POLYMER TRANSLOCATION THROUGH CONICAL PORES

Andri Sharma

A thesis submitted for the fulfillment of
the degree of Doctor of Philosophy

Department of Physical Sciences

Indian Institute of Science Education & Research (IISER) Mohali,
Sector 81 SAS Nagar, Manauli PO 140306 Punjab, India

March 2023

To my family …

Declaration

The work presented in this thesis has been carried out by me under the guidance of Dr. Rajeev Kapri at the Indian Institute of Science Education and Research Mohali. This work has not been submitted in part or in full for a degree, a diploma, or a fellowship to any other university or institute. Whenever contributions of others are involved, every effort is made to indicate this clearly, with due acknowledgment of collaborative research and discussions. This thesis is a bonafide record of original work done by me and all sources listed within have been detailed in the bibliography.

Andri Sharma

Place: ______________

Date: ______________

In my capacity as the supervisor of the candidate's thesis work, I certify that the above statements by the candidate are true to the best of my knowledge.

Dr. Rajeev Kapri
Associate professor
Department of Physical Sciences
IISER Mohali

Place: ______________

Date: ______________

Abstract

In 1996, Kasianowicz et al. [1], studied the translocation of a RNA molecule through an $\alpha-$hemolycin pore. It was observed that the ionic current gets blocked whenever the RNA molecule passes through the pore. Since this landmark experiment, considerable efforts have been made in understanding the transport phenomena of macromolecules through biological nanopores. One of the most investigated aspect is the fabrication of various types of nanopores to enable rapid DNA sequencing. Computer simulation studies using coarse-grained models with varying complexities, have greatly enhanced our understanding of the translocation process through various kinds of channels. The goal of this thesis is to understand the translocation of a polymer through an extended conical shaped pore with attractive surface interactions and a driving force which varies spatially inside the channel, using coarse grained molecular dynamics simulations. We consider both flexible, and semiflexible polymers. In our study, the polymer is modelled as a coarse-grained bead-spring chain, where non-bonded monomers interact via a short ranged repulsive Lennard-Jones (rLJ) potential. The consecutive monomers of the chain is bonded via a harmonic potential. To model a semiflexible polymer, an additional bending potential is introduced between consecutive bonds. The semiflexibility of the polymer is controlled by tuning its persistence length. The attractive surface interaction between the polymer and the conical channel is given by the standard Lennard-Jones interaction. The system is in a heat bath modelled as a Langevin thermostat. Verlet algorithm is used to solve the Langevin equation of motion to update the positions and the velocities of the polymer beads. All the simulations are performed using LAMMPS software [2]. For each set of simulation parameters, the results presented are averaged over $1500 - 2000$ independent samples.

As a first problem, we study the translocation process when the polymer enters the pore from the narrow entrance and exits from the wider end of the conical channel [3]. We refer to this as "Forward Translocation". We find that the channel gives rise to non-

monotonic features in the total translocation time as a function of the apex angle of the channel. We also obtained the waiting time distributions of individual monomer beads inside the channel and found unique features that depend strongly on the driving force and the surface interactions. Polymer stiffness results in longer translocation times for all angles of the channel which is consistent with earlier reports [4, 5]. Further, non-monotonic features in the translocation time as a function of the channel angle changes substantially as the polymer becomes stiffer, which is also reflected in the changing features of the waiting time distributions. The total translocation time τ decreases with increasing force strength as expected. Furthermore, with increasing forces, the non-monotonic features also reduce significantly. A break up of the total translocation time into a filling, transfer and escape time provides valuable insight on the translocation dynamics. We construct a free energy description of the system incorporating entropic and energetic contributions in the low force regime to explain the simulation results.

In the second problem, we study the translocation process with the entrance and the exit ends interchanged[6]. Now the polymer enters the pore from the wider side and exit from the narrow end. We call this as “Reverse Translocation”. We again obtain the total translocation time and the waiting time distributions, and compare them with the results obtained in the “Forward Translocation” case. We find striking differences between the two cases which we discuss in detail. Comparison of our simulation with experimental results [7] shows a good agreement. We have also obtained the conditions for directional independence of the translocation process so that results for the forward translocation process overlaps with that of the reverse case. It is found that ratio of pore and polymer lengths plays an important role in distinguishing the directional-dependent translocation processes. We find that the two process appears to be same under two circumstances (a) for a very rigid polymer chain, and (b) for a very long polymer chain.

As a third problem, we study the effect of different pore-polymer interactions as a function of pore length on the translocation of different polymers. The transition in the behavior of average translocation time with pore and polymer length is studied. For an extended pore with pore apex angle zero (i.e., a cylindrical pore), we find that the average translocation time scales nicely with the pore and the polymer lengths with same set of exponents for all ranges of the force considered in our study. However, for a conical pore, the average translocation time shows different behaviour for shorter and longer pore lengths and we do not observe a scaling behavior.

List of Figures

1.1 3D Structure showing the cross-section of α-hemolycin ion channel. The internal dimension of the channel is self-assembled from seven subunits in the bilayer to form a heptamer structure. The dimension varies from 1.5 nm (the narrowest lysine opening) to 3.6 nm (the widest vestibule) opening[8, 9]. 4

1.2 (a) Cartoon picture illustrating the set-up of polymer translocation through α-hemolysin pore embedded in a phospholipid-membrane. Negatively charged DNA molecules along with the salt ions are electrically driven across the pore. Ionic currents are measured with and without the DNA passage, and it is seen that with DNA passage ionic current drops by 90%. (b) The two current blockades at different time intervals are for two events of translocation for different DNA molecules.[10] 6

1.3 Schematic of $'i'$ bond vectors in freely rotating chain model in 2-d space, where the projection along the bond vector contributes to the correlation value while the normal components cancel out. The bond angle between vectors is θ, and the bond length is 'b'. 10

1.4 Plot showing the decay of bond-bond correlations as a function of rigidity along the chain contour. The rigidity of the chain varies from [2:128], as shown in the plot with colored number keys. The solid lines along each correlation plots is a fit of correlation exponent relation $(\exp(-|j-i|b/l_p))$ derived from WLC model. 11

1.5 Schematic diagram showing the emergence of curvature, with the radius of curvature R, when the beam is bent. The cost of the bending of the beam is stored as bending energy in the rod. 13

1.6 Figure showing the translocation of a flexible polymer of chain length 128 through a slit: (a) Snapshot of translocation dynamics, (b) Waiting-time distribution, $w(s)$, as a function of translocation co-ordinate, s (empty squares). A fit to the waiting time graph is provided with the TP-theory (filled squares). 18

1.7 Plots of Lennard-Jones potential(U_{LJ}), harmonic potential(U_{harm} and finite extensible non-elastic potential (U_{fene}). Out of the three potentials, first two potentials are used in our simulations. U_{LJ} is between two neighboring beads, while U_{harm}/U_{fene} acts between directly connected beads. The zeroes of U_{harm} and U_{fene} are shifted to the minima point (r_0) of U_{LJ} at ($2^{1/6}, -\epsilon = -1$). 22

2.1 Snapshots from the simulation for various stages of the translocation process of a semiflexible polymer with $N = 64$ beads, through a conical channel of length $L_p = 16\sigma$, half apex angle α and channel entrance width d. (a) Equilibrium polymer conformation on the *cis* side of the channel with one end fixed at the pore entrance. Subsequent polymer conformations (b) midway through the translocation process, (c) showing a possible hairpin formation near the channel exit and (d) when the polymer has successfully translocated to the *trans* side of the channel. 28

2.2 External force f_{ext} as a function of the length of the channel along its axis x, plotted for different apex angles α at a fixed $f_0 = 1.0$ according to Eq. 2.5. With increasing α, external force drops rapidly with x as expected. 31

2.3 (a) Waiting time distribution $w(s)$ of a flexible polymer through a flat channel ($\alpha = 0°$) as a function of scaled translocation coordinate s/N, for weak forces $f_0 = 0.1, 0.2$. (b) Waiting time distribution for strong forces : $f_0 = 1.0, 2.0$. (Inset) $w(s)$ for force values, $f_0 = 4.0$. 33

2.4 Variation of different time components (τ_s) with external force f_0 for a flat channel ($\alpha = 0°$) in log scale. Here, $\tau = \tau_f + \tau_p + \tau_e$. 34

2.5 Variation of total translocation time τ with external force f_0 for a flat channel ($\alpha = 0°$). $\tau \sim 1/f_0^\gamma$ with $\gamma \approx 1.78$. 35

2.6 Total translocation time (τ) of flexible polymer as a function of apex angle (α) for different external forces f_0. (Inset) The magnified plot of τ versus α at larger force values shows the disappearance of maxima-minima peaks. 36

2.7 Plots of time components for flexible polymer ($\kappa = 0$): passage time (τ_p) and escape time (τ_e) contributions to total translocation time (τ), s.t. $\tau = \tau_p + \tau_e$. Fig.(a-d) is for different values of external force. 37

2.8 Waiting time distributions of a flexible polymer for different α. In (a) we show the variation for $f_0 = 0.1$. (Inset) The plot of $w(s)$ for a flat channel serves as a control. Increasing force values to (b) $f_0 = 0.2$, (c) $f_0 = 0.5$ and (d) $f_0 = 1.0$ leads to dramatic changes in the distribution. 39

2.9 Total translocation time versus α for a semiflexible polymer for four different bending rigidities $\kappa = 1, 2, 4$ and 8. In (a) the variation is shown for $f_0 = 0.2$. (Inset) Magnified plot at lower α for $\kappa = 1.0$ and 2.0. As external force is increased : (b) $f_0 = 0.5$ (c) $f_0 = 1.0$ and (d) $f_0 = 2.0$, τ increases almost linearly with α. 41

2.10 Plots of time components for semi-flexible polymer: passage time (τ_p) and escape time (τ_e) contributions to total translocation time (τ), s.t. $\tau = \tau_p + \tau_e$. Fig.(a-d) represents and compares the time components for increasing rigidity of polymer for external force, f_0 =0.2. 42

2.11 Phase plot of total translocation time τ in the $\kappa - \alpha$ plane for two forces (a) f_0=0.2. and (b) $f_0 = 1.0$. 44

2.12 Phase plot displaying the dependence of τ on α's and κ's at lower force value, $f_0 = 0.2$, in (a-e) and for force 1.0 in (f) respectively. (a) The color variations clearly project two minima for the lower κ and lower α range. (b) It displays one minimum for higher α values. (c) Phase plot for rigid polymer at lower α values, τ monotonically decreases up to $\approx 5^\circ$ and then increases after that(fig. (d)). Fig.(e) is the total projection of τ. Fig.(f) is phase plot for force value 1.0, τ is a monotonic function of α for all κ values. 45

2.13 Waiting time distributions for various α at (a) $\kappa = 2$, and (b) $\kappa = 4$ for $f_0 = 0.2$. The distributions show distinct differences as the bending rigidity of the polymer is increased. 46

2.14 (a) Entropic part of the free energy ($\mathscr{F}_c + \mathscr{F}_e$) for a flexible polymer as a function of the translocation coordinate s for different α values showing non-monotonic behavior. (b) Energetic contribution to free energy for a flexible polymer from surface interactions ($\mathscr{F}_{pp}$) as a function of translocation coordinate s for various α values. (c) Entropic part of the free energy ($\mathscr{F}_c + \mathscr{F}_e$) for a semiflexible polymer ($\kappa = 8$) as a function of the translocation coordinate s for different α values showing largely monotonic behavior. (Inset) The barrier height decreases monotonically with α. (d) Energetic contribution to free energy for the semiflexible polymer from surface interactions ($\mathscr{F}_{pp}$) as a function of translocation coordinate s for various α values. 49

3.1 Variation of the magnitude of external force, f_x, along the conical channel for various cone angles (α). For any non-zero α value, f_x increases towards the narrow exit of the pore. 56

3.2 Schematic of an equilibrated flexible polymer sample for reverse translocation. The first bead of the chain is fixed at the entry of the conical pore, a few additional beads along with the first bead of the polymer are present at the pore entrance to restrict the entry of any polymer segments during the equilibration process. Inset shows the set-up for the forward translocation case, where the translocation takes place from the narrower end to the wider end of the conical channel. The color in the conical pores, represents the force gradient, f_x. 57

3.3 Plot of total time translocation (τ) for flexible polymer($\kappa = 0$) of length 64 beads along with the two time components: passage time (τ_p) and escape time (τ_e), s.t. $\tau = \tau_p + \tau_e$. Two simulation snapsorts are embedded in the plot to provide a visual scenario of the translocation process at lower and higher apex angle. 58

3.4 Comparison of forward (red) and reverse (blue) total translocation time (τ) vs. cone apex angle (α) at lower force value, $f_0 = 0.2$. Fig.(a-d) is plotted for $\kappa's$ =0, 2, 4 and 8 respectively. 60

3.5 Phase plot of τ for lower force ($f_0 = 0.2$). The three subplots (a-c) is for lower alpha values ($\alpha = [0 : 5]$) for different ranges of κ: (a) for $\kappa = [0 : 2]$, (b) for $\kappa = [2 : 4]$ and (c) for $\kappa = [4 : 8]$. Subplot (d) is for higher values of apex angle ($\alpha = [5 : 10]$) for the entire range of κ values i.e, for [0:8]. 62

3.6 Waiting time distributions, $w(s)$ vs. scaled translocation co-ordinate s/N ($N = 64$), for κ =0, and 4 respectively in Fig. (a), and (b) for $F_0 = 0.2$. The plots are for few intermediate apex angles to show the transition of $w(s)$ behaviour. 63

3.7 Residence time plot for flexible polymer with different polymer lengths (L =32, 64, 96, 128 and 256) for conical pore $\alpha = 1.5^{\circ}$, 3.5° and 10° in Figures (a), (b) and (c) respectively, for the force value, $f_0 = 0.2$. 65

3.8 Effect of increasing force on $w(s)$ pattern for longer flexible polymer chains (N =128(square) and 320(circle)) at $\alpha = 3.5^{\circ}$ for both the forward and reverse cases. Fig.(a) is for force, $f_0 = 0.4$ and Fig.(b) is for $f_0 = 0.8$. (filled circles and filled squares represent "reverse" case, and empty circles and empty squares represent "forward" case, respectively.) 67

3.9 Plots showing the overlap in waiting time distributions for the forward and reverse translocation process for a flexible polymer chain of length $N = 512$. In the same graph, $w(s)$ is plotted for the two force value: $f_0 = 0.8$ and $f_0 = 1.6$. The graphs with filled circle and filled square are for reverse translocation case and the empty circle and empty square represents forward translocation case. 67

4.1 Plots showing the variation of τ vs. α behaviour, with the change of pore-length, L_p from [5:10]. Here the polymer is flexible with length (N) 128 beads, and pore-length varies from 5σ to 10σ. 73

4.2 $\langle\tau\rangle$ as a function of N (in log-log scale) for three different driving forces when the polymer is translocating from an extended cylindrical pore (i.e., $\alpha = 0$) of length (a) $L_p = 5$, and (b) $L_p = 10$. The slopes mentioned in the plot are the values of the translocation exponent, defined by $\langle\tau\rangle \sim N^{\beta}$, for different driving forces. 74

4.3 $\langle\tau\rangle/N^{\gamma}$ as a function of L_pN^{ν} for an extended pore ($\alpha = 0$) for three different driving forces (a) 0.2, (b) 0.6, and (c) 1.0. The lines are the scaling function. 76

4.4 Schematic of sequenced pores with different lengths: 5, 10, and 15. The colorful beads of the pore are to denote different interactions between the pore and polymer beads. The polymer chain has repulsive interaction with the green static wall beads, the blue beads of the pore are attractive in nature, and the yellow part of the pore is repulsive in nature. Figures(a1-c1), are the pore designs for a pore length of 5 beads. Fig.a1 is an attractive pore, in pore b1, the middle pore is repulsive and in pore c1, the last three beads are repulsive and the rest of the beads are attractive in interactions. Figures(a2-c2), is the pore design for a pore of length 10 beads. The design of the pore with 10 beads is in the same ratio as the pore length of 5. Here pore (a2) is purely an attractive pore, the middle two beads of the pore (b2) are repulsive and the rest beads are attractive, and, in pore (c2), the last six beads are repulsive and first four beads are attractive. Similarly, Figures (a3-c3) is the sequenced pore in the same ratio as discussed above for pore length 15. 78

4.5 Comparison of τ vs. α for three different pore sizes L_p = 5, 10 and 15 for two different forces (f_0 =) 0.6 and 1.0. The length(N) of the flexible polymer chain ($\kappa = 0$) is 128 beads. 79

4.6 Total translocation time versus apex angle plots for a rigid polymer of length 128 for $f_0 = 1.0$, for two different pores ($L_p = 5$ and 10) described in Fig. 4.4. The curves in fig.(a,b) are for semi flexible polymer with rigidity 12.8, curves in fig.(c,d) are for $\kappa = 38.4$, and the curves in (e,f) represents polymer with rigidity 64 for pores: $L_P = 5$(a,c,e) and $L_P = 10$(b,d,f) respectively. 80

4.7 Scaled translocation time(τ) for the sequenced pore (Fig. 4.4) for three different pore lengths 5, 10 and 15. Plots (a), (b) is for force 0.6 and plots (c), (d) is for force 1.0 respectively. 81

Table of Contents

Chapter 1

Introduction **1**
1.1 Motivation: ”The Human Genome Project” 1
1.2 Definition: Polymer translocation 2
1.3 Translocation process in biological phenomena: 3
1.4 Progress in Theoretical and Experimental research: 3
1.5 Polymer Models 9
  1.5.1 Ideal chain: 9
    1.5.1.1 Freely jointed chain Model (FJC): 9
    1.5.1.2 Freely rotating chain model: 10
    1.5.1.3 Worm like Chain Model(WLC): 12
    1.5.1.4 WLC in continuous space(Derivation of bending energy) : 12
  1.5.2 Semiflexible chain: 14
  1.5.3 Real chain: 15
1.6 Theoretical description of translocation: 16
  1.6.1 Free energy description of polymer translocation: 16
  1.6.2 Tension propagation (TP) Theory for polymer translocation: 17
1.7 Langevin Equation 20
1.8 Computer Simulations 22
1.9 Overview of the thesis: 24

Chapter 2

Forward translocation of Semiflexible polymer through conical channels 27

2.1 Introduction 27

2.2 Model 29

2.3 Results and Discussions 32

2.3.1 Flexible Polymer 32

2.3.2 Semiflexible Polymer 40

2.4 Free Energy 44

2.5 Conclusions 51

Chapter 3

Reverse Translocation process of semiflexible polymer through conical channels 53

3.1 INTRODUCTION 53

3.2 MODEL AND METHOD 54

3.3 Results and Discussions 58

3.3.1 Total Translocation Time 58

3.3.2 Waiting Time Distributions 63

3.3.3 Effect of Polymer length: 64

3.4 Conclusions 68

Chapter 4

Effect of pore sequencing on translocation and scaling laws 71

4.1 Introduction 71

4.2 Effect of pore length 72

4.3 Effect of pore patterning 77

4.4 Conclusion 82

Chapter 5

Conclusion 85

Chapter A

Free Energy for Conical pore 89

Chapter 1

Introduction

1.1 Motivation: ”The Human Genome Project”

The fundamental unit of heredity is DNA (Deoxyribonucleic acid), which carries the genetic information of living species. DNA is a complex molecule where each molecule consists of two strands twisted to form a double helical structure[11]. The backbone of strands is made up of alternative sugar and phosphate groups, and these strands are bonded together with base pairs formed from four bases: Adenine(A) with Thymine(T), and Cytosine(C) with Guanine(G). The bases are organized in a sequence one after another to form a genetic code. Decoding the code extracts the information contained inside the DNA! With this knowledge in mind Human Genome Project (HGP) [12] was initiated in 1990 with a cost of 2.7 billion dollars to read the human genome, which has approx 3 billion base pairs. The project was closed in 2003, reporting a 1.3 billion base-pairs count of DNA in the human genome. A lot of engineering techniques and technologies have been developed over the years to extract information about the organism. Generation after generation, various techniques have been introduced to reduce the time and cost of DNA sequencing. Recently a third-generation DNA sequencing technique was invented, in which a single molecule of DNA is sequenced through a nanopore[13–15]. Here, different current blockades are measured across the pore due to different nucleotide patterns in DNA, which are further used to identify different sequences of DNA. The process is called DNA sequencing through a nanopore. Since 1996, various experimental and computational research has been performed on this area of DNA sequencing. It is found that the method of DNA transport process through nanopores is very efficient in DNA identification, as it minimizes the noise by preventing interference with other neighboring nucleotides, and at the same time is very cost-effective.

1.2 Definition: Polymer translocation

Polymer translocation terminology is used for the transport process of macromolecules from one side to the other side of the nanopore. The translocation problem is treated at the mesoscale level, and hence theoretically, the translocation process is studied by setting various coarse-grained models. Fine and detailed simulation techniques are used via force fields to incorporate the realistic chemical nature of the molecules, surrounding environment (e.g solvents), and the pores. The translocation process initiates when the first bead of the molecule enters the pore from one side of the pore (the cis side), and the process is successfully completed when all the beads of the molecule are transported through the pore to the opposite side, i.e. on the trans side of the pore. The extent to which polymer has passed through the pore or channel is decided by the polymer segment, s, on the trans side. The successive passing of monomers, adding to the increase of successfully translocated segment, **s**, on the trans side, is the net result of the forces from the cis-side segment, pore-polymer interactions, external driving force, and entropy force from the segment on the trans-side side itself. The nature of the translocation process depends on various factors: polymer length, pore length, external driving force, pore friction, bead-solvent interactions, pore-polymer adsorption strength, etc.

1.3 Translocation process in biological phenomena:

Real evidence of polymer translocation can be seen inside a biological cell. A biological cell consists of various proteins, ions, and polymers like DNA, RNA, etc, and is encapsulated inside a bi-layer membrane. The membrane holds the cell along with its constituents as a complete unit. The biomolecules leave the cell from the pores present on the bi-layer membrane and the passage of the molecules is one of the processes which makes the cell function. This is an example of multiple spontaneous translocations from a very complex environment.

There are various applications of single file threading in biotechnology. A few important examples are virus injection inside a host cell [10, 16–18], the transfer of DNA from bacteria to host cells, or gene swapping between two bacteria, and controlled drug delivery. These applications lead a lot of interest in experimental and theoretical research to deeply and thoroughly understand polymer translocation.

1.4 Progress in Theoretical and Experimental research:

Here are the chronology of progresses achieved in the last 3 decades, to study and evaluate the physics of polymer transportation.

In 1996, Kasianowicz et al. [1] demonstrated an experiment showing the translocation process through α-hemolycin pore (Fig. 1.1)[1], they observed the appearance of current blockades in the presence of RNA inside the pore, which is otherwise absent in the absence of the molecules inside the pore. This indicates the presence of a polymer inside

---

[1] Raw data for the alpha-hemolysin pore geometry is collected from Protein Data Bank[19].

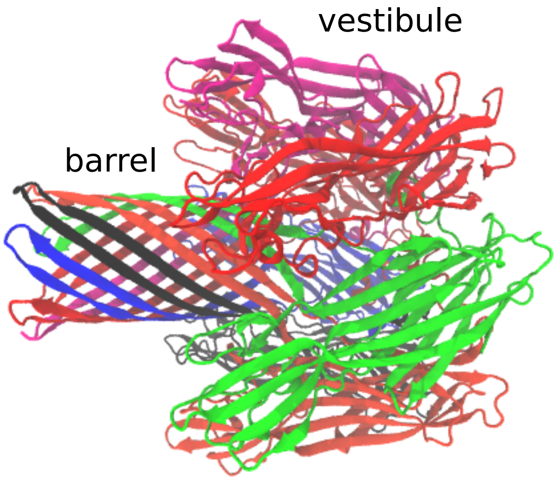

Figure 1.1: 3D Structure showing the cross-section of α-hemolycin ion channel. The internal dimension of the channel is self-assembled from seven subunits in the bilayer to form a heptamer structure. The dimension varies from 1.5 nm (the narrowest lysine opening) to 3.6 nm (the widest vestibule) opening[8, 9].

the channel. The duration of time for which the blockades appear is proportional to the length of the molecules passing the channel. The achievements from the result of this experiment paved the way to study DNA sequencing, both experimentally and theoretically. In 1995, Baumgärtner et.al. [20] studied the effect of pore curvature on the translocation process of polymers. It was found that, the gain in the conformational entropy of the polymer due to a curved membrane, facilitates the drive of polymer across the membrane. This leads to a spontaneous transport process, where the polymer is transported from a lower curved region to a higher curved region of the pore.In 1996, Sung et.al. [21], introduced a new statistical model of polymer translocation through a pore in a membrane, where the free energy barrier concept across the membrane was used to explain the diffusion process. They built the formalism from the Fokker-Plank equation, where they assumed that the friction coefficient was proportional to polymer length(N). The calculated translocation time was proportional to $N^{2+\nu}$, ν equals to 1 in Rouse model and

$\frac{1}{2}$ in Zimm model. Later in 1999, Akeson et.al. [22], showed that it is possible to distinguish between different kinds of composition in polymer through sequencing. In their experiment, two different types of current blockades were observed for the two different compositions, polycytidylic acid (poly A) and polyadenylic acid (poly C), of the same single RNA molecule. Later, in a paper by Muthukumar[23], the same Fokker-Planck[24] formalism was used to derive the translocation time. The only difference was that the friction coefficient was not a constant length-dependent number, but rather a parameter that depends on the ratchet potential which depends explicitly on the pore details. The assumption of local interaction between the pore and the monomer helped to improve the results for translocation time dependence on N. It was seen that long polymers, τ are proportional to N, as was experimentally observed in [1]. These were a few pioneering works in the area of polymer transport. For the last three decades, research are in progress to find various scaling laws and behavior of τ with other translocation parameters, for example, the chain length, and the pore length. In 2001, Amit Meller et.al. [10, 25] presented a letter describing the behaviour of τ with the chain length (Fig. 1.2). The experiment was carried out for α hemolysin pore, it was seen that the translocation process is faster with shorter chain length in comparison to longer chain length [26], and the velocity of translocation was seen to be a non-linear function of the applied voltage across the channel.

In 2007, Kaifu et.al. [27] performed Langevin dynamics simulation to establish relation between τ and pore polymer interactions ϵ. Here it was seen that for strong pore-polymer interactions, the translocation probabilities increases, and τ shows non-monotonic dependence on chain length for strong ϵ and the weak force, whereas for strong ϵ and strong force τ scales as $N^{2\nu}$, where ν is Flory's exponent. The non-universal scaling explicitly emphasizes the non-equilibrium nature of the polymer translocation problem. It was also shown for the first time that for strong attractive interactions, where single file translocation are ensured, τ can be divided into three different time: filling time τ_1, passage time τ_2 and escape time τ_3, s.t. $\tau = \tau_1 + \tau_2 + \tau_3$. This fragment analysis helped a lot to evaluate

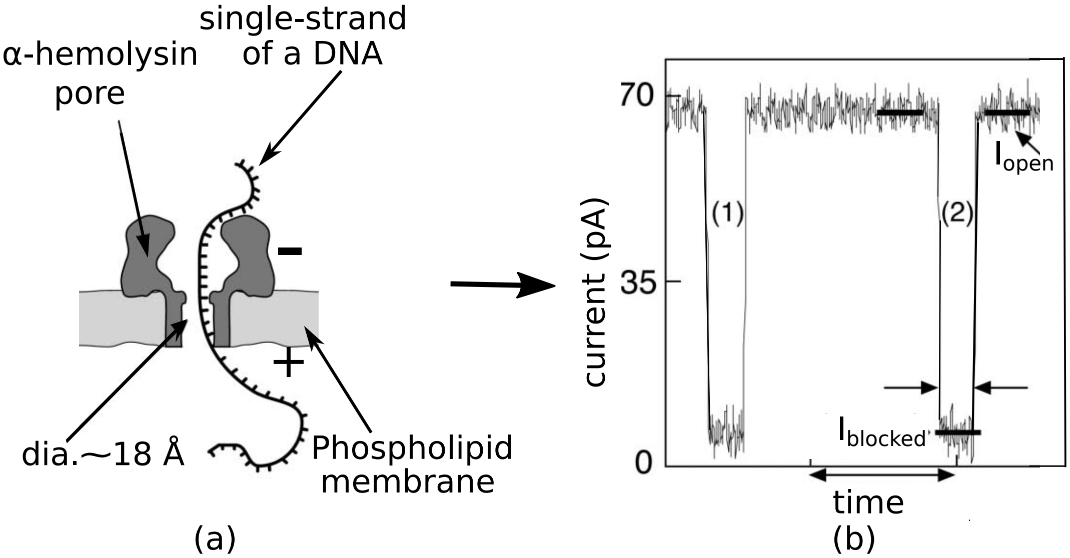

Figure 1.2: (a) Cartoon picture illustrating the set-up of polymer translocation through α-hemolysin pore embedded in a phospholipid-membrane. Negatively charged DNA molecules along with the salt ions are electrically driven across the pore. Ionic currents are measured with and without the DNA passage, and it is seen that with DNA passage ionic current drops by 90%. (b) The two current blockades at different time intervals are for two events of translocation for different DNA molecules.[10]

the role of attractive pores on the cis and trans side polymer segments. In a series of papers by Gauthier [28, 29], Monte Carlo technique was used to find the translocation time for flexible polymers through small nanopores. Here, it was established that for a long polymer chain, the translocation time (τ) scales as $\approx N^{1+\nu}$ for the Rouse model and as $N^{2\nu}$ in the case for Zimm model. Apart from studying the translocation process through nanopores and extended-pores, various other kind of biological inspired pore structures has been explored to study the effects of pore-polymer interactions [30–32].

Study of confined polymers and translocation of polymers through different geometrical pores other than single bead pores, like extended pores, conical pores, circular pores, spherical channels, corrugated channels, etc. [33, 34], paved the way to study sequencing of DNA and RNA, which has a lot of applications in the field of medicine and biotechnology. During the last few decades, a number of experimental and theoretical work has been performed to understand the dynamics of the transportation of such biomolecules [1, 4, 5, 21, 23, 27–29, 31, 35–40, 40–51, 51–61, 61–75]. For polymer driven translocation, tension propagation theory [46, 48–50, 52] is used to set up scaling laws at different force regime [47]. In a recent study[76], translocation through a conical channel was studied, where the complexity of the pore was captured in a two-stage process as capture and threading processes. Apart from flexible chain study, translocation problems for semi-flexible chains have been studied. It is seen that for long polymer $N = 256$, the more rigid the polymer is less is the propagation tail, and the retraction vector increases respectively[52, 77]. The effect of rigidity on τ has also been studied[33, 52, 54, 58, 59, 65, 77, 78]. Along with free energy description of translocation, and tension propagation theory, flory theory or(blob theory)[4, 79] are also used to find the scaling laws of τ with translocation parameters, like chain lengths, pore geometries, etc.

The transport of DNA through a nanopore/nanochannel is facilitated by the application of an electric field across the channel, giving rise to an electrostatic force that pulls the DNA into the channel. Due to the reduction in conformational entropy of a polymer in confinement, the geometry of the nanochannel has been found to strongly affect the dynamics of the translocation process. For example, in DNA sequencing using biological nanopores like α-hemolysin and MspA, it has been observed that the shape of the channel plays a vital role in determining the ionic current through it [10, 24, 30, 68, 72, 73, 80, 81]. Compared to the α-hemolysin pore, where the cylindrical shape of the beta-barrel dilutes the ion current specific to an individual nucleotide of the DNA inside the channel, thus making sequencing difficult, the narrow constriction of the cone-shaped MspA allows better resolution of current signatures corresponding to individual nucleotide [36, 82, 82, 83].

In a bid to control the transport dynamics of the DNA inside the nanochannel to achieve better sequencing, experimental approaches have shifted to the building of bio-inspired nanopores and nanochannels with similar transport properties [84–88]. These artificial solid-state nanochannels not only allow the control of the shape of the channel and tunability of its surface properties but are also stable to changes in pH, temperature and mechanical oscillations. Asymmetrical conically shaped nanopores have been found to have excellent sensing applications, with the nanopore tip acting as a sensing zone [89–94]. Conical nano capillaries show ionic current rectification at low salt concentrations. Further, chemical modifications of the inner surfaces of a conical nanochannel can lead to a reversal in the ion current rectification direction. A combination of a conical nano funnel with a cylindrical nanochannel was shown to significantly reduce the threshold external voltage required to trigger the translocation of DNA through the channel [93].

Theoretical studies of polymer translocation through conical nanochannels have shown that the escape of a confined flexible polymer from a conical channel is a pore-driven process and can proceed without an external force [4, 5]. The asymmetric shape of the channel ensures that the polymer has a larger entropic penalty near the constriction which gives rise to an entropic force leading to the escape of the polymer from the larger opening. Further, the passage time is a non-monotonic function of the apex angle of the cone for a given length of the channel. Langevin dynamics studies of flexible polymer translocation through conical channels have shown that translocation is dependent on channel structure and interactions of the polymer with the channel [73, 76, 95]. Most biopolymers and proteins are however semiflexible with an energy cost associated with bending, characterized by the bending rigidity κ of the polymer. The natural question to ask is how the stiffness of the polymer affects the translocation dynamics. It is with this motivation that we characterize the translocation dynamics of a semiflexible polymer through an interactive conical nanochannel. In this thesis, we investigated the translocation process from both the openings of the conical channel separately to underline the directional dependencies of the translocation dynamics.

1.5 Polymer Models

In theory, a polymer is modelled as a long chain of repeated monomer units. The monomers are connected with each other via some physical potentials. Depending on the type of interactions, a polymer chain can be categorised as: (i) an ideal chain, (ii) a semiflexible chain or (iii) a real chain.

1.5.1 Ideal chain:

Ideal chains are chains with no correlation between polymers monomer at long distance, they do not have any excluded volume interaction. They are allowed to cross each other. A few ideal chain models [96, 97] which are mostly used in theoretical studies are listed below.

1.5.1.1 Freely jointed chain Model (FJC):

It is the simplest model to model an ideal chain, there is no constraint on configurations and the bond angle θ and the torsion angle ϕ are allowed to take every possible value in the configuration space. The bond lengths (b) of the chain are constant, with no correlations between different bonds, such that the end-to-end distance ($\vec{R}_{\mathbf{n}}$) of the chain is the end-to-end vector which is the sum of individual bond vectors ($\vec{r}_i$):

$$\vec{R}_{\mathbf{n}} = \sum_{i=1}^{\mathbf{n}} \vec{r}_i \tag{1.1}$$

where **n** is the total number of bonds. Since, there is no direction preference in FJC, the ensemble average $\vec{R}_{\mathbf{n}}$ of chains is always zero, i.e. $\langle \vec{R}_{\mathbf{n}} \rangle = 0$. Whereas, the statistical measure of chain models is identified from the non-zero mean square end-to-end distance, and is given by:

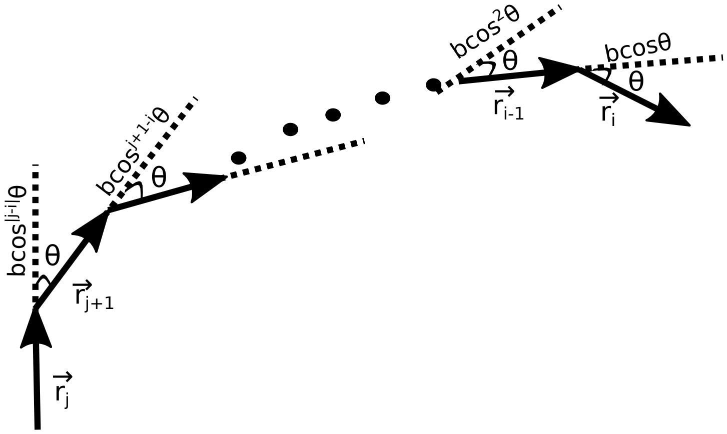

Figure 1.3: Schematic of ′i′ bond vectors in freely rotating chain model in 2-d space, where the projection along the bond vector contributes to the correlation value while the normal components cancel out. The bond angle between vectors is θ, and the bond length is ′b′.

$$\begin{aligned} \langle R^2\rangle &= \sum_{i=1}^{n}\sum_{j=1}^{n}\vec{r}_i\cdot\vec{r}_j && (1.2)\\ &= b^2\sum_{i=1}^{n}\sum_{j=1}^{n}\langle\cos\theta_{ij}\rangle && (1.3)\\ &= nb^2. && (1.4)\end{aligned}$$

1.5.1.2 Freely rotating chain model:

In this model, unlike FJC, the bond angles (θ) are fixed but torsion angle (ϕ) are free to span over all values (see Fig. 1.3). The correlation between the bond vectors is then given by the equation:

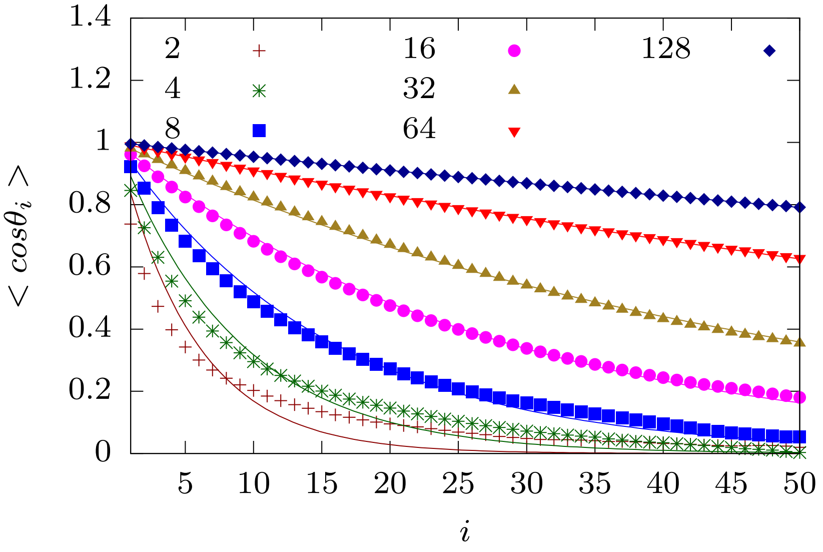

Figure 1.4: Plot showing the decay of bond-bond correlations as a function of rigidity along the chain contour. The rigidity of the chain varies from [2:128], as shown in the plot with colored number keys. The solid lines along each correlation plots is a fit of correlation exponent relation ($\exp(-|j-i|b/l_p)$) derived from WLC model.

$$\langle r_i r_j \rangle = b^2 \cos^{|j-i|} \theta. \tag{1.5}$$

Since, the torsion angle,ϕ, is free to rotate over the space, the components along the bond vectors contribute to the statistical average while the components normal to the axis cancel out. The end-to-end distance of the chain then becomes:

$$\langle R^2 \rangle = \mathbf{n} b^2 \frac{1+\cos\theta}{1-\cos\theta}, \tag{1.6}$$

where, **n** is the no. of bonds, and b is the length of each bond. From eq.1.6 we see that, for the case $\theta > 0$, $\langle R^2 \rangle$ for FRC model differs from the FJC model.

1.5.1.3 Worm like Chain Model(WLC):

The WLC model is often used to introduce the notion of rigidity in chains. Here the constraint is over the bond angle θ, i.e $\theta << 1$. The correlation between the bond vectors can be used to establish a relationship with the stiffness of the chain :

$$\begin{aligned}\langle r_i r_j \rangle &= b^2 \cos^{|j-i|}\theta \\ &= b^2 \exp[|j-i| \ln(\cos\theta)] \\ &= b^2 \exp[-|j-i| b/l_p],\end{aligned} \tag{1.7}$$

where, $l_p = \frac{-b}{\ln(\cos\theta)}$ is defined as the persistence length. The persistence length, l_p, measures the decay of bonds correlations in a chain. Correlation for stiffer polymers, i.e with higher persistence length, decays slowly in comparison to a less stiff polymer. As we can see in Fig. 1.4, the dark-blue plot is decaying very slowly, which is for $\kappa = 128$, in comparison to the brown curve, which is for $\kappa = 2$.

1.5.1.4 WLC in continuous space(Derivation of bending energy) :

One of the simplest ways to obtain the energy cost of bending is to study the beam bending technique[98]. A straight beam, with no bending, is deflected from its neutral axis, say from zero angles to some angle θ, as seen in Fig. 1.5. The beam is bent from the end side, such that the length of the beam along the axis is unaffected hence called the neutral axis, while the portion above and below the neutral axis is extended and compressed respectively. The arc hence formed can be mapped to a circle of radius R as the radius of curvature. Let's take a small portion of the arc with neutral arc length $L_0 = R\theta$, let z be the perpendicular distance above this arc with arc length $L_z = (R+z)\theta$. So the extent of

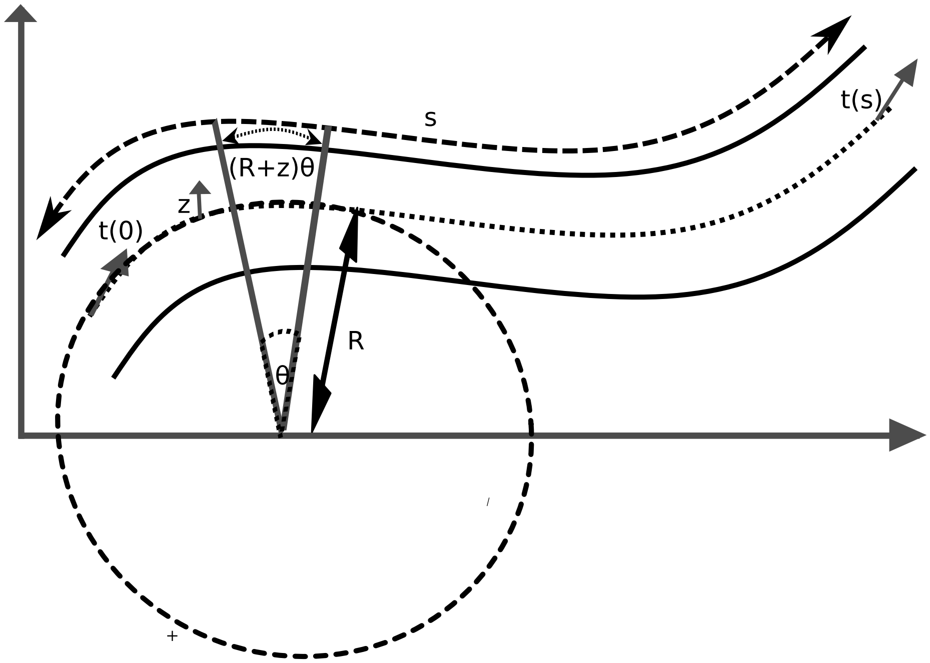

Figure 1.5: Schematic diagram showing the emergence of curvature, with the radius of curvature R, when the beam is bent. The cost of the bending of the beam is stored as bending energy in the rod.

the compression or extension:

$$\Delta L = L_z - L_0 = \frac{z}{R} L_0. \tag{1.8}$$

The strain is given by $\frac{\Delta L}{L}$, here small deformation is considered, such that the energy cost of this strain is the quadratic function of stretching or bending. In the simplest picture of bending, the stress-energy density is given as:

$$W = \frac{1}{2} Y \epsilon^2, \tag{1.9}$$

Y is Young's modulus of the material and $\epsilon = \frac{\Delta L}{L}$. The energy of the bending then is given by the equation:

$$E_{bend} = L_0 \int_{\partial\Omega} dA \frac{Y}{2}\frac{z^2}{R^2} \tag{1.10}$$

$$= L_0 I \frac{Y}{2R^2} \tag{1.11}$$

where $\partial\Omega$ is the cross-section perpendicular above the neutral beam axis, and $I = \int_{\partial\Omega} z^2 dA$ is the geometric moment due to the bending. By considering the assumption that the total energy can be written as the sum of energies of all the material particles along the same curvature, we rewrite:

$$E_{bend} = K_{eff} \int_0^L ds \frac{1}{R(s)^2} \tag{1.12}$$

where $K_{eff} = YI$. One can define $\frac{1}{R(s)}$ as the curvature which can also be written as the derivative of the tangent vector. Hence

$$E_{bend} = \frac{K_{eff}}{2} \int_0^L \left| \frac{dt}{ds} \right|^2 ds. \tag{1.13}$$

This is the continuous form for the discrete bending potential energy $U_{bend}(\theta_i) = \kappa(1 - \cos\theta_i)$, which incorporates stiffness by adding angle dependent interactions between the successive bonds (i.e., ith and $(i+1)$th bonds), respectively.

1.5.2 Semiflexible chain:

In theory, one can define a polymer chain to be completely flexible (as per FJC model). But in practice, almost every molecule posses rigidity due to its composition. The biomolecules have various ranges of stiffness and the WLC model is one of the useful models, in theory, to introduce controlled semiflexibility in chains. As discussed above, Eq.1.13 is the best way to talk about the degree of stiffness in chains from the cost of bending through the parameter(K_{eff}). Bending energy maps the elasticity of the chain between the beads. To compute the semiflexible chains, the discretized form of E_{bend}, i.e. U_{bend} is preferred in simulations, where the parameters and index have their usual definitions as described in the WLC section.

1.5.3 Real chain:

In real chain, the nearby monomer-monomer interaction or the interaction between the surrounding molecules is taken into account by an excluded volume interaction. The real chain conformations are decided upon the type of monomer-monomer interactions. It can be either attractive in nature or repulsive. Generally, in literature, these interactions reveal a lot about the surrounding solvents. If the chain is in good solvent then the monomer-monomer interactions are strong, or in other words, there is an attractive well between them. And in the situation when the monomer-solvent interactions (athermal solvents) are more strong in comparison to monomer-monomer interactions, then the monomers have hardcore repulsion between them. In theory, we use Week-Chandler-Anderson (WCA) potential or the Lennard-Jones (LJ) potential to incorporate the above-mentioned interactions.

In a real chain, the repulsion between monomer-monomer beads tends to swell the chain which causes the loss of conformational entropy. The chain then acquires an equilibrium size due to the balance between both competitive forces. The energetic contribution from excluded volume is equal to the energy associated with N numbers of excluded monomers occupying volume $'v'$, within a pervaded volume $V(= N/R^3)$, with no interactions between monomers:

$$F_{energetic} = \frac{K_B T v N^2}{R^3}. \tag{1.14}$$

The entropy free energy contribution is equal to the energy required to stretch an ideal coil to its end-to-end distance 'R':

$$F_{entropy} = \frac{K_B T R^2}{N b^2}. \tag{1.15}$$

The minimum of both the energies gives the equilibrium size of the chain and it is approx proportional to $N^{3/5}$.

1.6 Theoretical description of translocation:

1.6.1 Free energy description of polymer translocation:

In the above section, the free energy of a free real chain is discussed. But when the chain is in some confinement, the form of the equation is changed. During the translocation process, the chain is supposed to cross a barrier. Due to the barrier, the number of conformations of the chain reduces in comparison to the free real chain. The decrease in entropy increases the free energy due to the excluded volume effect in confinement. This develops a free energy barrier across the channel, and to successfully translocates on the opposite side of the pore, the chain has to overcome this barrier. The nature of translocation through various symmetric pores, e.g. nanopore, and cylindrical pores has been explained by establishing free energy for various regions during the transport process. This formalism is valid for the relatively small driving force and equilibrium conformations of polymer chains from m segments on the *trans*-side (compartment 1) and the remaining $N - m$ on the *cis*-side (compartment 2). The equilibrium partition function for the two compartments is given individually by Z_1 and Z_2, s.t. the total partition function is the product of the partition functions of both the compartments. Similarly, for an extended pore, the partition functions for the three regions can be written in the same way.

$$Z_2(m) = m^{\gamma-1} e^{-\mu m/K_B T}, \tag{1.16}$$

and

$$Z_1(N-m) = (N-m)^{\gamma-1} e^{-\mu(N-m)/K_B T}. \tag{1.17}$$

The total Free energy then is given by $-K_B T(\ln Z_1 + \ln Z_2)$

$$F_{total}(m) = (1-\gamma_2)\ln m + (1-\gamma_1)\ln N - m - m\frac{\Delta\mu}{K_B T}, \tag{1.18}$$

where $\Delta\mu$ is the chemical potential difference between the two sides. The chemical potential difference decides the favorable and unfavorable passage of segments on the trans side, for the positive value of $\Delta\mu$ the process is favorable whereas, for the negative value, it is an unfavorable escape. From this theory, one can study the polymer translocation process as a function of chain lengths (N). Along with it, the nucleation point (the condition for successful translocation) of the translocation can be calculated by finding the minima of Eq.(1.18) w.r.t. the trans coordinate (m).

1.6.2 Tension propagation (TP) Theory for polymer translocation:

Tension propagation formalism is used to explain the single file translocation dynamics of a polymer chain through nanopores. The length of the polymer chain considered in the theory is finite. For a polymer of chain length, N_0, the translocation process of the polymer is tracked by the segment on the *trans*-side of the pore which is defined as translocation coordinate s. The translocation coordinate s varies from 0, at the beginning of the translocation process, to N_0, on the completion of the translocation process. The motion of the

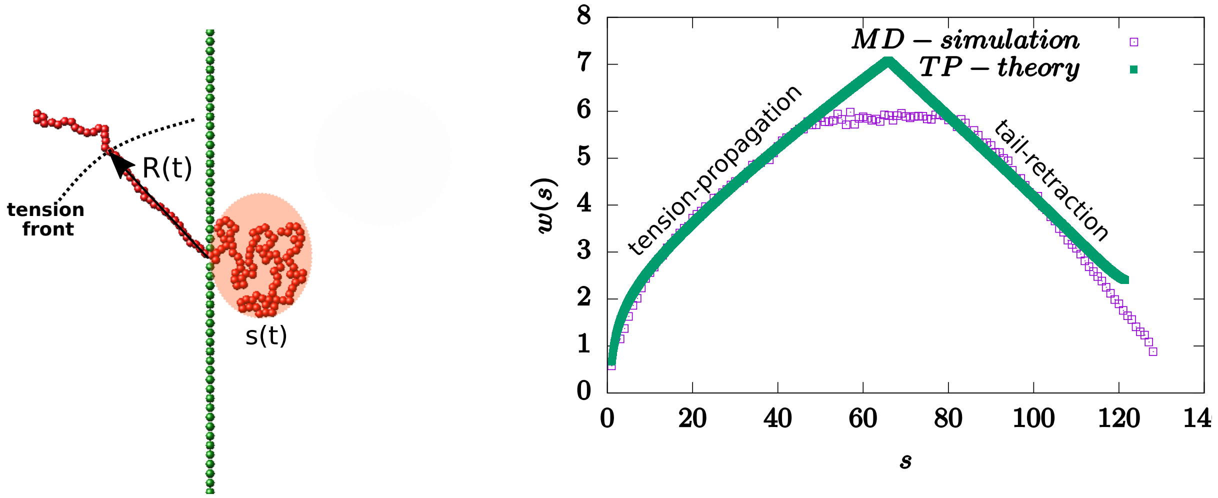

(a)

(b)

Figure 1.6: Figure showing the translocation of a flexible polymer of chain length 128 through a slit: (a) Snapshot of translocation dynamics, (b) Waiting-time distribution, $w(s)$, as a function of translocation co-ordinate, s (empty squares). A fit to the waiting time graph is provided with the TP-theory (filled squares).

translocation coordinate s is governed by a Langevin equation in the overdamped limit:

$$\tilde{\Gamma}(\tilde{t})\frac{d\tilde{s}}{d\tilde{t}} = (1-\gamma')\left[\frac{1}{\tilde{N}_0-\tilde{s}} - \frac{1}{\tilde{s}}\right] + \tilde{f}_{ext} + \tilde{\zeta}(\tilde{t}) \equiv \tilde{f}_{tot}. \tag{1.19}$$

The tilde sign in Eq.(1.19) is used to express the quantity in the dimensionless unit defined as: $\tilde{X} \equiv X/X_u$ [2]. In Eq. (1.19), $\tilde{\Gamma}(t)$ is the effective friction and is equal to the sum of the pore friction $\tilde{n_p}$ and the friction due to the drag force on the *cis*-segments, $\tilde{\zeta}(\tilde{t})$ is Gaussian white noise, $\gamma\prime$ is the surface exponent. The flux, $d\tilde{s}/d\tilde{t} = \tilde{\phi}(\tilde{t})$, of mobile monomers, $\tilde{N}$, is considered to be constant in space and time. In the TP theory for polymers, a tension force $\tilde{f}(\tilde{x},\tilde{t})$, arises due to a driving force exerted at the pore and it travels through the backbone of the polymer segments on the *cis*-side of the pore and is given by:

$$\tilde{f}(\tilde{x},\tilde{t}) = \tilde{f}_0 - \tilde{\phi}(\tilde{t})(\tilde{x}) \tag{1.20}$$

---

[2] Where the units are given by:time $t_u \equiv na^2/K_BT$, length $s_u \equiv a$, velocity $v_u \equiv a/t_u$, force $f_u = K_BT/a$, friction $\Gamma_u \equiv \eta$, flux density $\phi_u \equiv K_BT/\eta a^2$. Here a is the segment length, K_B is the Boltzmann constant, T is the temperature and η is the solvent friction.

where, $\tilde{f}_0 = \tilde{f}_{tot} - \tilde{\eta}_p \phi(\tilde{t})$ is the force at the pore entrance. The mobile and immobile domains on the *cis*-side are separated by a tension front, $\tilde{R}(\tilde{t})$, such that the region from the pore up to $\tilde{R}(\tilde{t})$ is always under the effect of the driving force (see Fig. 1.6(a)). The end-to-end distance of the mobile part of the polymer segments within the tension front can be used to calculate $\tilde{R}(\tilde{t})$,

$$\tilde{R}(\tilde{t}) = \tilde{A}_\nu \tilde{N}^\nu, \tag{1.21}$$

where $\tilde{A}_\nu$ is a prefactor which depends on the polymer chain and dimension of the system, $\tilde{N}$ is the last monomer under the tension force on the *cis*-side, and ν is the Flory exponent. The exact expression for the equation of motion for $\tilde{R}(\tilde{t})$ can be obtained using the iso-flux condition [46].

The force exerted on the part of the chain at the pore travels to the end of the chain on the cis-side through its backbone, and therefore the tension ($\tilde{R}(\tilde{t})$) propagates to the last bead of the polymer on the *cis*-side through the backbone of the chain. Once the number of monomers under tension propagation equals to the total number of monomer beads in the chain $\tilde{N}_0$, the propagation tail retracts and $\tilde{R}(\tilde{t})$ decreases. The effective friction is given by:

$$\tilde{\Gamma}(\tilde{t}) = \tilde{\eta}_p + \tilde{R}(\tilde{t}) \tag{1.22}$$

The solution of equations for tension front propagation and retraction are used to explain the waiting time distribution $w(s)$, obtained for the translocation of a polymer through a nanopore. As seen in Fig. 1.6(b), the initial rise in $w(s)$ is mapped to the tension propagation part obtained by $\tilde{R}(\tilde{t})$, and the decrease in $w(s)$ is mapped to the tail retraction part. Due to the single file translocation of polymer through a nanopore, the sum of the waiting-times solved for propagation and retraction gives the total translocation time.

1.7 Langevin Equation

The bio-molecular system is complex in structure and is surrounded by fluids, where its constituents atoms and molecules are in constant motion. In theory, the dynamics of the bio-molecules are studied by a coarse-grained model, where every entity of the system is captured by a physical potential. To get any closer to what the behavior of real molecules would look like, one needs to average thousands and thousands of these coarse-grained samples. Langevin equation is an example of such coarse-grained dynamics. It is used to study classical non-equilibrium processes like "polymer translocation". The equation consists of random source terms making the process stochastic. The stochastic differential equation is solved computationally to get a lucid picture of the underlying dynamics of the system. Here the random Brownian force is of thermal origin. In the case of the polymer translocation problem, the random distribution of the positions of the chain, is also a source of stochastic noise. Due to the thermal fluctuation term in the equation, the distribution of translocation parameters, like translocation time/velocity, is seen to be a Gaussian process. The Langevin equation for a bead of mass m, under an external potential U_{ext} is given as:

$$m\ddot{\vec{r_i}} = -\eta\dot{\vec{r_i}} - \nabla \sum (U_{LJ} + U_{harm} + U_{bend}) + \vec{f_{ext}} + \zeta. \tag{1.23}$$

The particle of mass m is subjected to coarse grained thermal environment via frictional force($-\eta\dot{\vec{r_i}}$) and random uncorrelated Gaussian random force ζ(t) (white noise), s.t.

$$\langle \zeta(t) \rangle = 0 \tag{1.24}$$

$$\langle \zeta_i(t)\zeta_j(t^{'}) \rangle = 2K_BT\eta\delta_{ij}\delta(t-t^{'}) \tag{1.25}$$

Equation (1.25) is known as fluctuation-dissipation relation. The average ($\langle\cdot\rangle$), is over different realizations of random forces, and $\delta(t)$ is the Dirac delta function. Eqs. (1.23), (1.24), and (1.25) are known as Langevin thermostats. The presence of an external force in the Eq. (1.23) makes it a driven process. The second term on the R.H.S of Eq.(1.23) is known as a force field, where U_{LJ} is known as Lennard-Jones potential, U_{harm} is harmonic potential and U_{bend} is cosine potential. U_{LJ} potential is a long-range potential between the neighboring beads within the cut-off region and is given by the expression:

$$U_{LJ}(r) = \begin{cases} 4\epsilon\left[\left(\frac{\sigma}{r}\right)^{12} - \left(\frac{\sigma}{r}\right)^{6}\right], & r \leq r_c \\ 0, & \text{otherwise}, \end{cases} \tag{1.26}$$

where $r_c = 2.5\sigma$ is the cut-off distance, σ is the size of the molecule, and ϵ decides the magnitude of attraction which is given by the depth of the potential below the point $(x, y) = (0, 0)$, The potential U_{harm} is between two connected beads of the chain. The other famous alternative for U_{harm} is U_{fene} potential which is preferred in molecular dynamic simulations and are given by Eq. (1.27) and Eq. (1.28), respectively.

$$U_{harm} = \frac{1}{2}K(r - R)^2, \tag{1.27}$$

$$U_{fene} = -K\ln\left(1 - (\frac{r}{R})^2\right), \tag{1.28}$$

where K is the spring constant, r is the distance between consecutive monomers, and R is their equilibrium separation. Fig. 1.7 compares different forms of above mentioned potentials. The value of spring constant(K) in U_{harm} and U_{fene} is chosen to be equal to 13 and the curves are shifted to -1 vertically so that the minimum of the plots coincides with the minima of U_{LJ} potential, $r_0 = 2^{1/6}\sigma$. In this thesis, we solve Langevin equation to get the coarse-grained dynamics of the polymer.

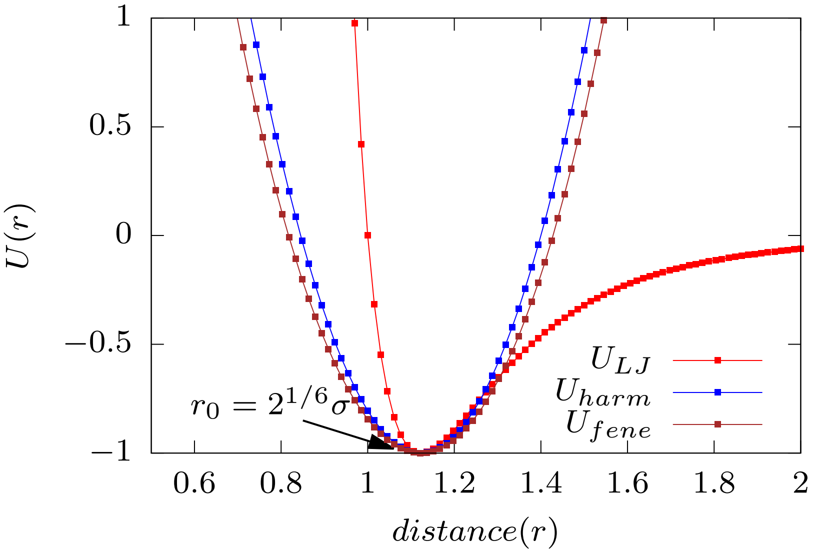

Figure 1.7: Plots of Lennard-Jones potential(U_{LJ}), harmonic potential(U_{harm} and finite extensible non-elastic potential (U_{fene}). Out of the three potentials, first two potentials are used in our simulations. U_{LJ} is between two neighboring beads, while U_{harm}/U_{fene} acts between directly connected beads. The zeroes of U_{harm} and U_{fene} are shifted to the minima point (r_0) of U_{LJ} at ($2^{1/6}, -\epsilon = -1$).

1.8 Computer Simulations

There are two approaches to perform simulations of the molecular system. The first one is a deterministic method called **Molecular dynamics** (MD), and the other method is a stochastic method known as **Monte Carlo** (MC).

The MD simulations are performed to obtain trajectories[3] of the molecular system. It gives temporal evolution of the states (or coordinates of beads in terms of computational) of the given system by solving the underlying dynamical equations, such as Newton's equation. The evolution is studied by computing the equations at extremely small time steps, usually in the order of femtoseconds ($10^{-15}s$) or in picoseconds ($10^{-12}s$)[4]. Molecular dynamics is a very useful tool in molecular physics, and lot of software are designed to incorporate the tools and techniques of MD. A few examples of such software are

---

[3] It is defined as the positions and velocities of the molecule as a function of time

[4] In Lennard Jones system all static and dynamic units are used in reduced units.

GROMACS, LAMMPS, CHARMM, NAMD, and AMBER. In the process, the acceleration of the particle is determined from the components of the force, which is further used to determine velocities and positions. The next updated position and velocity are then followed by the known states. There are different algorithms like Velocity Verlet, and leap-frog to perform integration over infinitesimal time steps. To begin the molecular dynamics simulation, all the atoms in the system are assigned initial positions and velocities. The velocity for each atom is assigned randomly from the Maxwell distribution at some temperature, T. The system is first equilibrated [5] at some desired temperature. The temperature of the system with n beads (of mass m) is related to the mean kinetic energy of the system by:

$$T = \frac{2}{3nK_B} \sum_{i=1}^{n} \frac{m_i v_i^2}{2}, \tag{1.29}$$

where, m_i and v_i are respectively the mass and the velocity of the i^{th} particle. Once the desired temperature is reached, the equilibration run is stopped followed by the production run.

In statistical mechanics, MC simulation is used to build the configuration space of the molecular system. The ensemble is generated by creating an acceptable sample space. The randomly chosen states must be feasible under the given thermodynamic conditions, which are decided by calculating probabilities of the accessible states. MC does not provide temporal dynamics of the system like MD. In contrast, every time step in MD is a new configuration in MC. On the other hand, in MD, one performs MC at every step. One of the popular MC methods for complex molecular systems is the Metropolis method. Monte Carlo simulation is a Markovian process, where a each state is defined from its previous state. The typical steps in the Metropolis algorithm are:

1. Initialise coordinates of n beads.

2. Randomly choose a bead i and displace its coordinates by random displacement,

---

[5] A system is said to be equilibrated if all the intensive parameters e.g. temperature, pressure, chemical potential, etc. are same in every spatial direction.

$\Delta x_i,\ \Delta y_i,\ \Delta z_i$ to obtain a new state.

3. Calculate the change in energy, ΔE, between the two states.
4. If $\Delta E < 0$, accept the new coordinates and repeat step 2.
5. If $\Delta E > 0$, choose a random number, $\psi \in [0, 1)$.
   (a) If $\psi < e^{\frac{-\Delta E}{K_B T}}$, accept the new coordinates and repeat step 2
   (b) If $\psi > e^{\frac{-\Delta E}{K_B T}}$, keep the original states and repeat step 2.

In the context of polymer physics, MC method is very efficient in studying the dynamics of polymer chains on a lattice.

In the thesis, we have used the MD approach and all the simulations are performed using LAMMPS software [2, 99].

1.9 Overview of the thesis:

The thesis is organised as follows:

In Chap. 2, we present our results on translocation of polymers though conical channels. The polymer enters the pore from the narrow end and exits from the wider end. We refer it as "forward translocation" process. The main objective of the study is to understand the influence of conical pore structure on the translocation process. The quantities of interest are the total translocation time τ, and the waiting time distribution $w(s)$. We also provide a Free energy description, in the quasi-equilibrium limit, to map the translocation dynamics at a lower force regime.

In Chap. 3, we present results for the case where the polymer enters from the wider end and exits from the narrow end of the conical pore. We refer this as "reverse translocation” process. We again obtain the same quantities of interest and compare them with the results obtained for the “forward” case. We found striking differences between the two cases. We also discuss the conditions when the results for the “forward” and the “reverse” cases are same.

In Chap. 4, we study the effect of pore length, polymer length, and pore patterning on the total translocation time τ. We also establish the scaling laws for the total translocation time with these parameters.

In Chap. 5, we summarise the results presented in the thesis.

Chapter 2

Forward translocation of Semiflexible polymer through conical channels

2.1 Introduction

In this chapter, we study the translocation dynamics of both flexible and semiflexible polymers through cone shaped nanochannels in the presence of a spatially varying external driving force and surface interactions, using coarse-grained Langevin dynamics simulations. The external force acting along the channel length mimics the voltage driven translocation of polymers, higher at narrower regions of the channel and lower near the larger channel openings. Using the results of the translocation dynamics of a flexible polymer through an flat channel ($\alpha = 0°$) as control, we first show that the asymmetric shape of the channel gives rise to non-monotonic features in the total translocation time as a function of the apex angle of the channel. The waiting time distributions of individual monomer beads inside the channel show unique features strongly dependent on the driving force and the surface interactions. Polymer stiffness results in longer translocation times for all angles of the channel. Further, non-monotonic features in the translocation

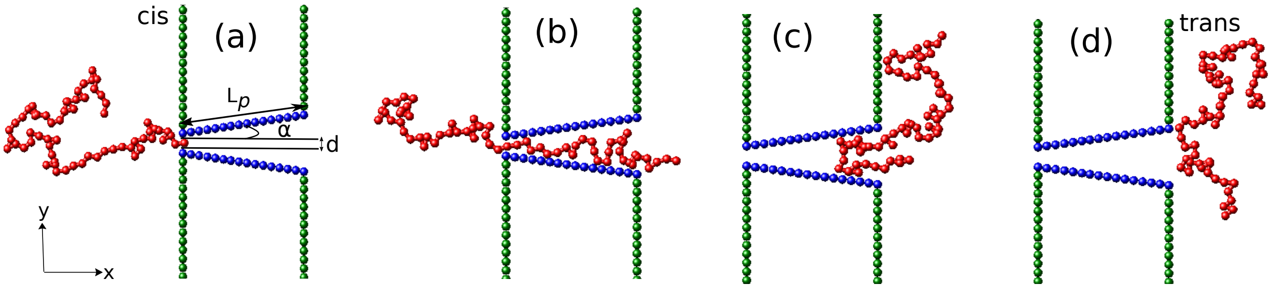

Figure 2.1: Snapshots from the simulation for various stages of the translocation process of a semiflexible polymer with $N = 64$ beads, through a conical channel of length $L_p = 16\sigma$, half apex angle α and channel entrance width d. (a) Equilibrium polymer conformation on the *cis* side of the channel with one end fixed at the pore entrance. Subsequent polymer conformations (b) midway through the translocation process, (c) showing a possible hairpin formation near the channel exit and (d) when the polymer has successfully translocated to the *trans* side of the channel.

time as a function of the channel angle changes substantially as the polymer becomes stiffer, which is reflected in the changing features of the waiting time distributions. The total translocation time τ decreases with increasing force strength as expected. A break up of the total translocation time into a filling, transfer and escape time provides valuable insight on the translocation dynamics. As the apex angle α (see Fig. 2.1for the definition of the system parameters) is varied, the translocation time shows non-monotonic features, consistent with earlier reports [4, 5, 73, 76, 95]. We construct a free energy description of the system incorporating entropic and energetic contributions in the low force regime to explain the simulation results. We comment on the detailed behavior of the waiting time distribution with varying force strengths and α. We next present a detailed study of the translocation dynamics of semiflexible polymers with increasing stiffness through this conical nanochannel. The non-monotonic features observed in τ with varying α differs significantly from that of the flexible polymer. The translocation time is also strongly dependent on the stiffness of the polymer. Further, with increasing forces, the non-monotonic features reduce significantly and total translocation time increases with increasing α for all values of polymer stiffness. We present phase plots of τ in the $\kappa - \alpha$ plane and mean waiting time distributions to characterize the translocation dynamics in detail. Finally, we provide free energy arguments using a quasi-equilibrium approximation valid at low forces to explain our observations.

In Sec. 2.2, we introduce the simulation model and methods where the governing equations are explained. This section also sets the notations used in the chapter. In Sec. 2.3, we present the results and discussion of our simulations for (a) flexible and (b) semiflexible polymer. In Sec. 2.4, we provide possible explanation for the observed behaviour at low forces via a free energy description. In Sec. 2.5, we conclude by discussing the importance of our results and possible future directions to extend the domain of physical relevance of this work.

2.2 Model

To model the conical channel in two dimensions, we consider the walls of the channel to be made up of two rows of fixed monomer beads of size σ and of length $L_p = N'\sigma$, where N' is the number of monomers making up a wall of the channel. The walls are symmetric about the $x-$axis with the apex angle of the channel α defined with respect to the x-axis as shown in Fig. 2.1. The diameter of the channel at the *cis* side is fixed at d to allow only a single monomer entry. To separate the *cis* and *trans* regions of the channel, vertical walls made up of fixed monomers beads are placed along the $y-$ direction.

The polymer is modeled via a coarse-grained bead-spring chain, where non-bonded monomers interact via a short ranged repulsive Lennard-Jones (rLJ) potential given by

$$U_{\text{bead}}(r) = \begin{cases} 4\epsilon\left[\left(\frac{\sigma}{r}\right)^{12} - \left(\frac{\sigma}{r}\right)^{6}\right] + \epsilon, & r < r_c \\ 0, & r \geq r_c \end{cases} \tag{2.1}$$

where ϵ gives the strength of the potential. The above truncated and shifted LJ potential has cut-off at $r_c = 2^{\frac{1}{6}}\sigma$. The interaction between consecutive monomers of the chain is harmonic with the interaction given by

$$U_{\text{bond}} = \frac{1}{2}K(r - r_0)^2, \tag{2.2}$$

where K is the spring constant and r_0 is the equilibrium separation between consecutive monomers.

To model a semiflexible polymer, an additional bending potential is introduced between consecutive bonds as follows :

$$U_{\text{bend}}(\theta_i) = \kappa(1 + \cos\theta_i) \tag{2.3}$$

where θ_i is the angle between the i^{th} and $(i-1)^{th}$ bond vectors. κ quantifies the bending rigidity of the polymer.

The interaction of the polymer beads with the vertical walls is modeled by the same repulsive Lennard-Jones (rLJ) introduced before for the polymer. The surface interaction of the conical channel with the polymer is however attractive, with the attraction between the beads of the polymer and the channel beads given by the standard Lennard-Jones interaction as :

$$U_{\text{channel}}(r) = \begin{cases} 4\epsilon\left[\left(\frac{\sigma}{r}\right)^{12} - \left(\frac{\sigma}{r}\right)^{6}\right], & r \leq r_c^{lj}. \\ 0, & \text{otherwise} \end{cases} \tag{2.4}$$

where $r_c^{lj} = 2.5\sigma$.

In addition to the forces on the polymer due to its interactions with the channel, it experiences an additional external force in the positive $x-$ direction, modeled as a potential gradient, Fig. 2.2 :

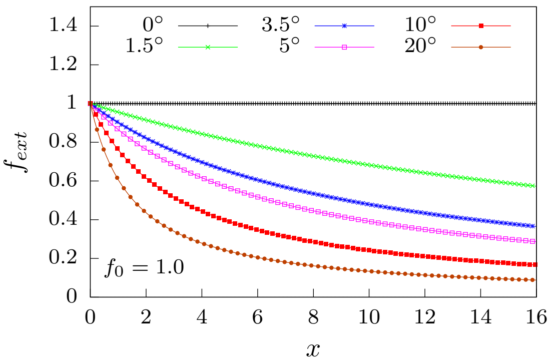

Figure 2.2: External force f_{ext} as a function of the length of the channel along its axis x, plotted for different apex angles α at a fixed $f_0 = 1.0$ according to Eq. 2.5. With increasing α, external force drops rapidly with x as expected.

$$f_{ext} = \frac{f_0 d}{(d + 2x \tan \alpha)} \tag{2.5}$$

where f_0 is the constant force expected in a linear channel with $\alpha = 0°$. Evidently, for a conical channel, the force decreases along its length.

The equation of motion for the position of the ith monomer of the polymer is given by

$$m\ddot{\vec{r}_i} = -\zeta\dot{\vec{r}_i} - \nabla U_i + \vec{f}_{ext} + \vec{\eta}_i, \tag{2.6}$$

where m is the mass of the monomer, U_i is the net potential faced by the monomer, ζ is the friction coefficient and $\vec{\eta}_i$ is a Gaussian random force with $\langle \eta_i(t)\eta_j(t^{'})\rangle = 2k_BT\zeta\delta_{ij}\delta(t-t^{'})$ where k_B is the Boltzmann's constant and T is the temperature. The equations are simulated in LAMMPS using the Verlet update scheme. The scales of length, energy, and mass are set by σ, ϵ, and m respectively. This sets the time scale as $\tau_0 = \sqrt{\frac{m\sigma^2}{\epsilon}}$. In these units, we choose $k_BT = 1.0$, $\zeta = 1.0$, $r_0 = 1.12$, $d = 1.25$ and $K = 10^3 k_BT/\sigma^2$. f_0 is varied in the range $0.1 - 2$ k_BT/σ and κ varies in the range $0 - 8$. The number of polymer beads $N = 64$ and pore beads $N' = 16$ are fixed in our simulations. The time step is set as $\Delta t = 0.001\tau_0$ and all results presented are averaged over $1500 - 2000$ independent samples.

We start our simulation by holding the first bead of the polymer at the narrow opening of the channel while the rest of the polymer segment is allowed to relax to its equilibrium conformation outside the channel. The translocation process is tracked by the translocation coordinate s. The counter for s starts once a bead of the polymer reaches the *trans* side after crossing the channel. The polymer is said to be successfully translocated if s is equal to the total number of beads N of the polymer and the simulation terminates. The speed with which the polymer traverses the channel gives a detailed idea of what is going on inside the channel. To trace the above effect, we focus on the waiting time $w(s)$, defined as the average time spent by a monomer inside the channel.

2.3 Results and Discussions

2.3.1 Flexible Polymer

We first look at the translocation dynamics of a flexible polymer through a flat channel $\alpha = 0^\circ$ which serves as a control. As the strength of the external force f_0 acting inside the channel is increased ($f_{ext} = f_0$ for a flat channel), the total translocation time (τ) of the polymer decreases.

To explain this behavior, we look at the waiting time distribution $w(s)$ of the polymer at different values of f_0 (Fig. 2.3). Tension propagation theory [46, 48, 50, 52] accurately predicts the waiting time distribution for a slit (channel of unit size). The waiting time, $w(s)$, is expected to rise with s as the tension due to the external force reaches the end of the polymer in the *cis* side. After that, the system is in the tail retraction stage and $w(s)$ starts decreasing with s. In our system, where the pore is extended and is attractive in nature, we observe several interesting features in $w(s)$ which are different from that obtained for the polymer translocating through a slit. These arise due to the interplay between surface interactions and the external drive.

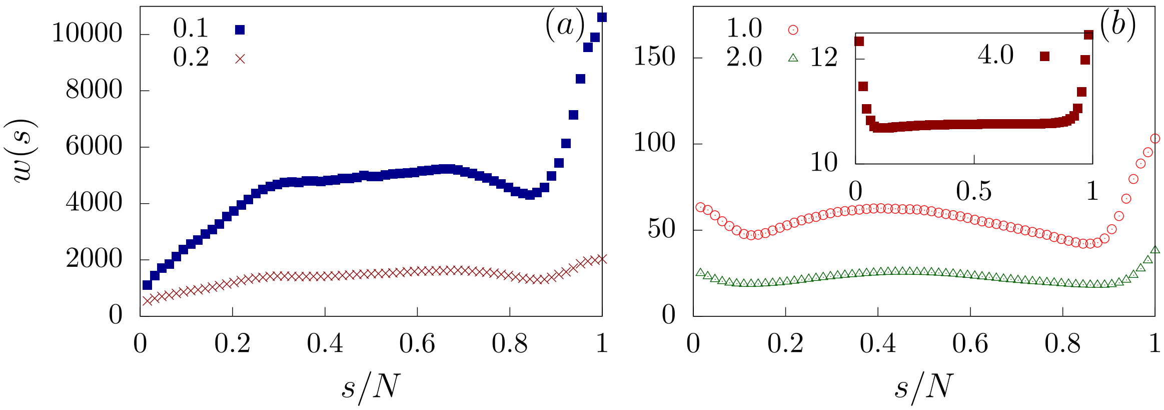

Figure 2.3: (a) Waiting time distribution $w(s)$ of a flexible polymer through a flat channel ($\alpha = 0°$) as a function of scaled translocation coordinate s/N, for weak forces $f_0 = 0.1, 0.2$. (b) Waiting time distribution for strong forces : $f_0 = 1.0, 2.0$. (Inset) $w(s)$ for force values, $f_0 = 4.0$.

For the initial part of the translocation, when the polymer enters the pore, the attractive nature of the pore and the external force, suck the polymer inside the pore. For smaller forces ($f_0 = 0.1, 0.2$) (Fig. 2.3(a)), $w(s)$ rises with s as the tension slowly reaches towards the end. However, as f_0 increases (see Fig. 2.3(b) with $f_0 = 1.0, 2.0$), the combined effect of the attractive pore and the external force pulls the initial monomers quickly inside the pore, thus reducing their waiting times. For the lower forces (Fig. 2.3(a)), we observe a flat regime, where $w(s)$ does not change with increasing s. Subsequently, once the tension has propagated to the end, the tail retraction part sets in, and $w(s)$ starts to fall. Dramatically, however, $w(s)$ shows a sharp rise for the end monomers of the polymer. This feature is true for all external force values. As the number of monomers left in the channel becomes lesser than the channel length and keeps decreasing, the net external force on the polymer decreases. Therefore, the attractive nature of the channel becomes a dominant factor for the end monomers resulting in increased waiting times. The behavior of the waiting times as explained above can be better understood if we divide the total translocation time as $\tau = \tau_f + \tau_p + \tau_e$ where (i) τ_f is the initial filling time, the time taken by the first monomer of the polymer to reach the exit without returning back into the channel; (ii) τ_p is the transfer time, the time taken from the exit of the first monomer into

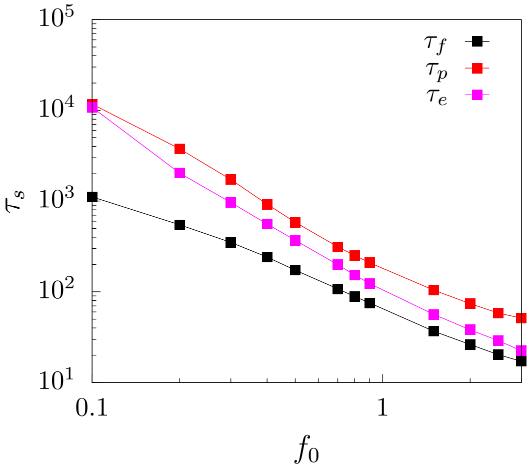

Figure 2.4: Variation of different time components (τ_s) with external force f_0 for a flat channel ($\alpha = 0°$) in log scale. Here, $\tau = \tau_f + \tau_p + \tau_e$.

the *trans* side to the entry of the last monomer from the *cis* side; and (iii) τ_e is the escape time, the time between the entry of the last monomer in the channel and its escape to the trans-side [55, 72]. τ_f depends strongly on the external drive and the surface interactions which sucks the polymer inside. τ_p depends on surface interactions and entropy of the polymer segment outside the channel on the *trans* side and less on the external force since these monomers see a constant force inside the channel. τ_e is strongly influenced by the attractive interactions which hold back the polymer as it exits the channel.

In Fig. 2.4, we have plotted the three translocation times as a function of the force. For low forces, τ_f is significantly smaller than τ_p and τ_e, suggesting that translocation is dominated by the transfer and escape dynamics. This explains the initial rise in $w(s)$ for small s as successive monomers spent longer times inside the channel. At larger forces, τ_f becomes comparable to the transfer and escape times. As explained earlier, the combined effect of surface interactions and external force pulls the monomer rapidly inside the pore. Therefore, the initial monomers show a dip in the waiting times.

In Fig. 2.5, we have plotted the total translocation time of the polymer as a function of the external force. The translocation time falls faster than $1/f_0$ for larger forces. This behavior is reminiscent of the effect of attractive pore-polymer interactions which pro-

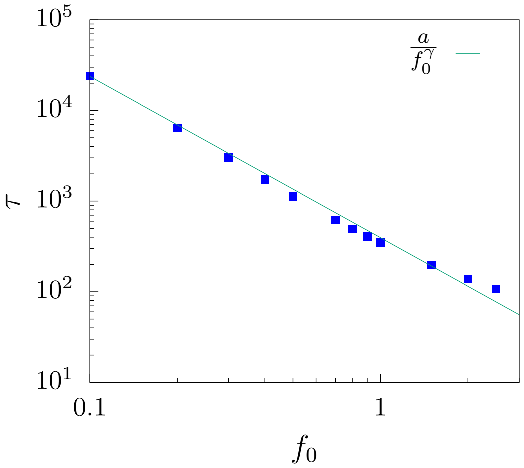

Figure 2.5: Variation of total translocation time τ with external force f_0 for a flat channel ($\alpha = 0°$). $\tau \sim 1/f_0^\gamma$ with $\gamma \approx 1.78$.

vides an additional pull on the monomer beads as they enter the pore. Such behavior of τ with f_0 for driven polymer translocation through extended channels have been reported earlier [27].

We next look at the situation for the conical channel ($\alpha \neq 0$). Since more polymer conformations are possible in the extended part of the channel compared to the constricted region, this shape asymmetry leads to a force of entropic origin which can facilitate movement of the polymer from the *cis* to the *trans* end. Therefore, in addition to the effects of the attractive surface interactions of the channel, the shape asymmetry influences the translocation process significantly. Further, the external force is space-dependent (Fig. 2.2), and decreases as we move from the *cis* to the *trans* side of the channel. This leads to a global decrease in the total translocation time (τ) when compared to a flat channel. Additionally, τ displays distinct non-monotonic features as α is varied (Fig. 2.6). We first analyze this non-monotonic behavior for very low forces (say $f_0 = 0.1$).

As α starts to increase, τ decreases as translocation are facilitated by the additional entropic drive when compared to $\alpha = 0°$ which drives the polymer inside the conical pore faster compared to a flat channel. This continues till a certain $\alpha = \alpha_1$ (see Fig. 2.6;

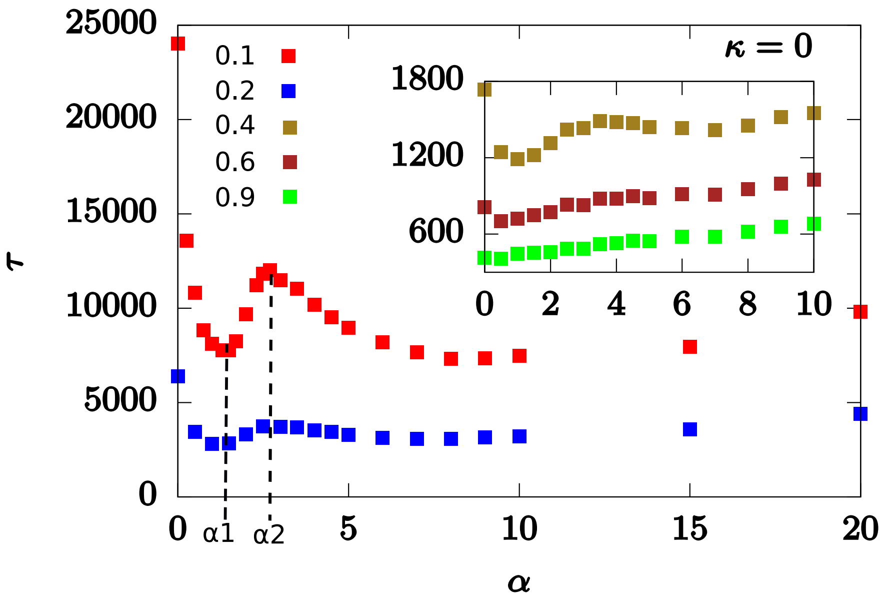

Figure 2.6: Total translocation time (τ) of flexible polymer as a function of apex angle (α) for different external forces f_0. (Inset) The magnified plot of τ versus α at larger force values shows the disappearance of maxima-minima peaks.

for $f_0 = 0.1$, $\alpha_1 \approx 1.5°$). Beyond this apex angle, τ starts increasing with α. Note that with increasing α, the attractive interactions along the length of the channel weaken. This lowering of the pull on the polymer near the entrance, leads to longer translocation times. It is again useful to split the total translocation time as was done for the flat channel. However, unlike a flat channel, a conical channel has a larger exit which results in the folding of the polymer back into the channel (see Fig. 2.1(c)). Therefore, for such channels it becomes convenient to split the translocation time into a passage time and an escape time, $\tau = \tau_p + \tau_e$. Passage time τ_p for a conical channel is defined as the the time elapsed between the entrance of the first and the last bead of the polymer at the pore entrance. The escape time τ_e is defined similar to that of the flat channel. It is the time taken after τ_p until all the polymer beads have exited the pore from the *trans* side. As we see, from Fig. 2.7(a), the non-monotonicity in τ for smaller α is completely governed by τ_p. The weakening of the surface interactions near the *cis* side is what dominates the behavior.

This increase in τ with α continues till it reaches $\alpha = \alpha_2$. Beyond α_2, τ starts decreasing

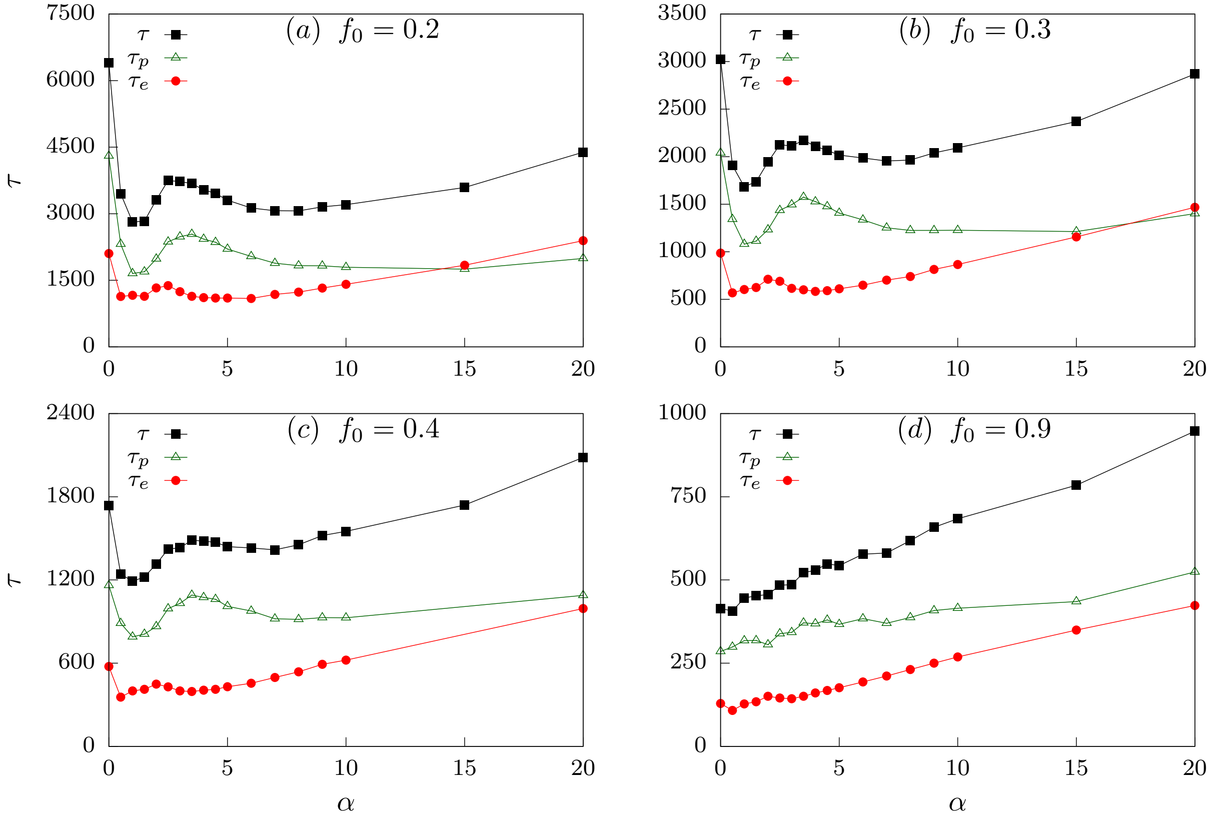

Figure 2.7: Plots of time components for flexible polymer ($\kappa = 0$): passage time (τ_p) and escape time (τ_e) contributions to total translocation time (τ), s.t. $\tau = \tau_p + \tau_e$. Fig.(a-d) is for different values of external force.

with α. This is a combined effect of the entropic drive and surface interactions. Due to wider pore exit, the pore filled with a polymer experiences an entropic drive. Further, the escape time (τ_e) also decreases because the attractive interaction near the pore exit becomes negligible and cannot hold the polymer inside the pore. With increasing α, we see a different behavior. At high α, τ_e starts increasing and surpasses τ_p at some α. This crossover can be explained by noting that the wider exit allows the folding of a polymer leading to hairpin formations inside the pore. The escape of the polymer becomes the rate-limiting step. Note that τ_p saturates beyond some value of α as the force that drives the entry and the subsequent passage of the polymer towards the exit do not change.

At higher forces ($f_0 > 0.4$; see inset of Fig. 2.6), τ increase with α because the surface interactions do not play a major role in this regime. The force along the channel axis is larger for smaller α. This ensures that at large force values, the translocation process is extremely fast. However, as α increases, the force along the channel axis decreases (see Fig. 2.2), and the translocation becomes slower.

We further verify our findings for the translocation time by looking at the waiting time distribution of the monomer beads (Fig. 2.8). At a force value of $f_0 = 0.1, 0.2$ (Fig. 2.8(a-b)), we note that as α is increased from $1.5°$ to $3.5°$, $w(s)$ for the initial beads increases dramatically. This is a result of weakening attractive interactions near the *cis*-side as the pore broadens. Note that for the end beads, $w(s)$ for $\alpha = 1.5°$ rises sharply because of the attractive interactions at the *trans*-side which prevent the exit of the polymer. This effect is reduced sharply for $\alpha = 3.5°$. As α is increased further, $w(s)$ reduces due to weakening attractive interactions near the exit and a greater entropic drive. At even higher $\alpha \geq 10°$, we start seeing the effects of the folding in of the polymer leading to increased $w(s)$ for all monomer beads when compared to $w(s)$ at lower α values. The dip in $w(s)$ for the last few monomers at large values of α is easily explained. With surface interactions lowered significantly and a large part of the polymer already outside the pore leading to higher entropy, the end monomers are sucked out extremely fast. For higher force

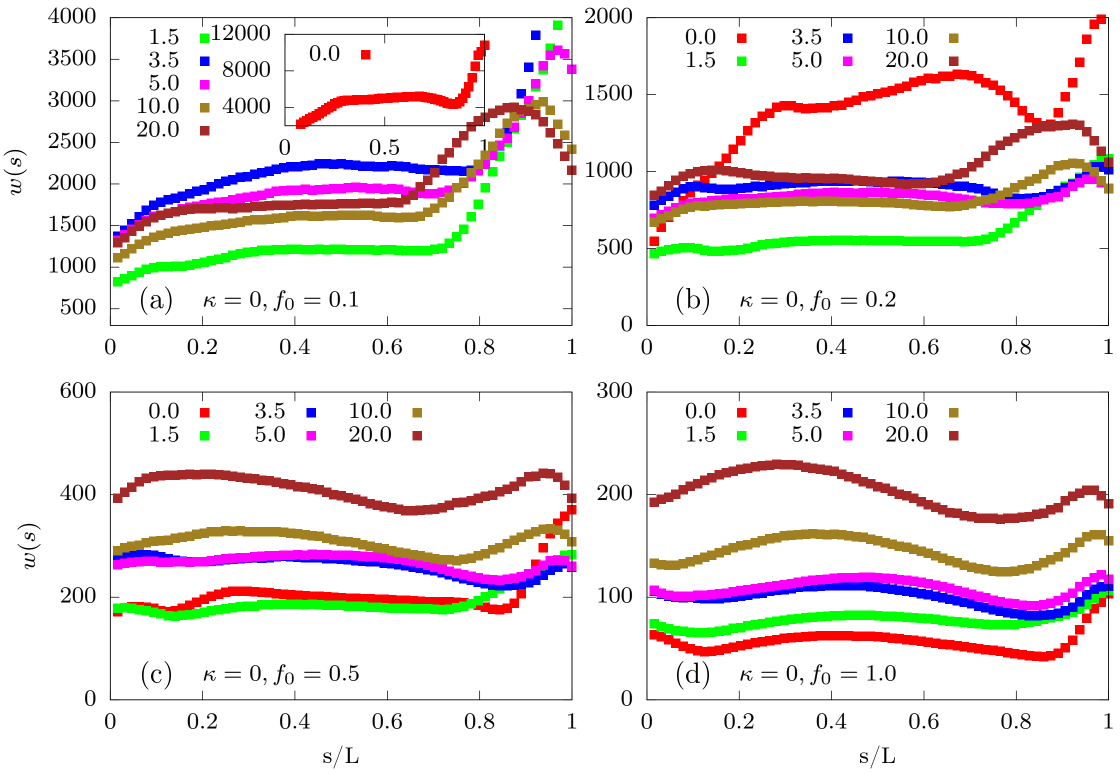

Figure 2.8: Waiting time distributions of a flexible polymer for different α. In (a) we show the variation for $f_0 = 0.1$. (Inset) The plot of $w(s)$ for a flat channel serves as a control. Increasing force values to (b) $f_0 = 0.2$, (c) $f_0 = 0.5$ and (d) $f_0 = 1.0$ leads to dramatic changes in the distribution.

values (Fig. 2.8(c-d)), $w(s)$ increases with α for all values of s. The net behaviour of $w(s)$ is consistent with the total translocation results for higher force value, (Inset of Fig. 2.6).

2.3.2 Semiflexible Polymer

We now discuss the translocation dynamics of a driven semiflexible polymer through the conical channel. We first look at the total translocation time as a function of the apex angle for different values of polymer rigidity and external driving force. In Fig. 2.9(a), we have plotted τ as function of α for a low external force value ($f_0 = 0.2$). The variation of the translocation time with apex angle still shows a non-monotonic feature as observed in the case of a flexible polymer. However, unlike that of the flexible polymer, rigid polymers do not show a sharp secondary peak in τ.

The total translocation time shows an initial decrease with increasing α indicating that as the apex angle increases, it becomes favorable for the polymer to exit the channel. This is a result of the enhanced entropic drive that we discussed for the flexible case. Beyond a critical value of α, τ starts to increase again. Note that the critical α shifts to larger values of apex angle and to higher values of τ as the rigidity of the polymer is increased (see Fig. 2.9(a)). This indicates that the translocation becomes more difficult with increasing stiffness of the polymer. This feature is consistent with earlier results of driven translocation of semiflexible polymers through extended channels [72, 77]. The largely monotonic increase in τ with increasing α is different from that of the flexible polymer. The effect of rigidity can be explained by looking at the multiple stages of the translocation process. At lower values of rigidity (say $\kappa = 2$, see Fig. 2.10(b)), τ_p plays a more significant role for most α values. This shows that the total translocation time is dictated by the filling of the pore as in the flexible case. However, with increasing rigidity (say $\kappa = 4$, see Fig. 2.10(c)), τ_e becomes the rate-limiting process. The increased influence of the escape time dynamics happens because the rigid polymer, which at this stage fills

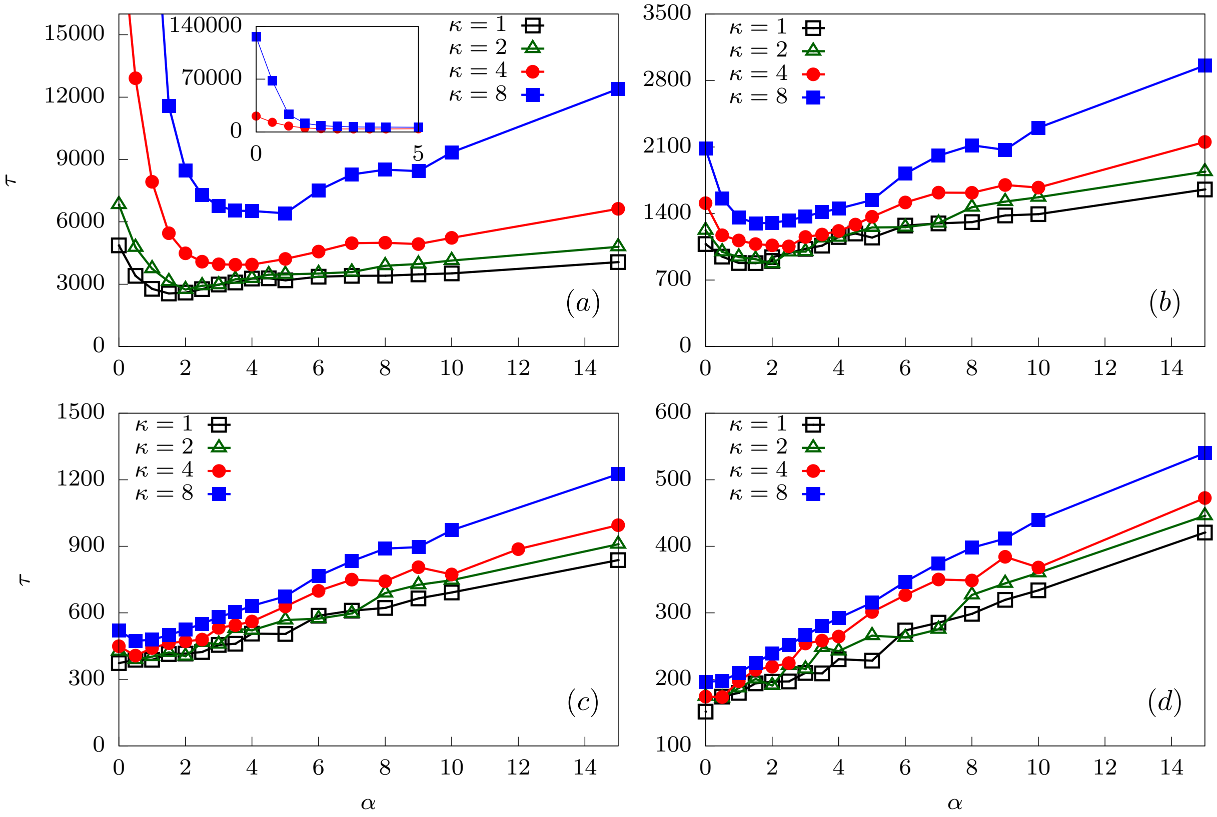

Figure 2.9: Total translocation time versus α for a semiflexible polymer for four different bending rigidities $\kappa = 1, 2, 4$ and 8. In (a) the variation is shown for $f_0 = 0.2$. (Inset) Magnified plot at lower α for $\kappa = 1.0$ and 2.0. As external force is increased : (b) $f_0 = 0.5$ (c) $f_0 = 1.0$ and (d) $f_0 = 2.0$, τ increases almost linearly with α.

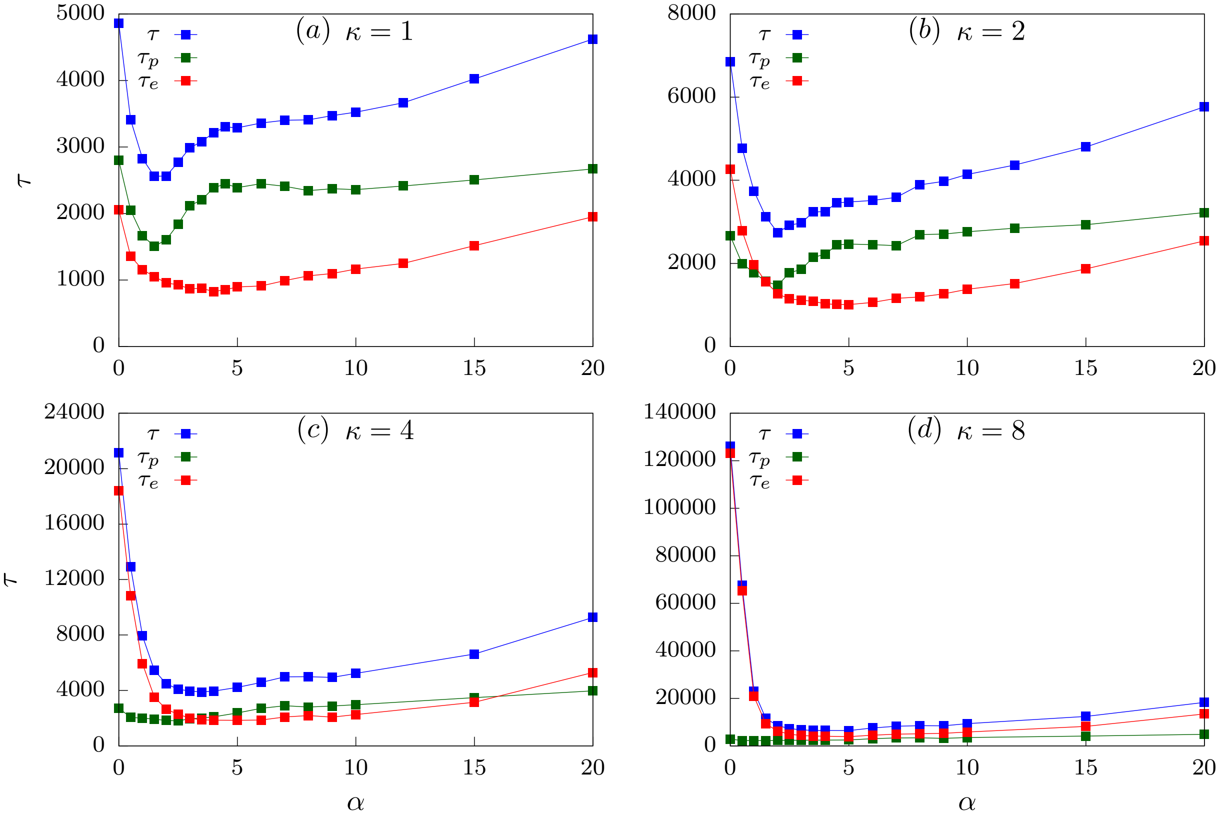

Figure 2.10: Plots of time components for semi-flexible polymer: passage time (τ_p) and escape time (τ_e) contributions to total translocation time (τ), s.t. $\tau = \tau_p + \tau_e$. Fig.(a-d) represents and compares the time components for increasing rigidity of polymer for external force, f_0 =0.2.

the channel, keeps deflecting between the two walls of the channel. This is a behavior typical of semiflexible polymers with increased rigidity [100]. The attractive interactions of the two walls keep the polymer pinned inside the channel for a long time, increasing the escape time τ_e. The monotonic increase of τ with α, as opposed to the appearance of a second peak for flexible polymers in the conical channel, can also be explained by the dominance of the escape time dynamics. The competition of the attractive interactions with the entropic drive, which results in the lowering of translocation time beyond α_2 for flexible polymers, is no longer the rate-limiting step. Rather, escape time dynamics which are dominated by the attractive interactions of the channel walls with the escaping beads influences the translocation process.

As the external force is increased, the non-monotonicity observed in the variation of τ with α starts decreasing (Fig. 2.9(b-d)). At very high forces, $f_0 \geq 1.0$ (see Fig. 2.9(d)), the total translocation time increases monotonically with the apex angle for all rigidities of the polymer. In Fig. 2.11 we construct phase plots for τ in the $\kappa - \alpha$ plane for various values of f_0. For small forces $f_0 = 0.2$, τ is maximum for stiffer chains and smaller apex angles (see Fig. 2.11(a), $\kappa > 3,\ 0^\circ \leq \alpha \leq 1^\circ$). For larger forces $f_0 = 1.0$, the phase plot shows a largely uniform increase in τ with increasing α for all κ values (see Fig. 2.11(b)). The maximum translocation times are observed when both κ and α are large. Separate phase plots for the entire range of α's and κ's are presented in Figs. 2.12(a-e) for lower force value ($f_0 = 0.2$), and for a higher force value ($f_0 = 1.0$) in Fig. 2.12(f).

We look at the waiting time distribution $w(s)$ of the semiflexible polymer as it moves from the *cis* to the *trans* side of the channel at low forces ($f_0 = 0.2$). In Fig. 2.13, we have plotted $w(s)$ for different values of the bending rigidity as the apex angle is varied. For low bending rigidity, $w(s)$ shows an increase with s initially and then a largely flat region at intermediate s, for all values of α (Fig. 2.13(a)). These results are similar to that for uniformly extended channels. Near the end, the attractive interactions prevent the exit of the polymer leading to larger waiting times. For stiffer polymers, the waiting times

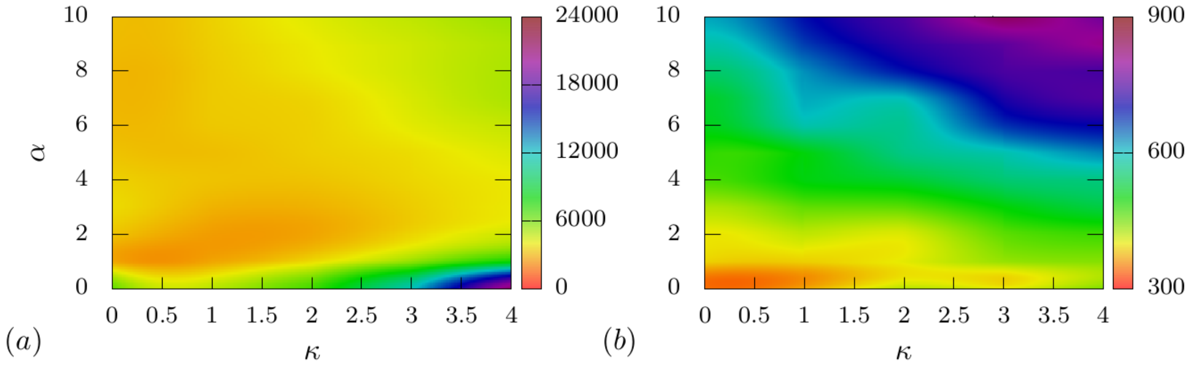

Figure 2.11: Phase plot of total translocation time τ in the $\kappa - \alpha$ plane for two forces (a) f_0=0.2. and (b) $f_0 = 1.0$.

for all monomers monotonically increase with α which is consistent with the behavior of total translocation time. As the polymer rigidity increases (Fig. 2.13(b)), the entropic gain in moving towards the *trans* end of the conical channel becomes lesser. The translocation dynamics of the end monomers are now dominated by attractive surface interactions. The end segment of the polymer keeps deflecting between the walls and is stuck in either wall for long periods, thereby increasing the waiting times.

2.4 Free Energy

It has been established that the relaxation time of a polyelectrolyte chain in equilibrium is much shorter than the translocation time for the typical range of chain lengths used and typical voltages applied in most experiments [60]. This implies that a polymer chain initially at equilibrium can be taken to be in quasi-equilibrium as it translocates across the nanochannel, especially for low external forces. In fact, the quasi-equilibrium approximation in such cases can be even extended to translocation of every segment of the polymer [60]. The quasi-equilibrium approximation obviously fails for high forces and longer lengths of the polymer. Using this approximation for low forces and chain lengths considered in our simulations, we construct the free energy landscape for the transloca-

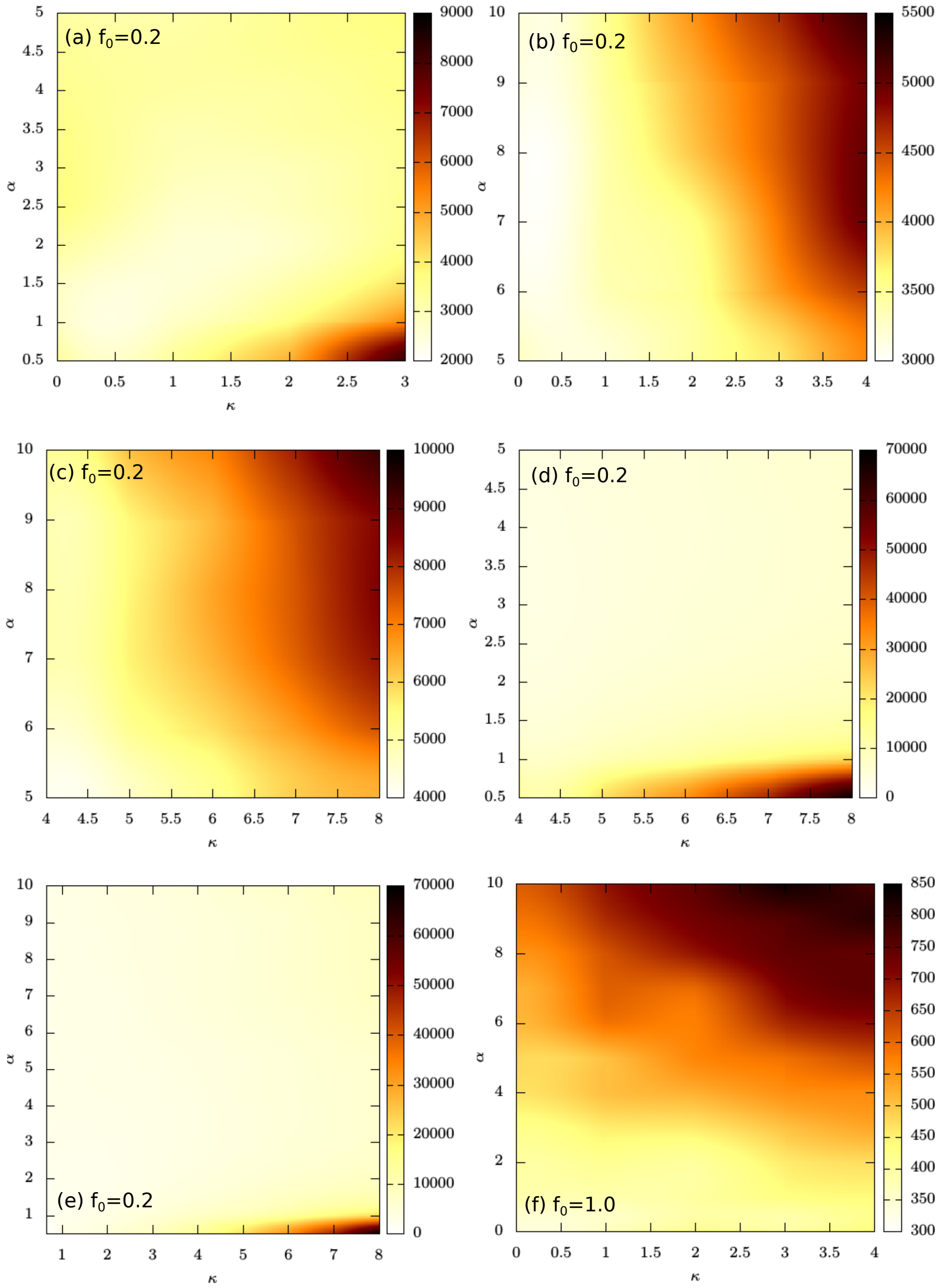

Figure 2.12: Phase plot displaying the dependence of τ on α's and κ's at lower force value, $f_0 = 0.2$, in (a-e) and for force 1.0 in (f) respectively. (a) The color variations clearly project two minima for the lower κ and lower α range. (b) It displays one minimum for higher α values. (c) Phase plot for rigid polymer at lower α values, τ monotonically decreases up to $\approx 5°$ and then increases after that(fig. (d)). Fig.(e) is the total projection of τ. Fig.(f) is phase plot for force value 1.0, τ is a monotonic function of α for all κ values.

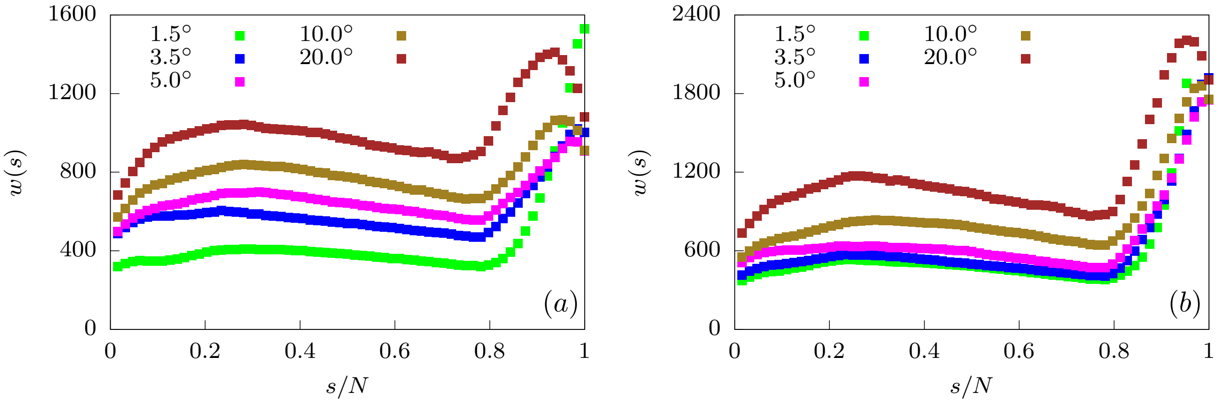

Figure 2.13: Waiting time distributions for various α at (a) $\kappa = 2$, and (b) $\kappa = 4$ for $f_0 = 0.2$. The distributions show distinct differences as the bending rigidity of the polymer is increased.

tion process to understand the translocation behavior obtained in our simulations.

There are several contributions to the free energy : (i) the entropic contribution coming from the confinement of the polymer segment inside the channel (ii) the entropic contribution due to the polymer segments outside the channel (ii) the energetic contribution due to surface interactions between the channel and the polymer and (iv) energetic contribution due to the external force.

The total free energy of the system in terms of the translocation coordinate can be written as

$$\mathscr{F}_t(s) = \mathscr{F}_e + \mathscr{F}_c + \mathscr{F}_{pp} \tag{2.7}$$

where $\mathscr{F}_c$ is the confinement-free energy, $\mathscr{F}_e$ is the entropic component due to polymer segments outside the channel, and $\mathscr{F}_{pp}$ is the free energy contribution due to the channel polymer interactions.

To construct $\mathscr{F}_e$ for a semiflexible polymer segment inside a conical channel, we use the approach in [4]. The contribution to the free-energy from a polymer of size R confined in an area A of the cone in two-dimensions is given as $\mathscr{F}_c \sim k_B T \left(\frac{R^2}{A}\right)^{\frac{1}{2\nu-1}}$ [101]. If N_p denotes the number of polymer beads confined inside the channel, then $R \sim \sigma N_p^{\nu}$, where

$\nu = 3/4$ is the Flory exponent in two-dimensions. A is dependent on the degree of confinement. If L denotes the length of the region inside the channel along the $x-$direction that holds the confined polymer and a the length which is empty, then A is given as

$$A = \frac{1}{4\tan\alpha}\left[(D_0 + 2(a+L)\tan\alpha)^2 - (D_0 + 2a\tan\alpha)^2\right]. \tag{2.8}$$

In the case of rigid polymers, the analysis can be extended by replacing the number of monomers N_p with the number of Kuhn segments $\tilde{N_p} \approx N_p\sigma/l_K$ where $l_K = 2l_p$ is the Kuhn length. l_p is the persistence length of the polymer. In two-dimensions, the bending rigidity is related to the persistence length as $\kappa/k_BT = l_p/2$. We would however like to express $\mathscr{F}_e$ in terms of the translocation coordinate s. Therefore, we extract the number of beads that are inside the channel from the simulations for a fixed translocation coordinate. As is expected, there would be several configurations of the polymer (with different values of N_p) inside the channel for a given s. The confinement-free energies of all such configurations are averaged to give $\mathscr{F}_c(s)$.

The free energy contribution from the polymer segments outside the channel is given as[29]:

$$\mathscr{F}_e = \begin{cases} \gamma' \log N_c & N_c > 1 \text{ and } N_t = 0 \\ \gamma' \log N_c + \gamma' \log N_t & N_c > 1 \text{ and } N_t > 1 \\ \gamma' \log N_t & N_c = 0 \text{ and } N_t > 1 \end{cases}$$

where N_c is the number of beads on the *cis*-side of the channel and N_T is the number of beads on the *trans*-side of the channel. Note that N_c and N_T are functions of the translocation coordinate s and are obtained from the simulation similar to the confinement free energy for every value of s. Further, $N_c + N_p + N_T = N$ at all times.

The free energy contribution from the surface interaction $\mathscr{F}_{pp}$ is obtained by summing over the LJ potential felt by each polymer bead when they are inside the channel. For a given translocation coordinate, we identify the number of beads inside the channel and calculate the total potential felt by the beads. As we mentioned before, for a given s, there would be multiple configurations of the polymer inside the channel (corresponding to the time steps for which $s = 1, 2, ...$). All such contributions are appropriately accounted for and the averaged free energy contribution $\mathscr{F}_{pp}$ due to surface interactions is evaluated numerically as the translocation coordinate changes.

In Fig. 2.14(a), we plot the total free energy contributions which are entropic in origin for a flexible polymer, arising due to the confined segments of the polymer and the segments outside the channel. The free energy contribution due to channel-polymer interactions is plotted in Fig. 2.14(b). The entropic contribution exhibits a free energy barrier for an intermediate s for all values of the channel angle α. This indicates that entropically it is more difficult for the polymer to enter the channel from the *cis*-side. However, the energetic contribution coming from the attractive LJ potential dominates the initial stages and the polymer is sucked into the channel. At intermediate s, the competition between the two leads to the comparatively larger waiting times observed in Fig. 2.8(b). As α is increased, we observe a clear non-monotonic behavior in the entropic part of the free energy. The free energy barrier increases as we go from $\alpha = 1.0^\circ$ to $\alpha = 2.7^\circ$ and decreases as α is increased further. This indicates that translocation would be more difficult from $\alpha = 1.0^\circ$ to $\alpha = 2.7^\circ$ and favorable as the channel angle increases. This is consistent with the behavior observed in the translocation time as a function of the channel angle, where for $f_0 = 0.1$, τ shows a peak at $\alpha \approx 2.7^\circ$ and decreases with increasing α. The energetic contribution $\mathscr{F}_{pp}$ does not show non-monotonic behavior at these values of α, with significant overlap in the free energy profiles (see Fig. 2.14(b)). As α is increased, $\mathscr{F}_{pp}$ becomes shallower indicating easier translocation and therefore decreasing τ.

In Fig. 2.14(c), we plot the total free energy contributions which are entropic in origin for a semiflexible polymer for various channel angles. Similar to the flexible polymer, the entropic contribution indicates a barrier at intermediate s. However, unlike the flexible

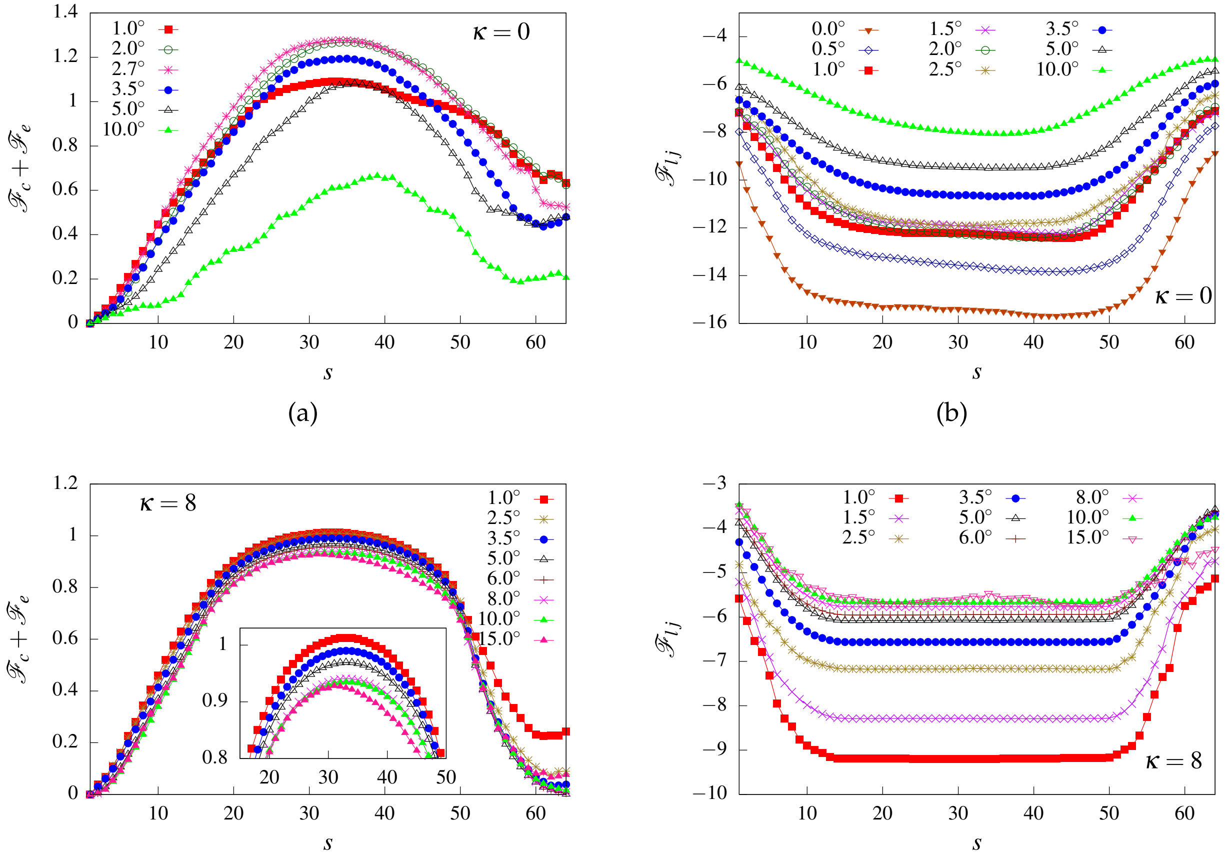

(a) (b) (c) (d)

Figure 2.14: (a) Entropic part of the free energy ($\mathscr{F}_c + \mathscr{F}_e$) for a flexible polymer as a function of the translocation coordinate s for different α values showing non-monotonic behavior. (b) Energetic contribution to free energy for a flexible polymer from surface interactions ($\mathscr{F}_{pp}$) as a function of translocation coordinate s for various α values. (c) Entropic part of the free energy ($\mathscr{F}_c + \mathscr{F}_e$) for a semiflexible polymer ($\kappa = 8$) as a function of the translocation coordinate s for different α values showing largely monotonic behavior. (Inset) The barrier height decreases monotonically with α. (d) Energetic contribution to free energy for the semiflexible polymer from surface interactions ($\mathscr{F}_{pp}$) as a function of translocation coordinate s for various α values.

polymer, this barrier reduces monotonically with increasing α. The corresponding free energy contribution due to channel-polymer interactions also becomes shallower monotonically as α is increased (see Fig. 2.14(d)). Therefore, for a semiflexible polymer, translocation becomes easier with increasing α. If we compare our analytical predictions with that of the simulation results in Fig. 2.9(a) for $\kappa = 8$, we find that translocation time indeed decreases with increasing α up to $\alpha = 6^\circ$ consistent with our predictions. However, for larger channel angles, the translocation time increases. This behavior is very different from the predictions from the free energy calculations.

To understand this behavior, it is crucial to look at the potential landscape inside the channel. At large channel angles, the strength of the potential due to the channel walls becomes negligible for large regions inside the channel. Even during the entry of the polymer from the cis side of the channel, the attractive potential becomes much weaker in the region close to the cis side for large angles. This hampers the pulling ability of the channel resulting in larger waiting times of even the initial beads of the polymer. As the polymer is pulled in, the segments of the stiff polymer inside the channel keeps getting deflected from one wall to the other. The potential near the center of the channel is negligible as is the external force and the polymer segments stay attached to either wall for a considerable time. This leads to increasing translocation times at higher channel angles. For smaller channel angles, the average positions of the polymer segments are much closer to the middle of the channel as both walls try to pull on them. With external force much stronger near the center, the polymer is pulled out faster. Note that for flexible polymers, the possibility of more conformations of the polymer as compared to stiffer chains at larger angles ensures that the situation is much more homogeneous and we do not observe much change at larger channel angles.

2.5 Conclusions

The translocation of polymers through asymmetric-shaped channels has sparked a lot of interest due to its significant advantages in bio-sensing applications. Buoyed by experimental studies using conical nanochannels, we have studied the translocation dynamics of a semiflexible polymer through such a channel under the influence of a spatially varying external drive and attractive surface interactions. The waiting time distribution shows rich features arising due to the polymer stiffness, surface interactions, and nature of the external drive. We attempt to understand some of these features using a free energy argument based on a quasi-equilibrium approximation which is applicable for smaller polymer lengths and low forces. The theory captures some of the non-monotonic features of the translocation dynamics. At higher stiffness and larger channel angles, the variable potential landscape arising from the surface interactions becomes dominant. This variability needs to be accounted for in order to provide a more accurate description of the dynamics.

In our analysis, we have ignored the role of electrostatic interactions [102]. The translocation rate depends on the charge density of the polymer and the density of the bulk concentration of the solvent in a confined pore. Low polymer charge density and low solvent concentration lead to lower translocation rates, while the translocation rate increases sharply for high polymer charge density at high solvent concentration. It will be interesting to ask how these rates could be modified when considering asymmetric channels like the one considered in this study.

Recent experiments have revealed that driven polymer translocation through synthetic nanopores is a two-stage process with translocation initially slowing with time before accelerating close to the end of the process [94]. In our detailed simulations, we show however that the translocation dynamics are strongly dependent on the stiffness of the polymer and surface interactions. Attractive surface interactions can considerably slow down the translocation process near the ends while increasing the angle of the conical pore may facilitate the process. We have considered one possible conical structure where the polymer enters the pore from the constricted side of the channel. In the next chapter, we will explore the detailed dynamics of the polymer as it enters from the wider end of the channel and see that it gives rise to significantly different dynamics due to the asymmetry of the channel.

Chapter 3

Reverse Translocation process of semiflexible polymer through conical channels

3.1 INTRODUCTION

In Chap. 2, we have studied the translocation of a semiflexible polymer that enters the pore from the narrower end and exits from the wider end of the conical channel. We refer this as "Forward translocation". In this chapter, we reverse the ends of the conical pore. Now the polymer enters from the wider end and exits from the narrower end. To distinguish this from the previous case, we call this as "Reverse translocation" process[6]. It has already been reported that the direction of transport through symmetric channels (e.g. a flat channel) does not effect the translocation properties[86]. But, as soon as the symmetry of the channel geometry breaks, which is the case for a conical pore, the translocation properties become direction dependent for the same simulation parameters [70, 94]. The nature of the force depends on the asymmetric design of the conical channels [4].

Similar to Chap. 2, we have considered the effect of pore asymmetry on the nature of the driving force by choosing a specific form of force (f_x) which depends on channel variables (α, x). We study the system using Langevin dynamics simulations. We concentrate in the weak force regime so that the pore effect on the polymer does not get washed out. Due to the asymmetry of the conical pore and the position dependent external force, each bead experiences a different velocity which results in the formation of different segment structures inside the pore. We have compared the translocation properties for both the ″forward″ and the ″reverse″ translocation processes and found that our simulation results agree well with the experimental studies [70, 94].

The chapter is organized as follows: In Sec. 3.2, we define our model and the simulation set-up. In Sec. 3.3, we discuss the results of the translocation dynamics in terms of the total translocation time and waiting time distributions. In Sec. 3.4, we conclude the chapter by providing the limiting cases for the directional dependent translocation processes.

3.2 MODEL AND METHOD

We simulate our model in 2-dimensions. We model a linear homopolymer of length N by a coarse grained bead-spring model. The consecutive beads of the chain are connected to each other via harmonic potential,

$$U_{\text{bond}} = \frac{1}{2}K(r - r_0)^2, \tag{3.1}$$

where K is the spring constant, and r_0 is the equilibrium separation between the consecutive monomers. The non-bonded beads interact via repulsive Lennard-Jones (LJ) potential, $U_{\text{bead}}(r)$.

$$U_{\text{bead}}(r) = \begin{cases} 4\epsilon\left[\left(\frac{\sigma}{r}\right)^{12} - \left(\frac{\sigma}{r}\right)^{6}\right] + \epsilon, & r < r_c \\ 0, & r \geq r_c, \end{cases} \tag{3.2}$$

where ϵ is the depth of the regular LJ potential. The truncated and shifted LJ potential has a cut-off at $r_c = 2^{\frac{1}{6}}\sigma$, where σ is the diameter of the bead. The static conical channel is constructed from $L_p = 16$ There exists a long range attractive LJ interaction between the polymer beads and the channel beads:

$$U_{LJ}(r) = \begin{cases} 4\epsilon\left[\left(\frac{\sigma}{r}\right)^{12} - \left(\frac{\sigma}{r}\right)^{6}\right], & r \leq R_c \\ 0, & \text{otherwise} \end{cases} \tag{3.3}$$

where $R_c = 2.5\sigma$ is the cut-off distance. The motion of polymer beads are governed by the Langevin dynamics (LD) equation:

$$m\ddot{\vec{r_i}} = -\eta\dot{\vec{r_i}} - \nabla \sum (U_{LJ} + U_{bond}) + \vec{f_{ext}} + \zeta, \tag{3.4}$$

where m and r_i are, respectively, the mass and the position of ith bead of the polymer, η is the friction coefficient of the fluid, and ζ is an uncorrelated random force which follows the fluctuation-dissipation relation, $\langle \zeta_i(t)\zeta_j(t')\rangle = 2K_BT\eta\delta_{ij}\delta(t-t')$. The polymer experiences a force-gradient, f_x, along the x-direction of the channel:

$$f_x = \frac{f_0 d}{(d + 2(16 * \tan\alpha)) - (d + 2(x * \tan\alpha))}, \tag{3.5}$$

where x varies from 0 (wider entrance) to 16 (narrow exit), f_0 is the magnitude of the force at the narrow opening of the conical channel, d is the diameter of the narrow end of the channel and α is the cone apex angle. In Fig. 3.1, we have plotted the variation of f_x along the cone x-axis as a function of α. The force f_x increases towards the narrower end of conical pore according to Eq.(3.5).

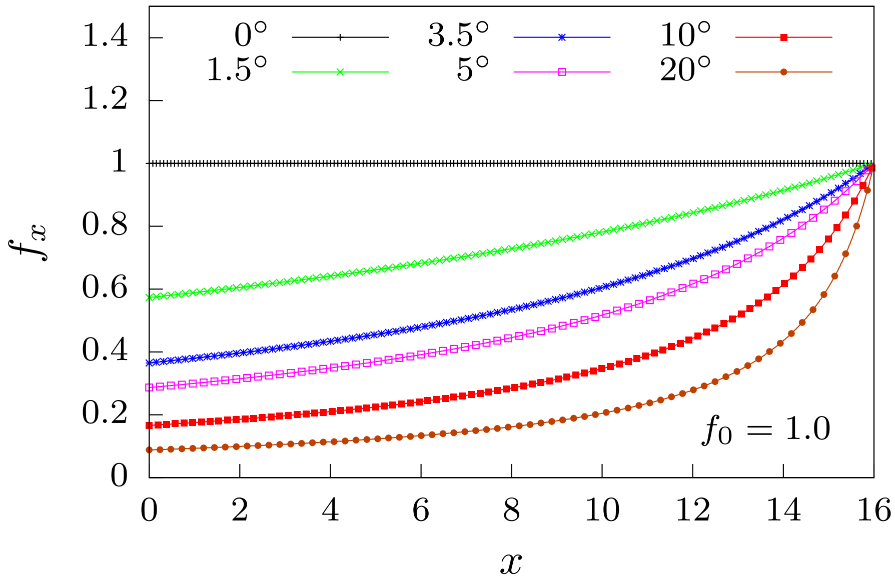

Figure 3.1: Variation of the magnitude of external force, f_x, along the conical channel for various cone angles (α). For any non-zero α value, f_x increases towards the narrow exit of the pore.

We set all the simulation parameters in reduced LJ units: ϵ (energy), σ (length), and m (mass). The dimensionless parameter k_BT, η are set to be equal to 1. The strength of the force at the narrow end is taken to be $f_0 = 0.2$ or stated otherwise. This value is found to be apt to capture the transport properties without washing out the role of the pore effect. Due to the wide opening at the entrance of the pore, there is no successful translocation in the absence of external force.

Before the translocation starts, the system needs to be equilibrated. We anchor the first bead at the axis of the pore entrance and allow the polymer beads to move according to Eq. (3.4). Since the pore entrance is wider, multiple beads can enter the pore while equilibrating. We therefore put additional beads at the pore entrance to prevent this to happen (see yellow beads in Fig. 3.2). Once the polymer attains an equilibrium configuration, the yellow beads are removed before we start monitoring the translocation process.

In our study we consider averaging over only those samples for which the process

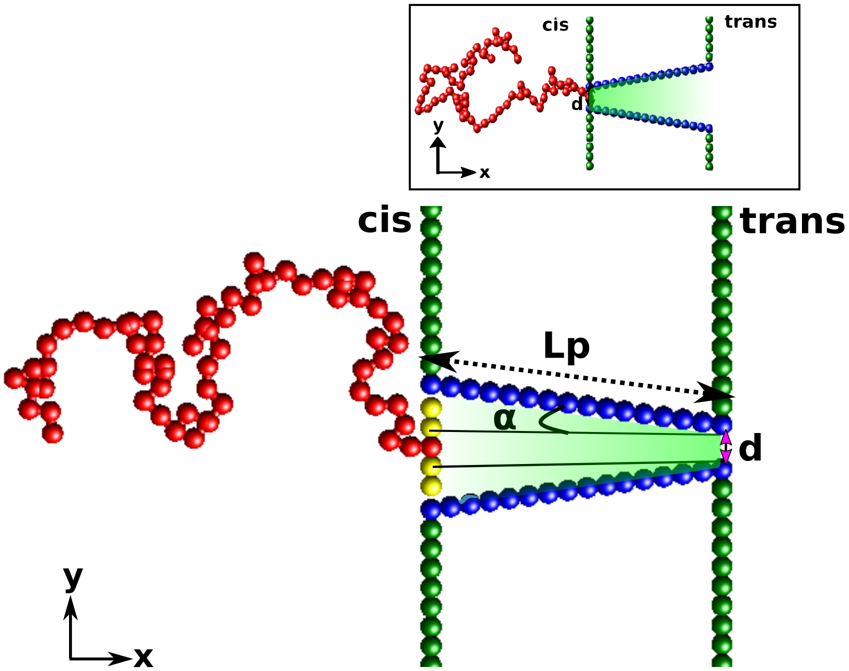

Figure 3.2: Schematic of an equilibrated flexible polymer sample for reverse translocation. The first bead of the chain is fixed at the entry of the conical pore, a few additional beads along with the first bead of the polymer are present at the pore entrance to restrict the entry of any polymer segments during the equilibration process. Inset shows the set-up for the forward translocation case, where the translocation takes place from the narrower end to the wider end of the conical channel. The color in the conical pores, represents the force gradient, f_x.

begins with the entry of the first bead of the polymer chain, otherwise, the sample is discarded. The total translocation time, τ, is the time lapse between the entrance of the first bead of the polymer chain into the channel from the *cis* side and the exit of the last bead from the narrow end (i.e., the *trans* side) of the conical channel. For each set of simulation parameters, the translocation time (τ) is averaged over 1500-2000 independent samples.

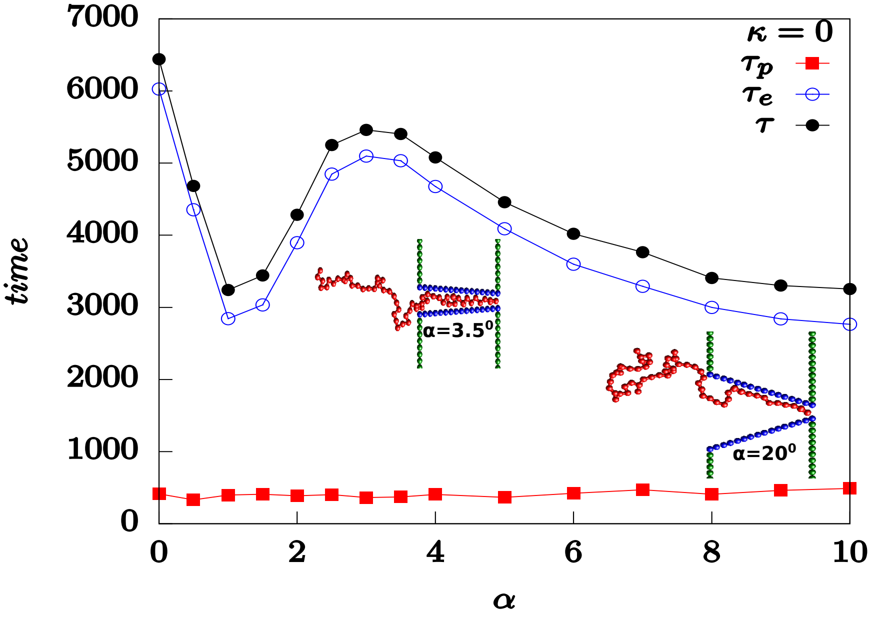

Figure 3.3: Plot of total time translocation (τ) for flexible polymer($\kappa = 0$) of length 64 beads along with the two time components: passage time (τ_p) and escape time (τ_e), s.t. $\tau = \tau_p + \tau_e$. Two simulation snapsorts are embedded in the plot to provide a visual scenario of the translocation process at lower and higher apex angle.

3.3 Results and Discussions

To see the effect of different pore geometries on the translocation process, we measure the average total translocation time (τ), one of the most fundamental properties of translocation dynamics. We also measure the residence time $w(s)$ of each monomer s, defined as the average time spent by monomer s inside the channel during the translocation process. This is another important quantity that quantifies the effect of the pore geometry.

3.3.1 Total Translocation Time

We first start with the case of a flexible polymer chain (i.e., $\kappa = 0$). For a flexible polymer, we find that the total translocation time (τ) shows a non-monotonic behavior when it is plotted as a function of cone apex angle α (see Fig. 3.3). As done in Chap. 2, the total time, τ, can be divided into two times, the passage time (τ_p) and the escape time (τ_e). The passage time is defined as the time taken for the first bead to reach the narrow exit such that the pore is completely filled, while the time taken from the passage phase to the exit of last bead from the narrow end is defined as escape time. Therefore, the total translocation time, $\tau = \tau_p + \tau_e$. The pattern of τ vs. α is decided by the time components of the major contributions. In the case of a flexible polymer, we see from Fig. 3.3) that major contribution to the total translocation time τ, which is shown by filled squares, is from the escape time τ_e (empty circles). As evident from Fig. 3.1, the magnitude of the external force f_x increases towards the narrower side of the pore for all αs. Therefore, the filling of the pore becomes much easier and hence the contribution of τ_p is much lesser in comparison to the escape time τ_e.

In Fig. 3.4(a), we have re-plotted the total translocation time τ as a function of α for the "reverse" translocation case for a flexible polymer. In the same figure, we have also plotted the results for the "forward" case (see Fig. 2.6) from Chap. 2 to make out differences between the forward and reverse translocation processes. From the figure, we can clearly see that for both the forward and reverse processes, the τ vs α curves show non-monotonic behavior. But, there are striking differences in the intermediate cone apex angles ($0.5° < \alpha < 9°$). For example, we see that the translocation time for the reverse case is much larger than the translocation time for the forward case in this region. Although, the complexity of the problem makes it extremely difficult to pinpoint the exact dynamics for the different behaviors of the forward and the reverse translocation processes, but, we can still give some reasoning to understand the qualitative differences.As seen in Fig. 3.4(a), for $\alpha \approx 3°$, we have $\tau_{reverse} \approx 1.5\tau_{forward}$. This observation is in agreement with the results of ping-pong experiment performed with a fabricated conical pore with apex angles in the range ($2.6° - 3.6°$) [7]. In this experiment, it was found that the translocation time in the reverse flow (i.e., from the wider to the narrower opening of the conical pore), is always larger than the translocation time in the forward flow. From the

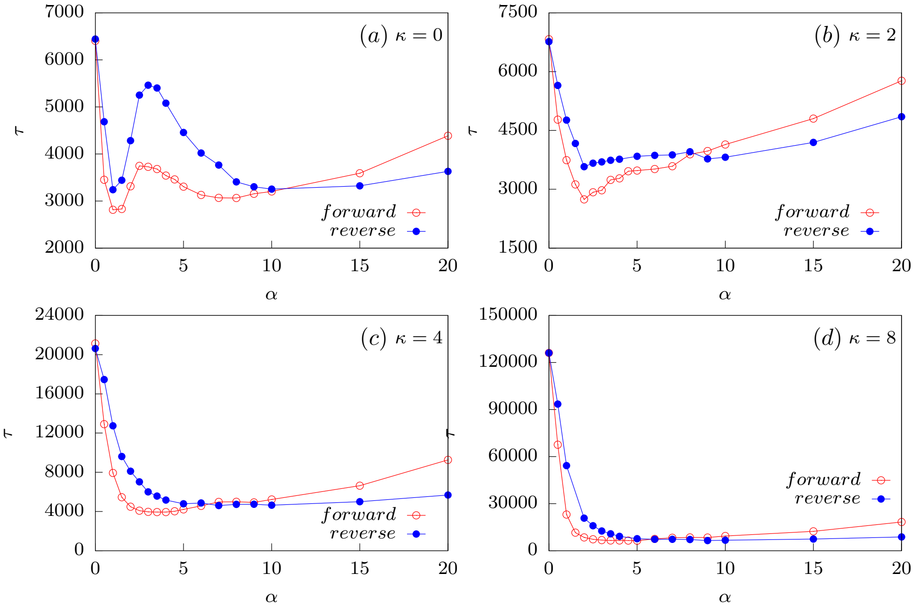

Figure 3.4: Comparison of forward (red) and reverse (blue) total translocation time (τ) vs. cone apex angle (α) at lower force value, $f_0 = 0.2$. Fig.(a-d) is plotted for $\kappa's$ =0, 2, 4 and 8 respectively.

geometry of the conical channel, we see that the wider y-extent of the cone for $\alpha \approx 3.5^\circ$ is apt enough to fit two beads simultaneously in a way that they are always in a close proximity to the attractive pore walls. The geometric construction and the entry of the flexible polymer from the wider end have the potential to form a block-like situation, where the polymer segment spends a lot of time inside the filled pore, either in a hairpin or in a coiled conformation (see an embedded snapshot in Fig. 3.3), and hence costs a lot of time to get out of the pore.

On introducing the rigidity in the translocating polymer, the situation becomes quite different. In Fig. 3.4(b-d), we have plotted the average translocation time for a semiflexible polymer for bending rigidity $\kappa = 2$, 4 and 8 as a function of pore apex angle α. In these figures, we can clearly see that the bending energy associated with polymer segments can overcome the fluctuations inside the pore, which results in the disappearance of differences in the translocation time between the forward and the reverse cases. From

Rigidity (κ)	Crossover angle (α_c)	Crossover time $\tau_c(\approx)$)
0	10°	3.2×10^3
2	9°	4.0×10^3
4	8°	4.5×10^3
8	6°	7.5×10^3
16	5°	1.4×10^4
32	4.3°	3.5×10^4
64	3.5°	10^5

Table 3.1: Values for the crossover angle (α_c) in the τ measure for the two processes: forward translocation and reverse translocation.With increasing rigidity (κ) of polymer, α_c shifts to lower alphas (col.2). Cross overtime (τ_c), on the other hand, increases with increase in rigidity of the polymer chain.

Fig. 3.4, it is evident that for lower values of α, the average translocation time for the reverse case is larger than that for the forward case (i.e., $\tau_{reverse} > \tau_{forward}$) for both the flexible and the semiflexible polymer. However, for larger values of α, the translocation time for the forward case is more than that for the reverse case. We will call the angle α at which this crossover takes place as crossover α and represent it by α_c. The translocation time at α_c will be represented by τ_c. In Table. 3.1, we have listed approximate values of α_c and τ_c for different bending rigidities of the polymer. With an increase in the polymer rigidity, we observe that α_c shifts towards a lower value. Therefore, one would expect that for a rod-like polymer chain (i.e., $\kappa \to \infty$), the channel will behave like a slit and the translocation process will be independent of the direction of the channel and the τ vs. α curves for both the forward and the reverse cases will overlap with each other.

In Fig. 3.5, we have plotted the phase diagram for the reverse translocation case. The explicit non monotonic feature in τ at lower cone apex angles α and for lower κ is clearly seen in Fig. 3.5(a-b). For higher values of κ, the translocation time τ decreases with α for lower α values (see Fig. 3.5(c)), but increases for higher values of the cone apex angles α (see Fig. 3.5(d)).

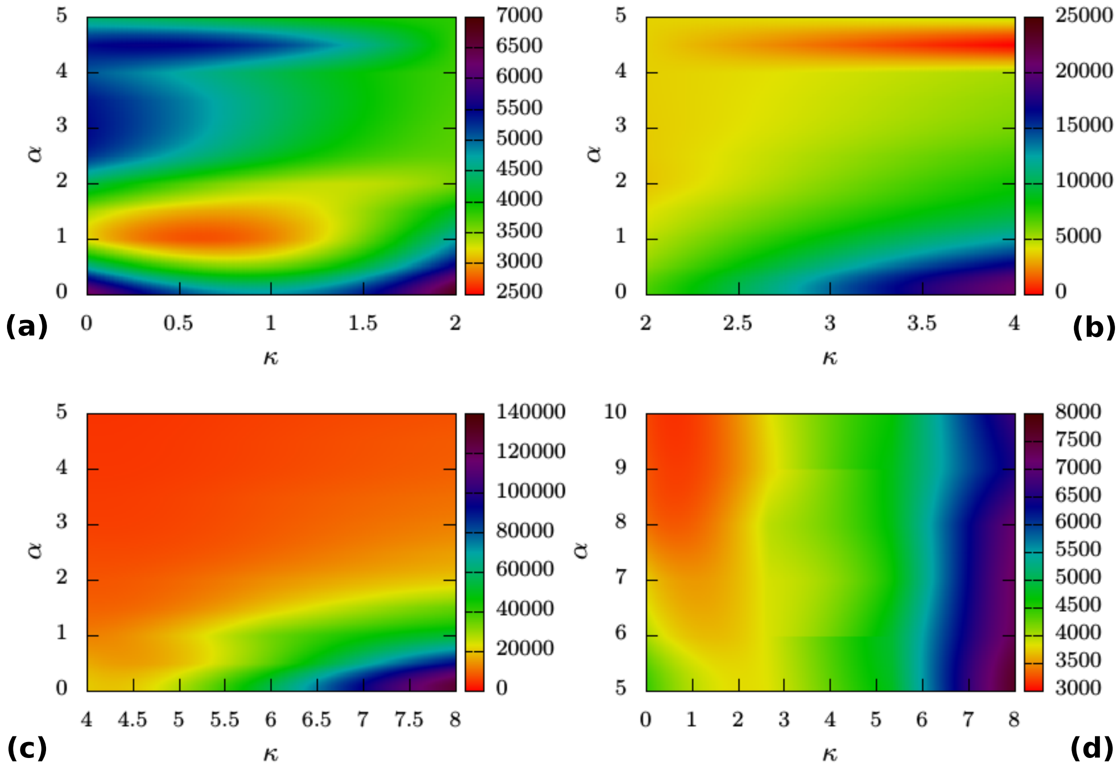

Figure 3.5: Phase plot of τ for lower force ($f_0 = 0.2$). The three subplots (a-c) is for lower alpha values ($\alpha = [0 : 5]$) for different ranges of κ: (a) for $\kappa = [0 : 2]$, (b) for $\kappa = [2 : 4]$ and (c) for $\kappa = [4 : 8]$. Subplot (d) is for higher values of apex angle ($\alpha = [5 : 10]$) for the entire range of κ values i.e, for [0:8].

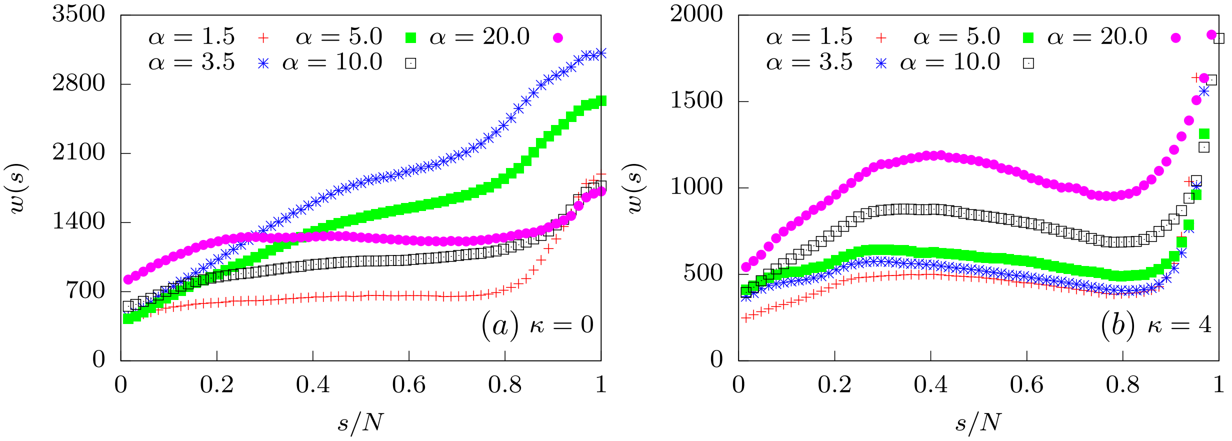

Figure 3.6: Waiting time distributions, $w(s)$ vs. scaled translocation co-ordinate s/N $(N = 64)$, for κ =0, and 4 respectively in Fig. (a), and (b) for $F_0 = 0.2$. The plots are for few intermediate apex angles to show the transition of $w(s)$ behaviour.

3.3.2 Waiting Time Distributions

The effect of pore polymer interactions on the translocation process can be studied from the waiting time distributions, $w(s)$. In Figs. 3.6(a) and 3.6(b), we have plotted $w(s)$, for various cone apex angles α, as a function of scaled translocation coordinate s/N for a polymer with bending rigidities $\kappa = 0$, and $\kappa = 4$, respectively. The length of the polymer used is $N = 64$ and the strength of the driving force at the narrow end is $f_0 = 0.2$. The geometry of the conical pore allows single-file exit from the narrow end and this constraint can be used to track the overall escape process. Unlike the exit process, multiple beads can enter the pore simultaneously. This allows coiling and hairpin formation of the polymer segments near the entry which can block the pore and hence stalls the translocation process. The extent of stalling depends on the pore apex angle α and the rigidity κ of the polymer. We have seen in Fig. 3.4(a) (filled circles) that in the reverse translocation case, the total translocation time for a flexible polymer in the range of cone apex angle α between 3° and 5° (i.e., $3^\circ < \alpha < 5^\circ$) varies a lot from the rest α values. This difference is also reflected in the waiting time distributions. From Fig. 3.6(a), we see that $w(s)$ plots for apex angles $\alpha = 3.5^\circ$(stars) and 5°(filled squares), exhibit very different behaviour than the rest of α values. For $\alpha = 3.5^\circ$ and 5°, there is no retraction or the plateau region in $w(s)$, and it rises sharply as a function of scaled translocation coordinate (s/N). However, for other values of α, the waiting time distributions $w(s)$ show retraction features.

On introducing the bending rigidity in the translocating polymer, we observe that unlike the flexible case, the waiting time distribution curves $w(s)$ for all cone apex angles α show tail retraction features (see Fig. 3.6(b) for $\kappa = 4$). An interesting observation from Fig. 3.6 is that irrespective of the values of α and κ, the $w(s)$ curve for the end monomers has a positive slope (i.e., $dw(s)/ds > 0$ as $s/N \to 1$). This reflects the fact that in the "reverse translocation" process, the escape of the polymer is single-file (i.e., one bead can come out from the pore) and is difficult. In contrast, for the "forward translocation" case, the $w(s)$ curve has a negative slope as $s/N \to 1$ (see Fig. 2.8) because in this case, the polymer can make coiled conformations near the wider exit and multiple beads can escape the channel easily.

3.3.3 Effect of Polymer length:

So far, we studied the translocation process for a polymer chain of fixed length having $N = 64$ beads. We have seen that for the "reverse translocation" case, $w(s)$ shows distinct features in the range $\alpha \in [3^\circ, 5^\circ]$ for a flexible polymer. In this range, $w(s)$ increases monotonically as a function of s/N. To see if this feature persists for the translocation of longer polymer chains, we study the behavior of waiting time distributions as a function of chain length N.

In Fig. 3.7, we have plotted $w(s)$ for a flexible polymer chain of different lengths N = 32, 64, 96, 128 and 256 for three different pore apex angles $\alpha = 1.5^\circ$, 3.5°, and 10° shown in Figs. 3.7(a), 3.7(b), and 3.7(c), respectively. These figures are for the "reverse translocation" process and these angles are representative for lower, intermediate, and higher cone apex angles. The effect of chain length on the translocation process can be

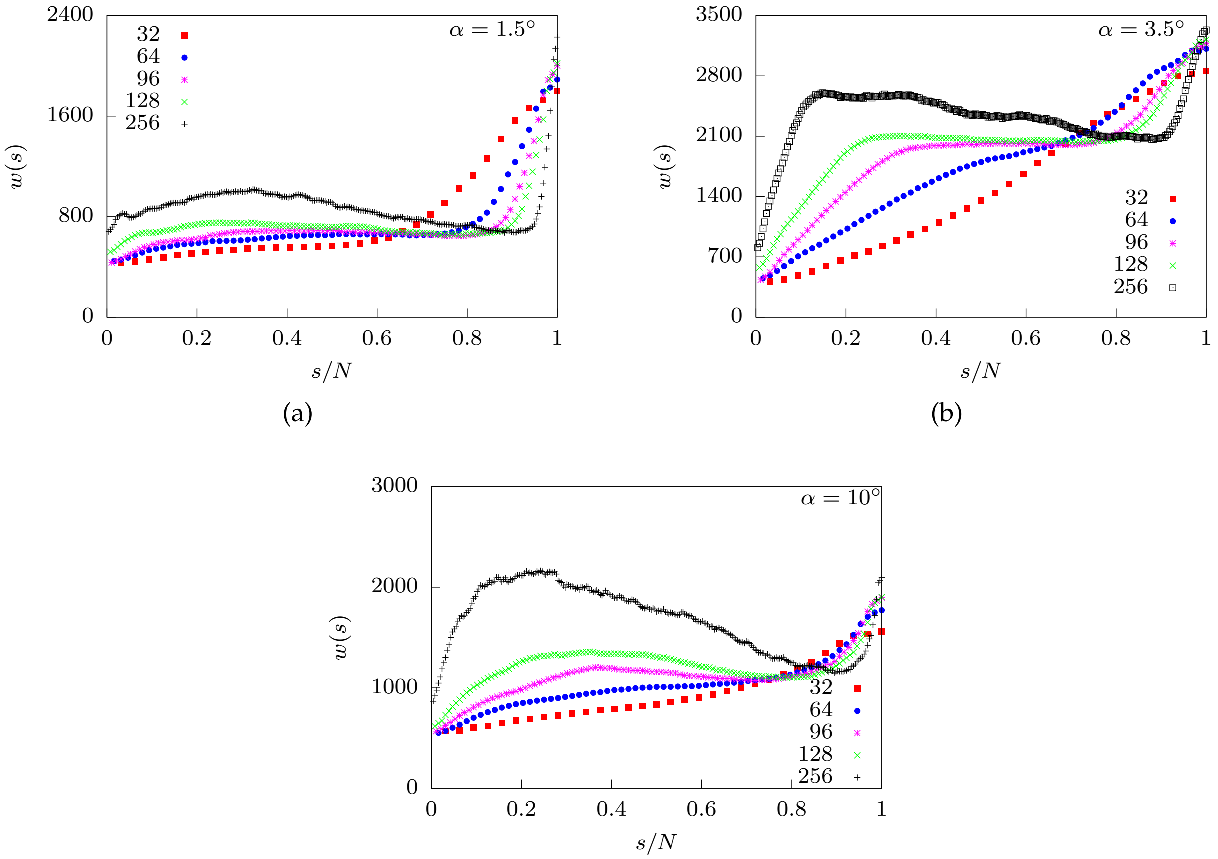

(a)

(b)

(c)

Figure 3.7: Residence time plot for flexible polymer with different polymer lengths (L =32, 64, 96, 128 and 256) for conical pore $\alpha = 1.5°$, $3.5°$ and $10°$ in Figures (a), (b) and (c) respectively, for the force value, $f_0 = 0.2$.

witnessed with the appearance of a plateau and tail retraction patterns in $w(s)$ with the increase in the polymer lengths. As expected, the total translocation time τ increases with the increase in the length of a translocating polymer for all cone apex angles α. However, the waiting time distributions for different chain lengths depend on the cone apex angles.

For $\alpha = 3.5°$, $w(s)$ increases monotonically for subsequent transition coordinates for smaller polymer lengths, i.e, for N = 32 and 64 (Fig. 3.7(b)). With the increase in chain length, e.g. for $N = 96$, a plateau starts emerging at approximately $s/N \approx 0.3$ and persists till $s/N \approx 0.75$. This plateau region is due to the force balance experienced by the polymer segments inside the pore. However, for a longer polymer chain (e.g. N =256 (squares)), the entropy from the polymer segment on the trans-side drives the polymer faster and the plateau region of $w(s)$ converts slowly to a tail-retraction part. In addition to this, for a longer flexible polymer chain, the extent of tail propagation along the backbone of the polymer segments reduces. Hence, the emergence of tail retraction keeps shifting to a lower s/N value with the increase in chain lengths.

We have also plotted the residence time as a function of s/N for various polymer lengths for lower (i.e., $1.5°$) and higher (i.e., $10°$) cone apex angles in Fig. 3.7(a) and Fig. 3.7(c), respectively. For these α values, we see that, for a short polymer chains (i.e., for $N = 32$ and 64), $w(s)$ is an increasing function of s/N. But, the rise in $w(s)$ is much slower in comparison to the rise for apex angle $3.5°$. With the increase in polymer chain lengths, $w(s)$ exhibits a tail retraction behavior, which is more enhanced in comparison to the tail retraction part for $\alpha = 3.5°$.

Next, we compare the behavior of $w(s)$ for the "forward" and the "reverse" processes for the translocation of longer chain lengths from the conical pore with apex angle $\alpha = 3.5°$. In Fig. 3.8, we have plotted the residence time $w(s)$, for both the "forward" and the "reverse" cases, as a function of s/N for the polymer of lengths $N = 128$ and 320 at two different driving forces f_0. For a lower driving force $f_0 = 0.4$ (see Fig. 3.8(a)), we see that the tail retraction part becomes steeper for a longer chain for both the "forward" and "reverse" processes. However, for the chain lengths used in our study, we observed that the initial rise in $w(s)$, which is due to the tension propagation, is for this range of N values, we witness that in the case of reverse translocation, the propagation part (the initial rise in $w(s)$) is shorter than that for the forward case.

With the increase in the force value, $f_0 = 0.8$ (see Fig. 3.8(b)), the difference in the propagation part of $w(s)$ for the both processes starts to decrease.

By observing above features, our hypothesis is that for a very long polymer chain

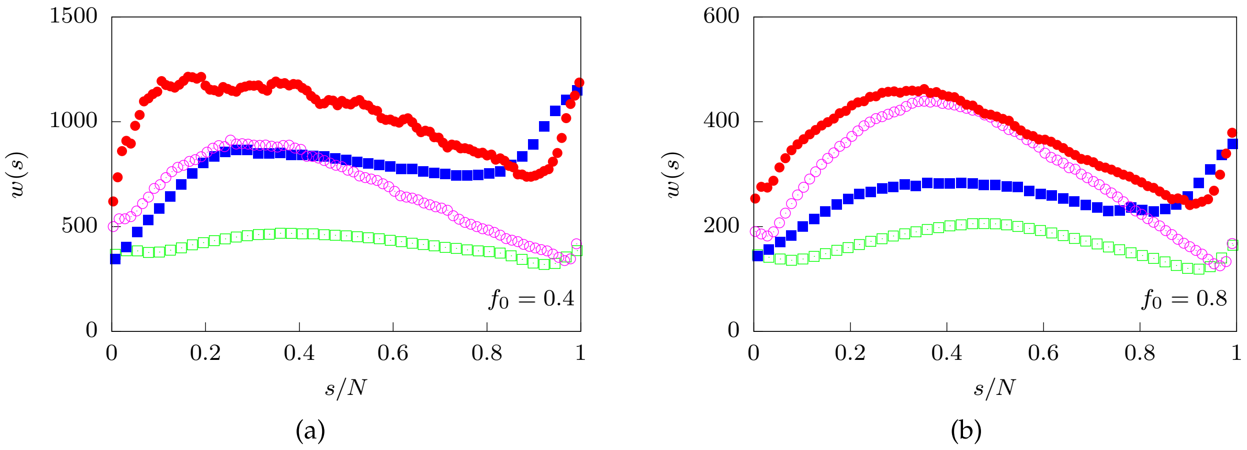

Figure 3.8: Effect of increasing force on $w(s)$ pattern for longer flexible polymer chains (N =128(square) and 320(circle)) at $\alpha = 3.5°$ for both the forward and reverse cases. Fig.(a) is for force, $f_0 = 0.4$ and Fig.(b) is for $f_0 = 0.8$. (filled circles and filled squares represent "reverse" case, and empty circles and empty squares represent "forward" case, respectively.)

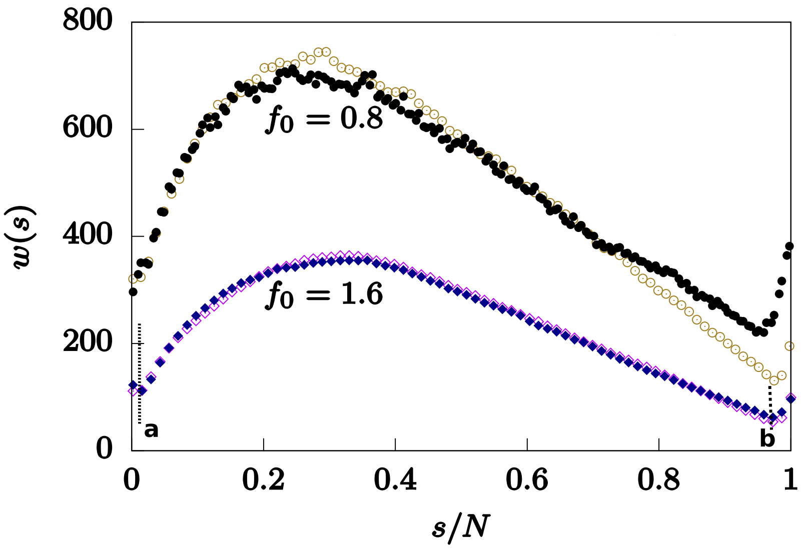

Figure 3.9: Plots showing the overlap in waiting time distributions for the forward and reverse translocation process for a flexible polymer chain of length $N = 512$. In the same graph, $w(s)$ is plotted for the two force value: $f_0 = 0.8$ and $f_0 = 1.6$. The graphs with filled circle and filled square are for reverse translocation case and the empty circle and empty square represents forward translocation case.

length the disparity in $w(s)$ for the "forward" and the "reverse" translocation processes will disappear completely and the translocation will appear to be a direction-independent process. To test this hypothesis, we have plotted in Fig. 3.9 the waiting time distribution curves $w(s)$ as a function of s/N for the polymer of length $N = 512$ at two different driving forces $f_0 = 0.8$ and $f_0 = 1.6$. We observe that even for $f_0 = 0.8$, the $w(s)$ curves for the "forward" and the "reverse" translocation processes show reasonable overlap, except at the tail retraction part (i.e., $s/N \to 1$). On increasing the magnitude of the force (i.e., $f_0 = 1.6$), the $w(s)$ curve for both the processes, including the retraction portion, merged completely. Note that the overlapped $w(s)$ curve for $f_0 = 1.6$ in Fig. 3.9 exhibits similar $w(s)$ curve (except an initial dip for $s/N \in [0, a]$, and a rise for $s/N \in [b, 1]$) for a polymer chain translocating through a slit. The dip at lower s/N values and the rise at higher s/N values store the information about the filling and the escape processes, respectively, for an extended and attractive pore.

3.4 Conclusions

In this chapter, we studied the driven polymer translocation through a conical pore when the polymer enters the pore from its wide opening and exits from the narrow end. We refer this process as "reverse translocation" to differentiate it with the "forward translocation" process, where the polymer enters the pore from the narrow end and exits from the pores wider end. Based on our previous study [3], we know that for lower force values, the translocation time τ is a non monotonic function of cone apex angle α. Therefore, we choose the value of force at the narrow end $f_0 = 0.2$. The samples are equilibrated accordingly before the translocation process starts. The reverse dynamics allows multiple bead entry of the equilibrated sample from the wider entrance of the conical pore, but the exit process is a single-file from the narrow end of the conical pore. For every successfully transported sample, we divide the translocation time τ into two times: (i) the passage time, and (ii) the escape time. The total translocation time τ is always equal to the sum of the two times. However, the major contribution is from the escape time.

It is found that the cone asymmetry (α) and the flexibility of the polymer chains (κ) play an important role in determining τ. For a flexible polymer, τ shows explicit non-monotonic behavior with the cone apex angle α. While the non-monotonic behavior fades away for rigid polymers. We found that for $\alpha \leq 1.5^\circ$, the total translocation time τ decreases as α is increased. However, for higher apex angles, i.e., $\alpha \geq 7^\circ$, τ increases as α is increased.

On comparing the "forward" and the "reverse" translocation processes, we observe that for a flexible polymer (i.e., $\kappa = 0$), the maximum disparity in τ is seen for the cone apex angle $\alpha \approx 3.5^\circ$, where $\tau_{reverse} >> \tau_{forward}$. This finding is in agreement with the experimental result [70]. The delay in τ for the reverse case is due to the coil and hairpin formation of polymer segments near the wide pore entrance. However, on increasing the rigidity of the polymers, the disparity in the translocation times between the two processes reduces. It is observed that for a very rigid polymer chain, the translocation process becomes direction independent and value of τ for both the "forward" and the "reverse" translocation are equal.

Furthermore, we find that the polymer dynamics through conical channels depends on the pore-polymer ratio. For a fixed pore length (L_p) and pore angle (α), we observe that the behaviour of $w(s)$ changes with the increase in polymer length N. We also see that, for longer chain lengths (e.g., $N = 512$), the waiting time distributions for the "forward" and the "reverse" cases overlap with each other and the translocation dynamics becomes direction independent.

Chapter 4

Effect of pore sequencing on translocation and scaling laws

4.1 Introduction

As discussed in previous chapters, the total translocation time τ, and the waiting time distributions $w(s)$ are key properties in polymer translocation process. A lot of information about the nature of the pore and polymer can be extracted from these quantities. The pore-polymer interaction plays an important role at every stage of the translocation process. In Chap. 2, we have seen the dominating role of the attractive channels during the exit process. Furthermore, for a pore of fixed length, we have seen that the behaviour of the total translocation time τ vs. the cone apex angle α transits from a non-monotonic dependence at lower force values (i.e, $f_0 < 0.7$), to a truly monotonic increasing function of apex angle α at higher force values (i.e, $f_0 > 0.9$).

In this chapter, we will extend our study to extended patterned pores, i.e., for pore with different types of pore-polymer interactions along its channel length. These interactions could be attractive or repulsive and are modelled by LJ potential. Depending upon the nature of the interaction at the opening of the pore, the polymer is either sucked in or thrown out of the pore. However, the presence of an external drive along the channel always facilitates the translocation process. We will study the effect of pore length L_p and the polymer length N in the translocation process.

The chapter is organized as follows: In Sec. 4.2, we study the effect of pore length L_p of conical as well as extended channel on the total translocation time, τ. In Sec. 4.3, we study the effect of pattered pores on τ. We establish scaling relations between τ, pore lengths and polymer lengths for extended as well as patterned pores. In Sec. 4.4, we conclude the chapter by providing a discussion on the obtained scaling exponents.

4.2 Effect of pore length

The Length of the pore plays an important role in the dynamics of the polymer chain translocating through a membrane channel. To demonstrate the effect of pore length on the total translocation time τ, we study the translocation of a flexible polymer of length $N = 128$ through conical pore of different lengths L_p ranging from 5σ to 10σ ($L_p \in [5\sigma, 10\sigma]$). We consider the pore to be attractive in nature and vary the cone apex angle α in the range between $0°$ to $5°$ ($\alpha \in [0°, 5°]$). The magnitude of the external driving force is kept fixed at 1 (i.e., $f_0 = 1$). In Fig. 4.1, we have plotted τ as a function of α for various L_p's. From the figure, we observe that, irrespective of the value of α, the total translocation time τ decreases with the increase of the pore length L_p.

For $\alpha = 0°$ the pore is cylindrical in geometry with diameter $d_0 = 2.25\sigma$, and allows only single-file translocation. For such a pore, the extent of the external force increases as the pore length is increased. For example, for a pore of length $L_p = 10\sigma$, the force experienced by number of beads are almost twice that of the beads for the pore of length $L_p = 5\sigma$. Therefore, the polymer can be driven easily through a longer pore. This can

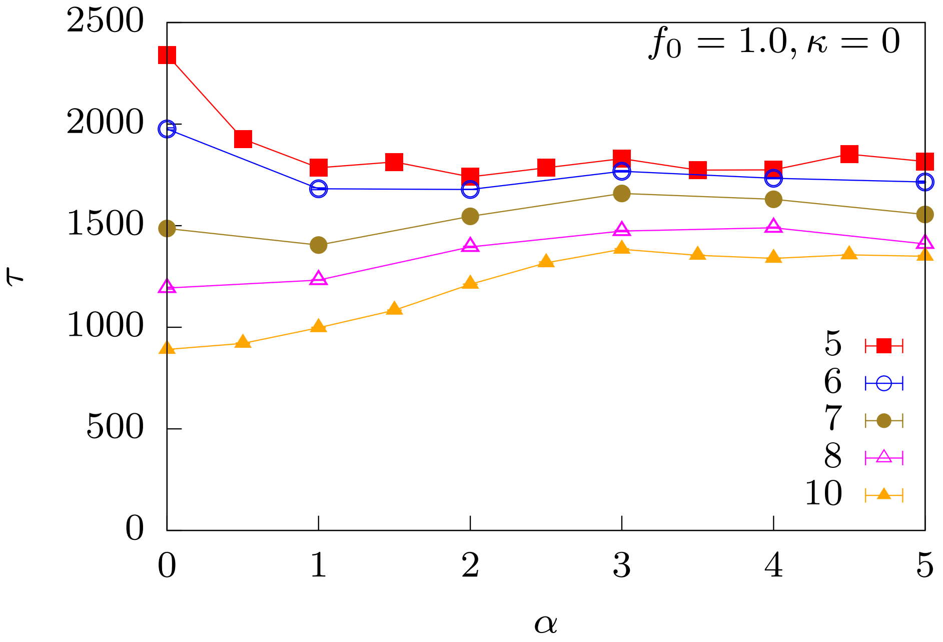

Figure 4.1: Plots showing the variation of τ vs. α behaviour, with the change of pore-length, L_p from [5:10]. Here the polymer is flexible with length (N) 128 beads, and pore-length varies from 5σ to 10σ.

be seen by lower τ value for $L_p = 10\sigma$ in Fig. 4.1. From the figure, we can see that for short pore lengths (e.g., $L_p = 5$, and 6), the translocation time τ decreases as α is increased and quickly gets saturated around $\alpha \approx 2^\circ$. This is because, on increasing α, the symmetry of the cylindrical channel gets broken. The diameter of the cylindrical channel at the narrow entrance remains the same as before ($d_0 = 2.25\sigma$), while the diameter at the wider end increases by an amount $2L_p \sin\alpha$ (i.e., $d_{L_p} = d_0 + 2L_p \sin\alpha$). Now due to more area available on the wider side of the conical channel, the single-file nature of the translocation process is no more true and more configurations of the polymer are possible and an entropic force [4] assists the polymer to escape faster from the channel.

However, for longer pore lengths, we see an opposite behavior. As the length of the pore increases, the diameter at the wider end increases proportionately. Since the external force inside the channel decreases as $f(x) \sim 1/x$, it also becomes weaker at the wider pore exit for longer pores. Further, since the pore is attractive in nature there is more possibil-

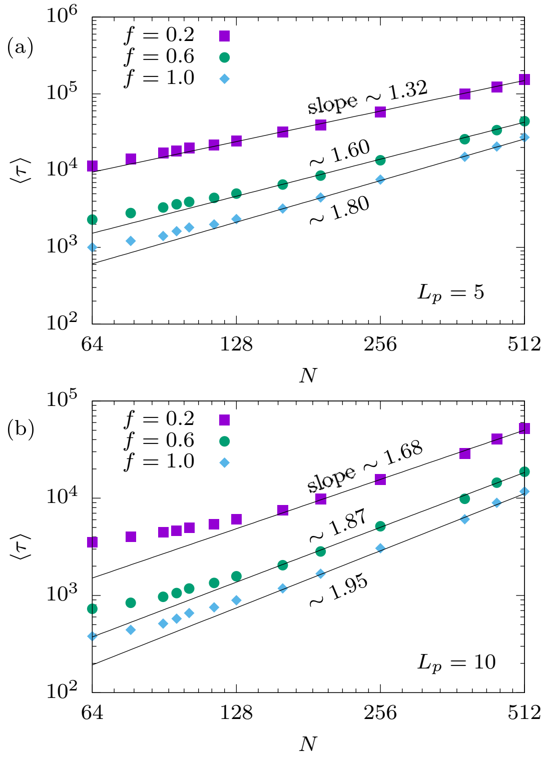

Figure 4.2: $\langle\tau\rangle$ as a function of N (in log-log scale) for three different driving forces when the polymer is translocating from an extended cylindrical pore (i.e., $\alpha = 0$) of length (a) $L_p = 5$, and (b) $L_p = 10$. The slopes mentioned in the plot are the values of the translocation exponent, defined by $\langle\tau\rangle \sim N^{\beta}$, for different driving forces.

ity for the polymer to have have a configuration where the two consecutive monomers of the chain occupy side-by-side position along $y-$direction at some location x in the channel. Combining all these factors, it was observed that the total force experienced by the polymer inside a longer pore is lesser than that for $\alpha = 0°$ and the total translocation time increases as the pore apex angle α is increased.

In Fig. 4.2(a) and 4.2(b), we have plotted the averaged total translocation time $\langle\tau\rangle$ as a function of chain length N for a flexible polymer translocating from a cylindrical pore (i.e., $\alpha = 0$) of lengths $L_p = 5$ and 10, respectively for various values of driving forces $f = 0.2$, 0.6 and 1.0. The translocation time exponent β is defined as $\tau \sim N^{\beta}$. For a flexible polymer translocating from a slit, it was found that the exponent $\beta < 1 + \nu$, where ν is the size exponent [48, 50]. In 1- and 2-dimensions $\nu = 1.0$ and 0.75, respectively. It is known that the value of exponent β depends on many factors such as chain length, chain flexibility, driving force, friction and pore structure. This is seen in our simulations as well. For smaller driving force $f = 0.2$, we found that the numerical value of the exponent for pore length $L_p = 5$ is $\beta = 1.32$, which is smaller than $1 + \nu = 1.75$. On increasing the pore length to $L_p = 10$, the value of the exponent becomes $\beta = 1.68$ but still less than 1.75. On increasing the driving force to $f = 0.6$, the translocation exponent for $L_p = 5$ is $\beta = 1.60 < 1.75$. However, for for pore length $L_p = 10$, the exponent becomes $\beta = 1.87 > 1.75$. For a driving force $f = 1.0$, the value of the translocation exponent for pore lengths $L_p = 5$ and 10 are 1.80 and 1.95, respectively, both are greater than 1.75 but less than 2. A similar behavior of increase in the exponent β is seen for translocation from a slit when the rigidity of the polymer is increased [52]. A plausible explanation could be that by increasing the pore length or the driving force reduces the embedded dimension for the polymer from two- to one and hence the upper bound for the translocation exponent for an extended pore should be 2.

We have seen that the translocation exponent β varies with the length of the extended pore. We now seek if it is possible to plot τ values for different pore lengths L_p and chain lengths N on a single curve. We use the following scaling form for this purpose

$$\langle\tau\rangle \sim N^{\gamma}\mathcal{F}\left(L_p N^{\nu}\right), \tag{4.1}$$

where ν is the size exponent and γ is some other exponent and $\mathcal{F}$ is the scaling function. In Fig. 4.3, we have plotted $\langle\tau\rangle/N^{\gamma}$ as a function of $L_p N^{\nu}$ for pore lengths L_p varying from 5 to 10, and the chain lengths N varying from 160 to 512. As we are working in 2-dimensions, we have used the size exponent $\nu = 0.75$. We found that a nice collapse is obtained for an exponent value $\gamma = 2.6 \pm 0.05$ for all the three driven force values $f_0 = 0.2$, 0.6 and 1.0. The scaling function is of the form $\mathcal{F}(x) \sim 1/x^p$ with p values $p = 1.5$, 1.1, and 1.0 for $f_0 = 0.2$, 0.6, and 1.0, respectively.

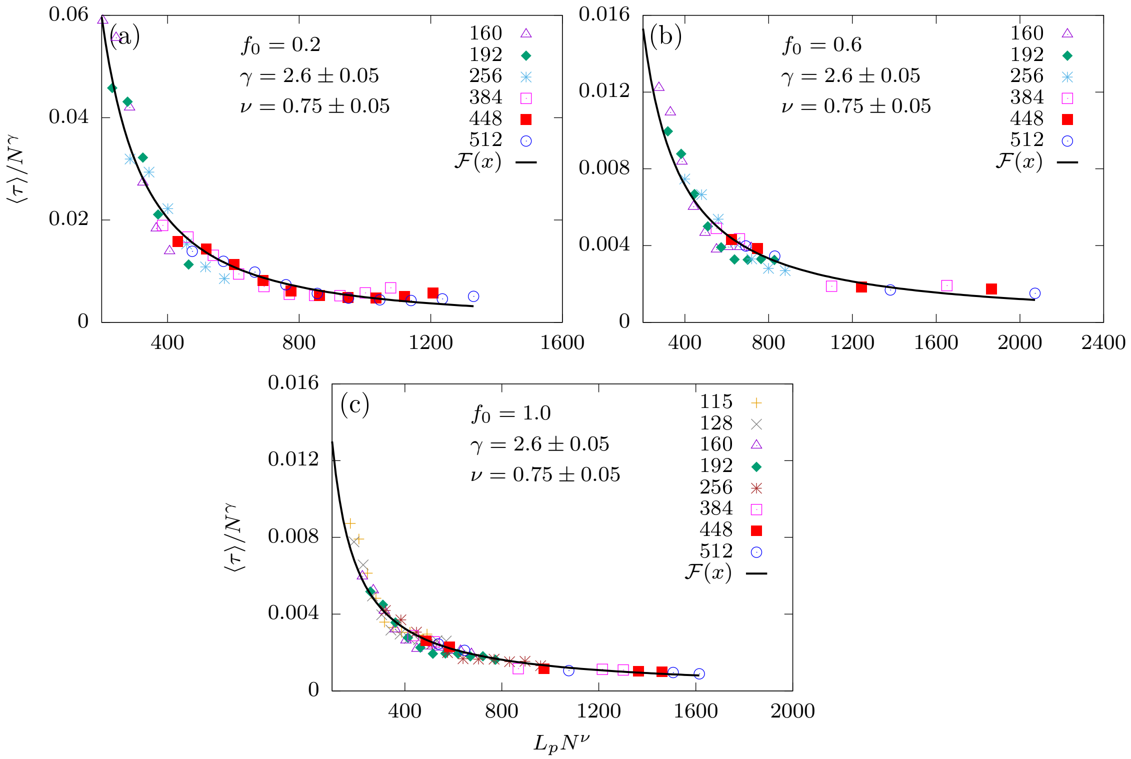

Figure 4.3: $\langle\tau\rangle/N^\gamma$ as a function of $L_p N^\nu$ for an extended pore ($\alpha = 0$) for three different driving forces (a) 0.2, (b) 0.6, and (c) 1.0. The lines are the scaling function.

4.3 Effect of pore patterning

In the previous section, we have studied the variation of total translocation time τ for an attractive pore. In this section, we will discuss the effect of pore patterning on τ for a flexible polymer of length $N = 128$. Figure 4.4 shows schematic diagram of three different pore patterns. The first row shows pores for length $L_p = 5$. The pore shown in Fig. 4.4(a1) is a completely attractive pore, while Fig. 4.4(b1) shows the pore with an attractive entrance and an attractive exit but separated by a repulsive bead in the middle, and Fig. 4.4(c1) has an attractive entrance but a repulsive exit. Such pore patterning has been studied earlier for cylindrical pores and many interesting results were obtained [72, 81]. In this thesis, we are studying pore patterning of a conical channel. Furthermore, we are also interested to know if the results change by increasing the length of the pore. We increase the pore length in such a manner that the ratio of pore patterning remains conserved. For example, in second and third rows of Fig. 4.4, we have plotted the pores for lengths $L_p = 10$, and $L_p = 15$, respectively. Figures clearly shows that the ratios of repulsive to attractive pore beads remains preserved on increasing the pore length. On increasing the length of the pore, the wide area at the exit of the pore also increases. We are interested to know how the total translocation time τ behaves for different type of pores.

In Fig. 4.5, we have plotted the total translocation time, for a flexible polymer of length $N = 128$, as a function of pore apex angle α for three different pore lengths $L_p = 5$, 10, and 15 at two different values of the driving force $f_0 = 0.6$ and 1.0. We clearly see that for shorter pore length, i.e., $L_p = 5$, the translocation time τ decreases with α and gets saturated for all the three type of pores for both the force values (see Figs. 4.5(a) and 4.5(d)). Further, we see that the pore with a repulsive exit (i.e., pore c1) favours faster translocation with a least value of τ at all angles. This is followed by the pore with an attractive entrance and exits and a repulsive bead in between (pore b1), and a fully attractive pore (pore a1). For a pore of intermediate length (i.e., $L_p = 10$), the translocation

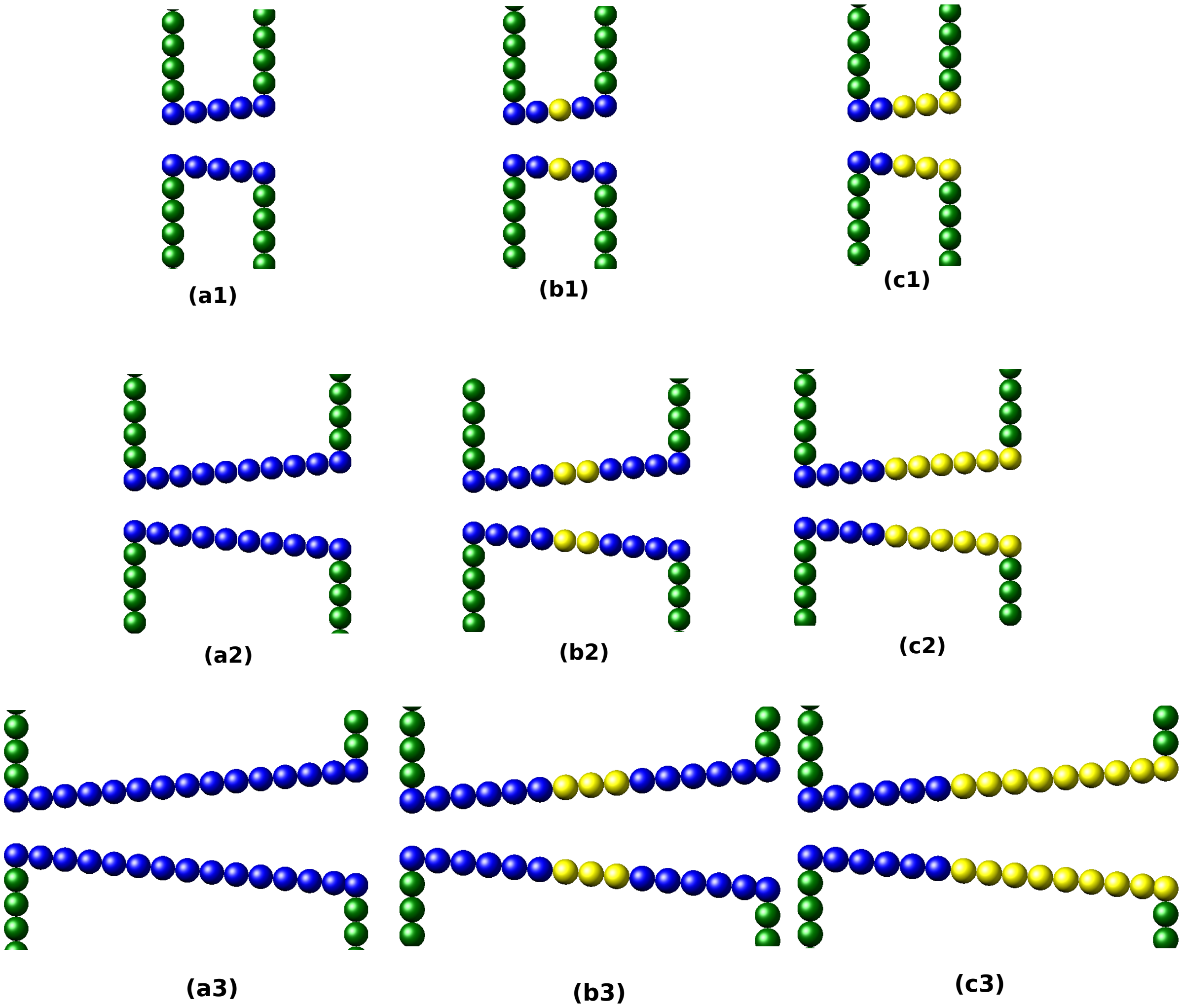

Figure 4.4: Schematic of sequenced pores with different lengths: 5, 10, and 15. The colorful beads of the pore are to denote different interactions between the pore and polymer beads. The polymer chain has repulsive interaction with the green static wall beads, the blue beads of the pore are attractive in nature, and the yellow part of the pore is repulsive in nature. Figures(a1-c1), are the pore designs for a pore length of 5 beads. Fig.a1 is an attractive pore, in pore b1, the middle pore is repulsive and in pore c1, the last three beads are repulsive and the rest of the beads are attractive in interactions. Figures(a2-c2), is the pore design for a pore of length 10 beads. The design of the pore with 10 beads is in the same ratio as the pore length of 5. Here pore (a2) is purely an attractive pore, the middle two beads of the pore (b2) are repulsive and the rest beads are attractive, and, in pore (c2), the last six beads are repulsive and first four beads are attractive. Similarly, Figures (a3-c3) is the sequenced pore in the same ratio as discussed above for pore length 15.

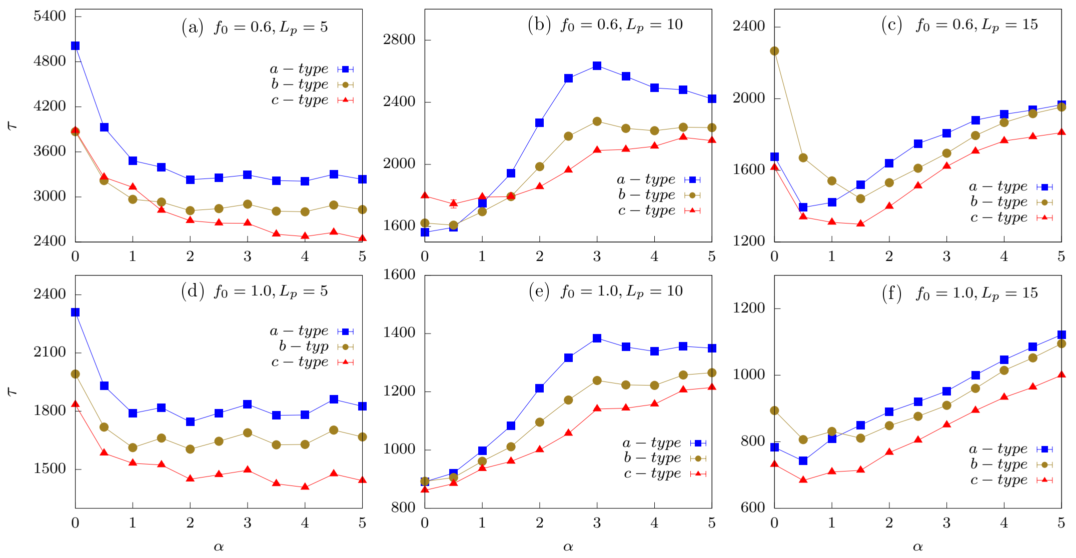

Figure 4.5: Comparison of τ vs. α for three different pore sizes $L_p = 5$, 10 and 15 for two different forces ($f_0 =$) 0.6 and 1.0. The length(N) of the flexible polymer chain ($\kappa = 0$) is 128 beads.

time τ increases with α for both $f_0 = 0.6$ and 1.0. It reaches a maximum at about $\alpha \approx 3°$ for pore types a2 and b2 and then decreases on increasing α and gets saturated (see Figs. 4.5(b) and 4.5(e)). The above feature is more pronounced for lower force values $f_0 = 0.6$ and on increasing the force value i.e. for $f_0 = 1.0$, τ gets saturated just after the peak is attained. On increasing the pore length further (i.e., $L_p = 15$), the translocation time first decreases with α. It reaches a minimum value at a different value of α for different type of pores and then increase till it gets saturated (see Figs. 4.5(c) and 4.5(f)).

We next look at the effect of patterned pores on rigid polymer chains. In Fig. 4.6, we have plotted the averaged total translocation time τ, as a function of apex pore angle α for a polymer of length $N = 128$ having different bending rigidities $\kappa = 12.8$, 38.4, and 64, translocating through conical pores of two different lengths $L_p = 5$ and 10. For the pore of length $L_p = 5$, we observe that τ decreases with α and gets saturated (see Figs. 4.6(a),(c),(e)). This is more pronounced for pores of types “a” and “b”. For pore of type “c”, we observe initial decrease for smaller values of κ but τ becomes almost constant for larger κ values (e.g., $\kappa = 64$ see Fig. 4.6(c)). However, for longer pore lengths

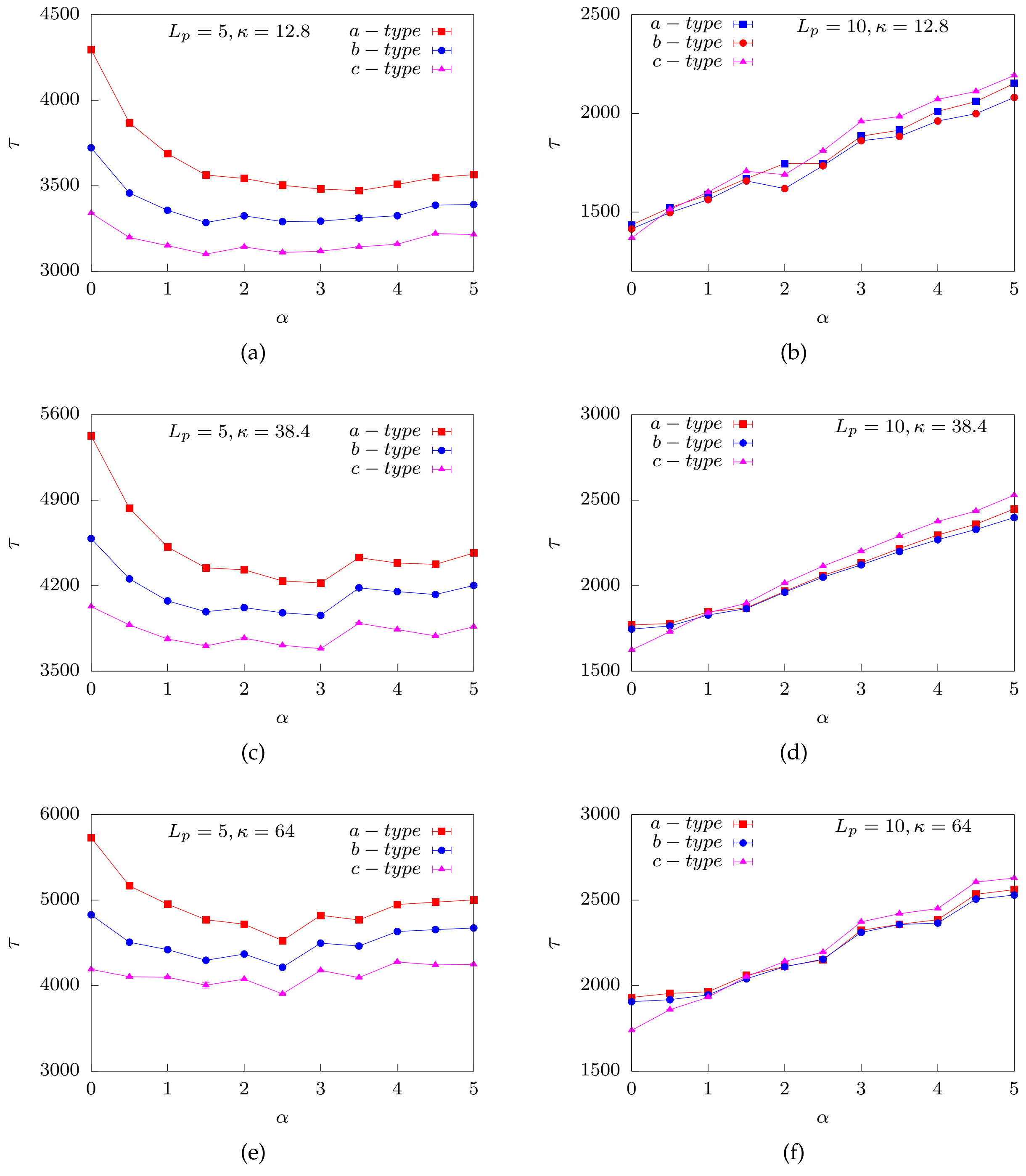

Figure 4.6: Total translocation time versus apex angle plots for a rigid polymer of length 128 for $f_0 = 1.0$, for two different pores ($L_p = 5$ and 10) described in Fig. 4.4. The curves in fig.(a,b) are for semi flexible polymer with rigidity 12.8, curves in fig.(c,d) are for $\kappa = 38.4$, and the curves in (e,f) represents polymer with rigidity 64 for pores: $L_P = 5$(a,c,e) and $L_P = 10$(b,d,f) respectively.

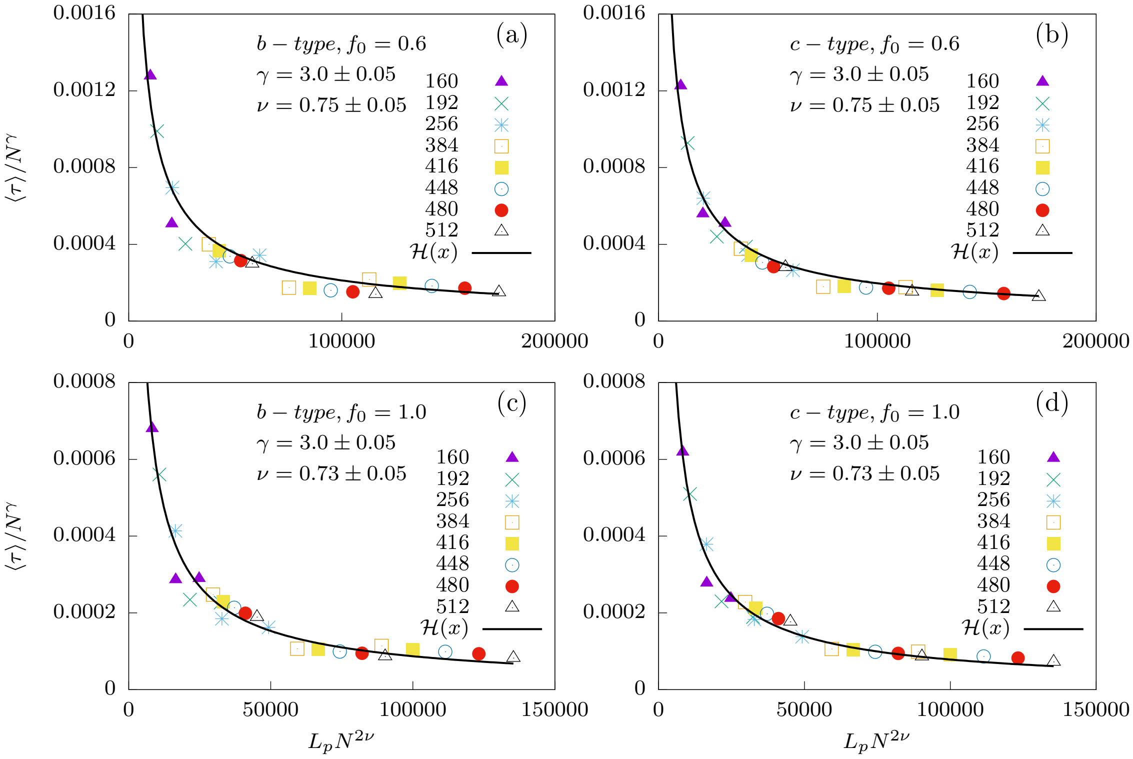

Figure 4.7: Scaled translocation time(τ) for the sequenced pore (Fig. 4.4) for three different pore lengths 5, 10 and 15. Plots (a), (b) is for force 0.6 and plots (c), (d) is for force 1.0 respectively.

(i.e.,. $L_p = 10$), we see that there is not much effect of the pore patterning on the net translocation time as the rigidity of the polymer chain is increased (see Figs. 4.6(b),(d),(f)).

To obtain the scaling of the averaged total translocation time with pore length L_p and chain length N for patterned pores, we again use the scaling relation of the form:

$$\langle\tau\rangle \sim N^{\gamma}\mathcal{H}\left(L_p N^{2\nu}\right), \tag{4.2}$$

where ν and γ is scaling exponents, and $\mathcal{H}$ is the scaling function. When $\langle\tau\rangle/N^{\gamma}$ is plotted as a function of $L_p N^{2\nu}$, for various pore lengths L_p and chain lengths N, the data collapse to a scaling curve $\mathcal{H}(x) \sim 1/x^q$. The value of the exponent q depends on the driving force but not on the pore type. At a force value $f_0 = 0.6$, the exponent is found to be $q = 0.75 \pm 0.01$, while for $f_0 = 1.0$ the exponent becomes $q = 0.81 \pm 0.01$. The data-collapse is shown in Fig. 4.7.

4.4 Conclusion

In this chapter, we have studied the effect of polymer length, pore length, and pore patterning on the total translocation time τ for both the cylindrical (i.e., $\alpha = 0$) and the conical pores with various apex angles α.

For a polymer of fixed length $N = 128$ (see Fig. 4.1), we found that the behavior of total translocation time τ switches from a decreasing function of α to a strictly increasing function of α on increasing the pore length from 5 to 10. The two opposite translocation behaviors seen for the shorter and the longer pore lengths are non-scalable, which shows the non-equilibrium nature of the driven polymer translocation process. We also observe that for a fixed pore apex angle α, the translocation time is a decreasing function of pore length (L_p). Since the extent of the external driving force is larger for longer pore lengths, the driven translocation process is favored for longer pores. This is found to be consistent for the translocation of rigid polymer from the patterned pores.

We find that, the average total translocation time $\langle\tau\rangle$ scales with the polymer lengths N as $\langle\tau\rangle \sim N^{\beta}$, where the translocation exponent β depends on the pore length L_p as well as the driving force. We found that for smaller driving force $f = 0.2$ the value of the exponent is $\beta < 1 + \nu = 1.7$ for pore lengths $L_p = 5$ and 10. However, for large driving force $f = 1.0$, the exponent $1.75 < \beta < 2.0$ for both the pore lengths. A plausible explanation could be that by increasing the pore length or the driving force reduces the embedded dimension for the polymer from two- to one and hence the upper bound for the translocation exponent for an extended pore should be 2.

We also found that the translocation time $\langle\tau\rangle$ scales with the pore length L_p and the polymer length N as $\langle\tau\rangle \sim N^{\gamma}\mathcal{F}(L_p N^{\nu})$, with $\gamma = 2.6 \pm 0.05$ and $\nu = 0.75$ for an attractive pore for all driven forces used in our study. The scaling function is found to be of the form $\mathcal{F}(x) \sim 1/x^p$ with p values 1.5, 1.1, and 1.0 for $f_0 = 0.2$, 0.6, and 1.0, respectively. For the patterned pores, $\langle \tau \rangle \sim N^{\gamma}\mathcal{H}(L_p N^{2\nu})$, with $\gamma = 3.0 \pm 0.05$ and $\nu = 0.75$. The scaling function is found to be of the same form $\mathcal{H}(x) \sim 1/x^q$ with $q = 0.75$ at $f_0 = 0.6$, and $q = 0.81$ at $f_0 = 1.0$.

Chapter 5

Conclusion

In this thesis, we have studied the dynamics of polymer translocation through conical pores.

In Chap. 2, we presented our results for the translocation of a semiflexible polymer through conical channels under the influence of a spatially varying external drive and attractive surface interactions. We considered the translocation dynamics of polymer directed from the narrow end to the wide end of the conical pores, and refer this process as "forward translocation". The translocation dynamics is measured by the total translocation time, τ, and the waiting time distributions, $w(s)$. The total translocation time is seen to be a non-monotonic function of cone apex angle α in the low force regime. To understand the effects arising due to the polymer stiffness, the surface interactions, and the nature of the external drive, we studied $w(s)$ for lower forces. We attempt to understand some of these features using a free energy argument based on a quasi-equilibrium approximation which is applicable for smaller polymer lengths and low forces. The theory captures some of the non-monotonic features of the translocation dynamics. For the case of higher stiffness and larger channel angles, the variable potential landscape arising from the surface interactions becomes dominant. This variability needs to be accounted for in order to provide a more accurate description of the dynamics. In our detailed simulations, we observe that the translocation dynamics are strongly dependent on the stiffness of the polymer and surface interactions. Attractive surface interactions can considerably slow down the translocation process near the ends while increasing the angle of the conical pore may facilitate the process.

In Chap. 3, we studied the driven translocation through a conical pore when the polymer enters the pore from its wide opening and exits from the narrow end. We refer this process as "reverse translocation" to differentiate it with the "forward translocation" process. Based on our studies on the "forward" translocation (i.e., Chap. 2), we choose the force value $f_0 = 0.2$ at the lower end. We measure τ and $w(s)$ to study the effect of pore asymmetries on the translocation process. We found that the cone asymmetry, which arises due to cone apex angle α, and the flexibility of the polymer chains, which arises due to the bending rigidity κ, play an important role in determining τ. For a flexible polymer, τ shows explicit non-monotonic behavior with the cone apex angle α. While this non-monotonic pattern fades away for two cases: (i) for rigid polymers, and (ii) for higher force values. We found that for $\alpha \leq 1.5°$, the total translocation time τ decreases as α is increased. However, for higher apex angles, i.e., $\alpha \geq 7°$, τ increases as α is increased. On comparing the "forward" and the "reverse" translocation processes, we observe that for a flexible polymer (i.e., $\kappa = 0$), the maximum disparity in τ is seen for the cone apex angle $\alpha \approx 3.5°$, where $\tau_{reverse} >> \tau_{forward}$. This finding is in agreement with the experimental result [70]. The delay in τ for the reverse case is due to the coil and hairpin formation of polymer segments near the wide pore entrance. However, on increasing the rigidity of the polymers, the disparity in the translocation times between the two processes reduces. It is observed that for a very rigid polymer chain, the translocation process becomes direction independent and value of τ for both the "forward" and the "reverse" translocation are equal. Furthermore, we find that the polymer dynamics through conical channels depends on the pore-polymer ratio. For a fixed pore length (L_p) and pore angle (α), we observe that the behaviour of $w(s)$ changes with the increase in polymer length N.

We also see that, for longer chain lengths (e.g., $N = 512$), the waiting time distributions for the "forward" and the "reverse" cases overlap with each other and the translocation dynamics becomes direction independent.

In Chap. 4, we presented our results for the effect of polymer length, pore length, and pore patterning on the total translocation time τ for both the cylindrical (i.e., $\alpha = 0$) and the conical pores with various apex angles α. For a polymer of fixed length $N = 128$ (see Fig. 4.1), we found that the behavior of total translocation time τ switches from a decreasing function to a strictly increasing function of α on increasing the pore length from 5 to 10. The two opposite translocation behaviors seen for the shorter and the longer pore lengths do not scale, which shows the non-equilibrium nature of the driven polymer translocation process. We also observe that for a fixed pore apex angle α, the translocation time is a decreasing function of pore length (L_p). Since the extent of the external driving force is larger for longer pore lengths, the driven translocation process is favored for longer pores. This is found to be consistent for the translocation of rigid polymer from the patterned pores. Further, we find that, the average total translocation time $\langle\tau\rangle$ scales with the polymer lengths N as $\langle\tau\rangle \sim N^{\beta}$, where the translocation exponent β depends on the pore length L_p as well as the driving force. We found that for smaller driving force $f = 0.2$ the value of the exponent is $\beta < 1 + \nu = 1.75$ for pore lengths $L_p = 5$ and 10, where $\nu = 0.75$ is the size exponent for a flexible polymer in 2D. However, for large driving force $f = 1.0$, the exponent is found to be $1.75 < \beta < 2.0$ for both the pore lengths. A plausible explanation could be that by increasing the pore length or the driving force reduces the embedded dimension for the polymer from two- to one-dimension and hence the upper bound for the translocation exponent for an extended pore should be 2, i.e., the size exponent $\nu = 1$. We also studied the behavior of τ with pore length L_p and the polymer length N. We found that the translocation time $\langle\tau\rangle$ scales as $\langle\tau\rangle \sim N^{\gamma}\mathcal{F}(L_p N^{\nu})$, with $\gamma = 2.6 \pm 0.05$ and $\nu = 0.75$ for an attractive pore for all driven forces used in our study. The scaling function is found to be of the form $\mathcal{F}(x) \sim 1/x^{p}$ with p values 1.5, 1.1, and 1.0 for $f_0 = 0.2$, 0.6, and 1.0, respectively. For the patterned pores, the scaling becomes

$\langle\tau\rangle \sim N^{\gamma}\mathcal{H}(L_pN^{2\nu})$, with $\gamma = 3.0 \pm 0.05$ and $\nu = 0.75$. The scaling function is found to have the same form $\mathcal{H}(x) \sim 1/x^q$ with $q = 0.75$ at $f_0 = 0.6$, and $q = 0.81$ at $f_0 = 1.0$.

Appendix A

Free Energy for Conical pore

When the size of the molecules are large in comparison to the size of the pores, they can be fully occupied inside the pores during the course of transport process. The free energy due to this confinement plays a very important role in translocation. For conical pores with different apex angles, the confinement effect will be different and can be estimated from the blob theory. According to blob theory the free energy contribution due to the confinement of polymer inside a d-dimension conical pore can be written as:

$$F_{conf}(N, \alpha, d) = \left[\frac{N^{\nu d}\, b^d \; \tan\alpha}{(D_0 + 2(a+L)\tan\alpha)^d - (D_0 + 2a\tan\alpha)^d} \right]^{1/(\nu d - 1)} \tag{A.1}$$

Here, N is the number of monomer beads confined inside the pore, α is half the apex angle of the cone, a is the horizontal distance up to which the pore portion is empty and L is the horizontal distance along the x-axis where the pore is filled. The projection of the cone length (which consist of 16 beads) along the x-axis is equal to ($a + L = 16\cos\alpha$), ν is the Flory's exponent which gives the size of the blob to the number of beads inside the blob as $R \approx N^{\nu}$. The force exerted on the polymer segment confined inside the pore can be obtained from the confinement free energy $f = -\partial F / \partial a$ and is given by

$$\begin{aligned} f_{conf} = \frac{1}{D_0(1-\nu d)} \left(\frac{(N^{\nu} b)}{D_0}\right)^{\frac{d}{\nu d - 1}} & \\ \left[\frac{\tan\alpha}{(1+\frac{2\tan\alpha(a+L)}{D_0})^d - (1+2\frac{2a\tan\alpha}{D_0})^d}\right]^{d\nu 1/(d\nu - 1)} & \\ \times \left[(1+\frac{2\tan\alpha(a+L)}{D_0})^{d-1} - (1+\frac{2a\tan\alpha}{D_0})^{d-1}\right] . & \quad \text{(A.2)} \end{aligned}$$

Note: The area / volume of the occupied cone while filling the pore is $((D_0 + 2a\tan\alpha)^d - D_0^d)/\tan\alpha$.

Bibliography

[1] John J Kasianowicz, Eric Brandin, Daniel Branton, and David W Deamer. Characterization of individual polynucleotide molecules using a membrane channel. *Proceedings of the National Academy of Sciences*, 93(24):13770–13773, 1996.

[2] Aidan P Thompson, H Metin Aktulga, Richard Berger, Dan S Bolintineanu, W Michael Brown, Paul S Crozier, Pieter J in't Veld, Axel Kohlmeyer, Stan G Moore, Trung Dac Nguyen, et al. Lammps-a flexible simulation tool for particle-based materials modeling at the atomic, meso, and continuum scales. *Computer Physics Communications*, 271:108171, 2022.

[3] Andri Sharma, Rajeev Kapri, and Abhishek Chaudhuri. Driven translocation of a semiflexible polymer through a conical channel in the presence of attractive surface interactions. *Scientific Reports*, 12(1):19081, November 2022.

[4] Narges Nikoofard, Hamidreza Khalilian, and Hossein Fazli. Directed translocation of a flexible polymer through a cone-shaped nano-channel. *The Journal of Chemical Physics*, 139(7):074901, 2013.

[5] Narges Nikoofard and Hossein Fazli. A flexible polymer confined inside a cone-shaped nano-channel. *Soft Matter*, 11(24):4879–4887, 2015.

[6] Andri Sharma. Translocation through conical pores: A direction-dependent process. *arXiv preprint arxiv.2210.16990*, 2022.

[7] Nicholas AW Bell, Kaikai Chen, Sandip Ghosal, Maria Ricci, and Ulrich F Keyser. Asymmetric dynamics of dna entering and exiting a strongly confining nanopore. *Nature communications*, 8(1):1–8, 2017.

[8] Veronica S DeGuzman, Clarence C Lee, David W Deamer, and Wenonah A Vercoutere. Sequence-dependent gating of an ion channel by dna hairpin molecules. *Nucleic acids research*, 34(22):6425–6437, 2006.

[9] David W Deamer and Daniel Branton. Characterization of nucleic acids by nanopore analysis. *Accounts of chemical research*, 35(10):817–825, 2002.

[10] Amit Meller, Lucas Nivon, and Daniel Branton. Voltage-driven dna translocations through a nanopore. *Physical Review Letters*, 86(15):3435, 2001.

[11] James D Watson and Francis HC Crick. The structure of dna. In *Cold Spring Harbor symposia on quantitative biology*, volume 18, pages 123–131. Cold Spring Harbor Laboratory Press, 1953.

[12] Francis S Collins, Ari Patrinos, Elke Jordan, Aravinda Chakravarti, Raymond Gesteland, LeRoy Walters, members of the DOE, and NIH planning groups. New goals for the us human genome project: 1998-2003. *Science*, 282(5389):682–689, 1998.

[13] Pushpendra K Gupta. Single-molecule dna sequencing technologies for future genomics research. *Trends in biotechnology*, 26(11):602–611, 2008.

[14] Eric E Schadt, Steve Turner, and Andrew Kasarskis. A window into third-generation sequencing. *Human molecular genetics*, 19(R2):R227–R240, 2010.

[15] Christoph Bleidorn. Third generation sequencing: technology and its potential impact on evolutionary biodiversity research. *Systematics and biodiversity*, 14(1):1–8, 2016.

[16] Harvey Lodish, Arnold Berk, Chris A Kaiser, Chris Kaiser, Monty Krieger, Matthew P Scott, Anthony Bretscher, Hidde Ploegh, Paul Matsudaira, et al. *Molecular cell biology*. Macmillan, 2008.

[17] Bruce Alberts, Alexander Johnson, Julian Lewis, Martin Raff, Keith Roberts, and Peter Walter. Molecular biology of the cell. garland science. *New York*, pages 1227–1242, 2015.

[18] Arnold J Storm, Cornelis Storm, Jianghua Chen, Henny Zandbergen, Jean-Francois Joanny, and Cees Dekker. Fast dna translocation through a solid-state nanopore. *Nano letters*, 5(7):1193–1197, 2005.

[19] Helen Berman, Kim Henrick, and Haruki Nakamura. Announcing the worldwide protein data bank. *Nature Structural & Molecular Biology*, 10(12):980–980, 2003.

[20] Artur Baumgärtner and Jeffrey Skolnick. Spontaneous translocation of a polymer across a curved membrane. *Physical review letters*, 74(11):2142, 1995.

[21] W Sung and PJ Park. Polymer translocation through a pore in a membrane. *Physical review letters*, 77(4):783, 1996.

[22] Mark Akeson, Daniel Branton, John J Kasianowicz, Eric Brandin, and David W Deamer. Microsecond time-scale discrimination among polycytidylic acid, polyadenylic acid, and polyuridylic acid as homopolymers or as segments within single rna molecules. *Biophysical journal*, 77(6):3227–3233, 1999.

[23] Murugappan Muthukumar. Polymer translocation through a hole. *The Journal of Chemical Physics*, 111(22):10371–10374, 1999.

[24] Amit Meller. Dynamics of polynucleotide transport through nanometre-scale pores. *Journal of physics: condensed matter*, 15(17):R581, 2003.

[25] Jeffrey Chuang, Yacov Kantor, and Mehran Kardar. Anomalous dynamics of translocation. *Physical Review E*, 65(1):011802, 2001.

[26] Elena Slonkina and Anatoly B Kolomeisky. Polymer translocation through a long nanopore. *The Journal of chemical physics*, 118(15):7112–7118, 2003.

[27] Kaifu Luo, Tapio Ala-Nissila, See-Chen Ying, and Aniket Bhattacharya. Influence of polymer-pore interactions on translocation. *Physical Review Letters*, 99(14):148102, 2007.

[28] Michel G Gauthier and Gary W Slater. A monte carlo algorithm to study polymer translocation through nanopores. i. theory and numerical approach. *The Journal of chemical physics*, 128(6):02B612, 2008.

[29] Michel G Gauthier and Gary W Slater. A monte carlo algorithm to study polymer translocation through nanopores. ii. scaling laws. *The Journal of Chemical Physics*, 128(20):05B619, 2008.

[30] Chiu Tai Andrew Wong and Murugappan Muthukumar. Polymer translocation through α-hemolysin pore with tunable polymer-pore electrostatic interaction. *The Journal of chemical physics*, 133(4):07B607, 2010.

[31] M Muthukumar. Polymer escape through a nanopore. *The Journal of chemical physics*, 118(11):5174–5184, 2003.

[32] Murugappan Muthukumar. *Polymer translocation*. CRC press, 2016.

[33] AM Berezhkovskii and IV Gopich. Translocation of rodlike polymers through membrane channels. *Biophysical journal*, 84(2):787–793, 2003.

[34] Peter Hänggi and Fabio Marchesoni. Artificial brownian motors: Controlling transport on the nanoscale. *Reviews of Modern Physics*, 81(1):387, 2009.

[35] Vladimir V Palyulin, Tapio Ala-Nissila, and Ralf Metzler. Polymer translocation: the first two decades and the recent diversification. *Soft matter*, 10(45):9016–9037, 2014.

[36] Daniel Branton, David W Deamer, Andre Marziali, Hagan Bayley, Steven A Benner, Thomas Butler, Massimiliano Di Ventra, Slaven Garaj, Andrew Hibbs, Xiaohua Huang, et al. The potential and challenges of nanopore sequencing. In *Nanoscience and technology: A collection of reviews from Nature Journals*, pages 261–268. World Scientific, 2010.

[37] Meni Wanunu. Nanopores: A journey towards dna sequencing. *Physics of life reviews*, 9(2):125–158, 2012.

[38] Stefan Howorka and Zuzanna Siwy. Nanopore analytics: sensing of single molecules. *Chemical Society Reviews*, 38(8):2360–2384, 2009.

[39] Ulrich F Keyser. Controlling molecular transport through nanopores. *Journal of The Royal Society Interface*, 8(63):1369–1378, 2011.

[40] Andrey Milchev. Single-polymer dynamics under constraints: scaling theory and computer experiment. *Journal of Physics: Condensed Matter*, 23(10):103101, 2011.

[41] Sergey M Bezrukov, Igor Vodyanoy, and V Adrian Parsegian. Counting polymers moving through a single ion channel. *Nature*, 370(6487):279–281, 1994.

[42] Pyeong Jun Park and Wokyung Sung. Polymer translocation induced by adsorption. *The Journal of chemical physics*, 108(7):3013–3018, 1998.

[43] Takahiro Sakaue. Nonequilibrium dynamics of polymer translocation and straightening. *Physical Review E*, 76(2):021803, 2007.

[44] Takahiro Sakaue. Sucking genes into pores: Insight into driven translocation. *Physical Review E*, 81(4):041808, 2010.

[45] Takuya Saito and Takahiro Sakaue. Process time distribution of driven polymer transport. *Physical Review E*, 85(6):061803, 2012.

[46] Jalal Sarabadani, Timo Ikonen, and Tapio Ala-Nissila. Iso-flux tension propagation theory of driven polymer translocation: The role of initial configurations. *The Journal of Chemical Physics*, 141(21):214907, 2014.

[47] Payam Rowghanian and Alexander Y Grosberg. Force-driven polymer translocation through a nanopore: An old problem revisited. *The Journal of Physical Chemistry B*, 115(48):14127–14135, 2011.

[48] Timo Ikonen, Aniket Bhattacharya, Tapio Ala-Nissila, and Wokyung Sung. Unifying model of driven polymer translocation. *Physical Review E*, 85(5):051803, 2012.

[49] Timo Ikonen, A Bhattacharya, T Ala-Nissila, and W Sung. Influence of pore friction on the universal aspects of driven polymer translocation. *EPL (Europhysics Letters)*, 103(3):38001, 2013.

[50] Timo Ikonen, Aniket Bhattacharya, Tapio Ala-Nissila, and Wokyung Sung. Influence of non-universal effects on dynamical scaling in driven polymer translocation. *The Journal of chemical physics*, 137(8):085101, 2012.

[51] Aniket Bhattacharya and Kurt Binder. Out-of-equilibrium characteristics of a forced translocating chain through a nanopore. *Physical Review E*, 81(4):041804, 2010.

[52] Aniket Bhattacharya. Translocation dynamics of a semiflexible chain under a bias: Comparison with tension propagation theory. *Polymer Science Series C*, 55(1):60–69, 2013.

[53] Hendrick W de Haan and Gary W Slater. Mapping the variation of the translocation α scaling exponent with nanopore width. *Physical Review E*, 81(5):051802, 2010.

[54] Aiqun Huang, Aniket Bhattacharya, and Kurt Binder. Conformations, transverse fluctuations, and crossover dynamics of a semi-flexible chain in two dimensions. *The Journal of Chemical Physics*, 140(21):214902, 2014.

[55] Kaifu Luo, Tapio Ala-Nissila, See-Chen Ying, and Aniket Bhattacharya. Translocation dynamics with attractive nanopore-polymer interactions. *Physical Review E*, 78(6):061918, 2008.

[56] Jack A Cohen, Abhishek Chaudhuri, and Ramin Golestanian. Active polymer translocation through flickering pores. *Physical review letters*, 107(23):238102, 2011.

[57] Jack A Cohen, Abhishek Chaudhuri, and Ramin Golestanian. Translocation through environments with time dependent mobility. *The Journal of chemical physics*, 137(20):204911, 2012.

[58] Jalal Sarabadani and Tapio Ala-Nissila. Theory of pore-driven and end-pulled polymer translocation dynamics through a nanopore: An overview. *Journal of Physics: Condensed Matter*, 30(27):274002, 2018.

[59] Pauli M Suhonen and Riku P Linna. Dynamics of driven translocation of semiflexible polymers. *Physical Review E*, 97(6):062413, 2018.

[60] Harshwardhan H Katkar and Murugappan Muthukumar. Role of non-equilibrium conformations on driven polymer translocation. *The Journal of chemical physics*, 148(2):024903, 2018.

[61] Rajesh Kumar Sharma, Ishita Agrawal, Liang Dai, Patrick S Doyle, and Slaven Garaj. Complex dna knots detected with a nanopore sensor. *Nature communications*, 10(1):1–9, 2019.

[62] Antonio Suma and Cristian Micheletti. Pore translocation of knotted dna rings. *Proceedings of the National Academy of Sciences*, 114(15):E2991–E2997, 2017.

[63] Antonio Suma, Lucia Coronel, Giovanni Bussi, and Cristian Micheletti. Directional translocation resistance of zika xrrna. *Nature communications*, 11(1):1–9, 2020.

[64] Calin Plesa, Daniel Verschueren, Sergii Pud, Jaco Van Der Torre, Justus W Ruitenberg, Menno J Witteveen, Magnus P Jonsson, Alexander Y Grosberg, Yitzhak Rabin,

and Cees Dekker. Direct observation of dna knots using a solid-state nanopore. *Nature nanotechnology*, 11(12):1093–1097, 2016.

[65] Jalal Sarabadani, Timo Ikonen, Harri Mökkönen, Tapio Ala-Nissila, Spencer Carson, and Meni Wanunu. Driven translocation of a semi-flexible polymer through a nanopore. *Scientific reports*, 7(1):1–8, 2017.

[66] Kehong Zhang and Kaifu Luo. Dynamics of polymer translocation into a circular nanocontainer through a nanopore. *The Journal of Chemical Physics*, 136(18):05B612, 2012.

[67] Kehong Zhang and Kaifu Luo. Dynamics of polymer translocation into an anisotropic confinement. *Soft Matter*, 9(6):2069–2075, 2013.

[68] Li-Zhen Sun and Meng-Bo Luo. Langevin dynamics simulation on the translocation of polymer through α-hemolysin pore. *Journal of Physics: Condensed Matter*, 26(41):415101, 2014.

[69] K Kiran Kumar and KL Sebastian. Adsorption-assisted translocation of a chain molecule through a pore. *Physical Review E*, 62(5):7536, 2000.

[70] Nicholas AW Bell, Kaikai Chen, Sandip Ghosal, Maria Ricci, and Ulrich F Keyser. Asymmetric dynamics of dna entering and exiting a strongly confining nanopore. *Nature communications*, 8(1):1–8, 2017.

[71] Timothée Menais. Polymer translocation under a pulling force: Scaling arguments and threshold forces. *Physical Review E*, 97(2):022501, 2018.

[72] Rajneesh Kumar, Abhishek Chaudhuri, and Rajeev Kapri. Sequencing of semiflexible polymers of varying bending rigidity using patterned pores. *The Journal of chemical physics*, 148(16):164901, 2018.

[73] Li-Zhen Sun, Haibin Li, Xiaojun Xu, and Meng-Bo Luo. Simulation study on the translocation of polyelectrolyte through conical nanopores. *Journal of Physics: Condensed Matter*, 30(49):495101, 2018.

[74] Paolo Malgaretti and Gleb Oshanin. Polymer translocation across a corrugated channel: Fick–jacobs approximation extended beyond the mean first-passage time. *Polymers*, 11(2):251, 2019.

[75] Rouhollah Haji Abdolvahab and Mohammadreza Niknam Hamidabad. Pore shapes effects on polymer translocation. *The European Physical Journal E*, 43(12):1–7, 2020.

[76] Li-Zhen Sun, Wei-Ping Cao, Chang-Hui Wang, and Xiaojun Xu. The translocation dynamics of the polymer through a conical pore: Non-stuck, weak-stuck, and strong-stuck modes. *The Journal of Chemical Physics*, 154(5):054903, 2021.

[77] Ramesh Adhikari and Aniket Bhattacharya. Driven translocation of a semi-flexible chain through a nanopore: A brownian dynamics simulation study in two dimensions. *The Journal of Chemical Physics*, 138(20):204909, 2013.

[78] Wancheng Yu, Yiding Ma, and Kaifu Luo. Translocation of stiff polymers through a nanopore driven by binding particles. *The Journal of chemical physics*, 137(24):244905, 2012.

[79] Narges Nikoofard, S Mohammad Hoseinpoor, and Mostafa Zahedifar. Accuracy of the blob model for single flexible polymers inside nanoslits that are a few monomer sizes wide. *Physical Review E*, 90(6):062603, 2014.

[80] Grégory F Schneider and Cees Dekker. Dna sequencing with nanopores. *Nature biotechnology*, 30(4):326–328, 2012.

[81] Jack A Cohen, Abhishek Chaudhuri, and Ramin Golestanian. Stochastic sensing of polynucleotides using patterned nanopores. *Physical Review X*, 2(2):021002, 2012.

[82] Ian M Derrington, Tom Z Butler, Marcus D Collins, Elizabeth Manrao, Mikhail Pavlenok, Michael Niederweis, and Jens H Gundlach. Nanopore dna sequencing with mspa. *Proceedings of the National Academy of Sciences*, 107(37):16060–16065, 2010.

[83] Bala Murali Venkatesan and Rashid Bashir. Nanopore sensors for nucleic acid analysis. *Nature nanotechnology*, 6(10):615–624, 2011.

[84] Cees Dekker. Solid-state nanopores. *Nanoscience And Technology: A Collection of Reviews from Nature Journals*, pages 60–66, 2010.

[85] Meni Wanunu and Amit Meller. Chemically modified solid-state nanopores. *Nano letters*, 7(6):1580–1585, 2007.

[86] Marc Gershow and Jene Andrew Golovchenko. Recapturing and trapping single molecules with a solid-state nanopore. *Nature nanotechnology*, 2(12):775–779, 2007.

[87] Binquan Luan, Gustavo Stolovitzky, and Glenn Martyna. Slowing and controlling the translocation of dna in a solid-state nanopore. *Nanoscale*, 4(4):1068–1077, 2012.

[88] Ulrich F Keyser, Bernard N Koeleman, Stijn Van Dorp, Diego Krapf, Ralph MM Smeets, Serge G Lemay, Nynke H Dekker, and Cees Dekker. Direct force measurements on dna in a solid-state nanopore. *Nature Physics*, 2(7):473–477, 2006.

[89] Jérôme Mathé, Aleksei Aksimentiev, David R Nelson, Klaus Schulten, and Amit Meller. Orientation discrimination of single-stranded dna inside the α-hemolysin membrane channel. *Proceedings of the National Academy of Sciences*, 102(35):12377–12382, 2005.

[90] C Chad Harrell, Youngseon Choi, Lloyd P Horne, Lane A Baker, Zuzanna S Siwy, and Charles R Martin. Resistive-pulse dna detection with a conical nanopore sensor. *Langmuir*, 22(25):10837–10843, 2006.

[91] Wen-Jie Lan, Deric A Holden, and Henry S White. Pressure-dependent ion current rectification in conical-shaped glass nanopores. *Journal of the American Chemical Society*, 133(34):13300–13303, 2011.

[92] Vivek V Thacker, Sandip Ghosal, Silvia Hernández-Ainsa, Nicholas AW Bell, and Ulrich F Keyser. Studying dna translocation in nanocapillaries using single molecule fluorescence. *Applied physics letters*, 101(22):223704, 2012.

[93] Jinsheng Zhou, Yanqian Wang, Laurent D Menard, Sergey Panyukov, Michael Rubinstein, and J Michael Ramsey. Enhanced nanochannel translocation and localization of genomic dna molecules using three-dimensional nanofunnels. *Nature communications*, 8(1):1–8, 2017.

[94] Kaikai Chen, Ining Jou, Niklas Ermann, Murugappan Muthukumar, Ulrich F Keyser, and Nicholas AW Bell. Dynamics of driven polymer transport through a nanopore. *Nature Physics*, 17(9):1043–1049, 2021.

[95] Bin Tu, Shiyang Bai, Benzhuo Lu, and Qiaojun Fang. Conic shapes have higher sensitivity than cylindrical ones in nanopore dna sequencing. *Scientific reports*, 8(1):1–11, 2018.

[96] Masao Doi, Samuel Frederick Edwards, and Samuel Frederick Edwards. *The theory of polymer dynamics*, volume 73. oxford university press, 1988.

[97] Michael Rubinstein, Ralph H Colby, et al. *Polymer physics*, volume 23. Oxford university press New York, 2003.

[98] Rob Phillips, Jane Kondev, Julie Theriot, et al. *Physical biology of the cell*. Garland Science, 2009.

[99] Steve Plimpton. Fast parallel algorithms for short-range molecular dynamics. *Journal of computational physics*, 117(1):1–19, 1995.

[100] Theo Odijk. The statistics and dynamics of confined or entangled stiff polymers. *Macromolecules*, 16(8):1340–1344, 1983.

[101] Takahiro Sakaue and Elie Raphaël. Polymer chains in confined spaces and flow-injection problems: some remarks. *Macromolecules*, 39(7):2621–2628, 2006.

[102] Sahin Buyukdagli, Jalal Sarabadani, and Tapio Ala-Nissila. Theoretical modeling of polymer translocation: From the electrohydrodynamics of short polymers to the fluctuating long polymers. *Polymers*, 11(1):118, 2019.